Master's thesis

2022

Markus Aasen Anker

NTNU
Norwegian University of
Science and Technology
Faculty of Information Technology and Electrical
Engineering
Department of Electric Power Engineering

Markus Aasen Anker

Powertrain Sizing of an All-Electric Commuter Aircraft for the Norwegian Short-Haul Network

June 2022

NTNU
Norwegian University of
Science and Technology

NTNU
Norwegian University of
Science and Technology

NTNU
Norwegian University of
Science and Technology

Powertrain Sizing of an All-Electric Commuter Aircraft for the Norwegian Short-Haul Network

Markus Aasen Anker

Energy and Environmental Engineering
Submission date: June 2022
Supervisor: Jonas Nøland
Co-supervisor: Kieran Duncan

Norwegian University of Science and Technology
Department of Electric Power Engineering

1 Acknowledgement

I want to thank my supervisor, Jonas Nøland, for his constant flow of ideas, laying the foundation for the scope of this thesis. He has also given valuable insight into electric aviation's technical aspects and has motivated me with his creativity and interest in this project. I would also like to thank my co-supervisor, Kieran Duncan, who, despite running a start-up company, has been available and has responded whenever I have needed help. He has also given insightful information into the industry of electrical aviation. Finally, I need to thank my friends for the long and joyous breaks and my family for their continuous support and encouraging words throughout the process.

Markus Aasen Anker
09.06.2022

2 Sammendrag

Mens utslippene knyttet til luftfart øker, er overgangen fra fossilt drivstoff til mer bærekraftige energikilder nødvendig. Denne overgangen inkluderer innfasing av elektriske fremdriftssystemer, og flere selskap har lansert planene for helelektriske batteridrevne fly. En utfordring er den lave spesifikke energien i batterier og den høye vektøkningen forbundet med det elektriske fremdriftssystemet. Vektutfordringene fører til at elektrifiseringen vil begynne på kortdistanseflygninger, og det norske kortbanenettet er pekt ut som et av de mest lovende markedene. Hovedmålet med denne oppgaven er å teste muligheten for elektriske flyvninger på det norske kortbanenettet og identifisere hovedutfordringene for en storstilt elektrifisering av flynæringen.

Oppgaven gjennomfører en omfattende analyse av norske kortdistanseflygninger. Blant annet, inkluderer den en detaljert flyprofil for 1500 gjennomførte flygninger. Denne dataen er prosessert for å frembringe en standardprofil for flyets fremdriftskraft med hensyn på tid. Resultatene er brukt i en vektestimeringsalgoritme med de beste elektriske komponentene for luftfart. Et 9- og 19-passasjerers fly har blitt brukt som referanse for algoritmen og en rekke scenarier, med ulike tekniske og lovmessige utfordringer, har blitt testet.

Scenariene viser at vekt er en stor utfordring for elektrifiseringen. Vektøkningen ved det elektriske fremdriftssystemet fører til at den maksimale vekten på flyene overgår den de er designet for. Denne vektøkningen forverres betydelig når regler for redundans og energireserver legges til. Det fører til at utsikten for implementasjon av elektriske fly er usikker, spesielt grunnet den høye vekten assosiert med batteriet.

Avslutningsvis understreker scenariene påvirkningen små endringer har på den totale vekten av flyet. Dette er blant annet vist ved å inkludere et gir mellom motor og propell. Dette gir en stor vektreduksjon av motoren, og fører også til at flyets vekt minsker. Scenariene viser også at høye spenninger vil føre til lavere vekt på grunn av en signifikant reduksjon i størrelsen på kablene om bord. Nødvendigheten av å inkludere batteritap er vist ved at det øker størrelsen og dermed effektkravene for kjølesystemet.

3 Abstract

As the emissions caused by the aviation sector are growing, the need to transition from fossil fuels to more sustainable energy sources is vital. This transition includes the implementation of electric drivetrains, and multiple companies have announced the launch of all-electric battery-driven aircraft. However, the specific energy of batteries is low, and the weight attributed to the electric propulsion system is high. The weight issue will initially enable short-distance aviation, and the Norwegian short-haul network is identified as one of the most promising markets. The main goal of this thesis is to test the viability of electric flight on the Norwegian short-haul network and identify the main obstacles to scaling up the electrification of aviation.

This thesis conducts a comprehensive analysis of the Norwegian commuter network. It includes detailed-level mission profile data of 1500 real-world flights. These data are further processed to obtain an overall standard profile for the propulsion power with respect to time.

The results are incorporated into a weight-sizing algorithm using state-of-the-art (SotA) electrical components. Two handpicked cases, a 9- and 19-passenger aircraft, have been investigated further. A myriad of scenarios has been considered, including technological and regulatory constraints.

The scenarios show that weight is a significant challenge for aircraft electrification. Even for short routes, the weight addition of the electric powertrain surpasses the maximum takeoff weight (MTOW) for the selected aircraft. Moreover, redundancy and reserve energy requirements are the most pressing issues as they add significant weight gains. With these requirements attached, the prospects for electrification are bleak, mainly due to the high weight addition of the battery.

Finally, the scenarios underline the system-level aspects affecting the aircraft's weight. The propulsion system achieves significant weight savings by implementing an indirect geared drive due to weight reductions in the motor. Additionally, high-voltage distribution results in weight savings due to reduced cabling size. The necessity to consider battery losses is also shown as it increases the size of the thermal management system (TMS), which also lifts the power requirements for handling the losses.

Nomenclature

Δ_{res}	Energy reserves in battery $[s]$
$\dot{Q}_{bat,TMS}, \dot{Q}_{conv,TMS}, \dot{Q}_{CB,bat,TMS}$	Heat losses in the battery, DC/DC-converter and battery breaker caused by the power provided to the TMS $[W]$
$\dot{Q}_{cable,1}, \dot{Q}_{cable,2}$	Heat losses in cables for EPS and TMS $[W]$
$\dot{Q}_{CB,bat}, \dot{Q}_{CB,TMS}, \dot{Q}_{CB,motor}$	Heat losses in the circuit breakers for the battery, TMS and motor $[W]$
$\dot{Q}_{conv}, \dot{Q}_{inv}, \dot{Q}_{inv,TMS}$	Heat losses in the DC/DC-converter, motor inverter and TMS inverter $[W]$
$\dot{Q}_{TMS}, \dot{Q}_{EPS}$	Total heat losses in the TMS circuit and the EPS $[W]$
$\dot{Q}_{tot}, \dot{Q}_{gear}, \dot{Q}_{motor}, \dot{Q}_{bat}$	Total, gear, motor and battery heat losses $[W]$
$\eta_{bat}, \eta_{gear}, \eta_{motor}, \eta_{conv}$	Efficiency of battery, gear, motor and DC/DC-converter
$\eta_{CB,uni}, \eta_{CB,bi}, \eta_{inv}, \eta_{cable}$	Efficiency of unidirectional, and bidirectional circuit breakers, inverter and cables
ρ	Air density $[kg/m^3]$
θ	Climb angle $[^\circ]$
a	Aircraft acceleration $[m/s^2]$
C_L, C_D, μ_f	Coefficient of lift, drag and friction
e_{bat}	Specific energy of battery $[Wh/kg]$
F_{prop}	Propulsion force $[N]$
F_{tire}, F_{slope}, N	Tire, slope and normal force $[N]$
g	Gravitational acceleration $[m/s^2]$
h_{TMS}	Thermal management system power per extracted heat loss $[W/W]$
K_g,	Gear constant
k_{bat}	Battery's utilization factor $[m/s]$
L, D, W	Lift, drag and weight force $[N]$
L/D	Lift-to-drag ratio

$L_{cable,1}, L_{cable,2}$	Length of cable for the EPS and TMS circuit $[m]$
m_0, m_f, m_{pl}	Empty, fuel and payload weight $[kg]$
m_{bat}, m_{TMS}	Weight of battery and TMS $[kg]$
$m_{cable,1}, m_{cable,2}$	Weight of cables for EPS and TMS $[kg]$
$m_{CB,bat}, m_{CB,TMS}, m_{CB,motor}$	Weight of battery, TMS and motor breaker $[kg]$
$m_{conv}, m_{inv}, m_{inv,TMS}$	Weight of DC/DC-converter, motor inverter and TMS inverter. $[kg]$
$m_{tot}, m_{gear}, m_{motor}$	Total aircraft, gear and motor weight $[kg]$
$P_{bat,TMS}, P_{conv,TMS}, P_{CB,bat,TMS}$	Power of the battery, DC/DC-converter and battery breaker caused by the power provided to the TMS $[W]$
$p_{bat}, p_{motor}, p_{conv}$	Specific power of battery, motor and DC/DC-converter $[W/kg]$
$P_{cable,1}, P_{cable,2}$	Power in the cables for the EPS and TMS $[W]$
p_{cable}	Specific power of distribution grid $[kg/A/m]$
$P_{CB,bat}, P_{CB,TMS}, P_{CB,motor}$	Power of circuit breakers protecting battery, TMS and motor $[W]$
$p_{CB,uni}, p_{CB,bi}, p_{inv}$	Efficiency of unidirectional, and bidirectional circuit breakers and inverter $[W/kg]$
$P_{conv}, P_{inv}, P_{inv,TMS}$	Power of DC/DC converter, motor inverter and TMS inverter $[W]$
$P_{takeoff}, P_{climb}, P_{cruise}, P_{descent}$	Takeoff, climb, cruise and descent power $[W]$
$P_{thrust}, P_{prop}, P_{gear}, P_{motor}$	Thrust, propulsion, gear and motor power $[W]$
p_{TMS}	Heat loss extracted per thermal management mass $[W/kg]$
PAX	Number of passengers
R	Aircraft's range $[m]$
S	Projected wing surface area $[m^2]$
$t_{takeoff}, t_{TOC}, t_{TOD}, t_{landing}$	Takeoff, Top-of-climb, Top-of-descent and landing time $[s]$
v,	Speed of aircraft $[m/s]$
v_∞,	Cruise speed of aircraft $[m/s]$

V_{DC}	Voltage level of DC distribution $[V]$
$V_{takeoff}$	Takeoff speed $[m/s]$

List of Figures

List of Tables

Contents

4 Introduction

4.1 Background and motivation

The aviation industry has experienced steady growth in passengers and transportable goods in recent years. Despite experiencing an offset due to the COVID-19 pandemic, the decline is expected to be temporary and reach pre-pandemic levels by 2023 before continuing its growth [17]. The aviation industry is currently responsible for approximately 5% of Anthropocene temperature change [18] and 2.7% of the global CO_2-emissions [19]. On its current trajectory, with annual growth in demand of 4.3%, the industry is expected to increase its emissions in the coming years. [20]. This growth could lead the industry to account for 20% of the world's total CO_2 emissions by 2050 [21].

Despite the expected growth in demand, a joint aviation sector has pledged a goal for carbon net neutrality by 2050 per the goals of the Paris climate accord [22]. The measures necessary to reach this goal include technological development and the transition from fossil fuels to sustainable ones. Within this measure is the transition to fully electrified aircraft.

The benefits attributed to the transition to all-electric aircraft are broader than just the emission reductions. Compared to conventional aircraft, the electrical drive train is more efficient. Conventional jet engines experience significant energy losses in their thermodynamic cycle. These are not present in an electric drive train where the efficiency goals are around 90% [23, 24]. The transition will also reduce other harmful emissions such as NO_x and CO polluting the air, especially in areas close to airports [25]. Due to fewer rotating parts in the electric drivetrain, it is also expected to increase reliability and reduce noise pollution, proven to lower the life quality of people living nearby airports [26]. The noise reduction could also increase the operating window for airports situated in urban areas where the operation is limited due to noise requirements [27]. Additional benefits include design optimization, reduced operation costs, and increased mobility [28].

Despite the advantages, electric aviation is in its infancy. Only one all-electric aircraft has been fully certified for operation [29]. The Velis Electro produced by Pipistrel is a two-person all-electric trainer designed to have around 50 minutes of flight [30]. The challenges facing the transition toward electric aircraft are plentiful. The main disadvantage is attributed to the energy storage. While conventional aircraft utilize the high power density of jet fuels with a specific power of 11900 Wh/kg [24], modern batteries have are substantially lower, with the most promising compositions reaching 250 Wh/kg. The low specific energy of batteries makes the energy storage in an all-electric aircraft heavy which is a significant disadvantage for an aircraft. The high power consumption needed in aviation is also a concern as it requires lightweight, high power components. All these concerns are secondary to safety concerns, as faults in the electric circuit could lead to devastating outcomes.

These problems have hindered the development of all-electric aircraft up until now. However, in recent years the field has seen a growing interest, and multiple companies

Table 1: Overview of announced all-electric aircraft

Company	**Model**	**Launch year**	**Capacity**	**Source**
Heart Aerospace	ES-19	2026	19	[14]
Wright electric	Spirit	2026	100	[31]
Elfly	-	2029	9	[32]
Eviation	Alice	2024	9	[7]
Zeroavia	-	2024	10-20	[33]
Bye Aerospace	eFlyer 800	-	12	[34]
Tecnam	P-Volt	2026	9	[35]
NASA	X-57 Maxwell	-	2	[36]

have announced launch dates for their all-electric aircraft. The designs range from complete retrofits, where the conventional propulsion unit of an existing design is replaced by an electrical, to new designs utilizing the design freedom offered by electrification. In Table 1, some of the companies currently developing all-electric aircraft are presented.

The table shows that the first aircraft is expected to be ready and certified by 2024. However, as neither of these designs has completed their maiden flights, the progress could be overly optimistic.

This thesis aims to explore the viability of all-electric aircraft and give an insight into the challenges facing the companies trying to electrify the aviation sector. It will also present a critical view of the prospects of electrification.

Many research articles have tried to shed light on the opportunities and challenges facing the implementation of all-electric flights. Thorough reviews for the components necessary for an electrical aircraft are conducted in [37, 19, 38] with more. Sizing procedures are also presented in the literature as in [39, 40]. Estimation of range, capacity, and power requirements for all-electric aircraft are shown in [24, 41]

However, many of the articles use future projections for the technology development [42, 43, 44]. Many of these are optimistic, and they require huge technological development, which could be overly optimistic, and expect that research programs are ready ahead of their time. The time used to advance from a successful prototype to a commercially available product is long [45].

Additionally, many technical aspects are often overlooked. These aspects can include effects such as thermal management system (TMS) design, system losses, and the effects of the different phases of flight. An example is the assumption of 100% efficiency for batteries where the heat dissipation of the battery is neglected. Regulations will also affect the design and sizing of the electric aircraft due to redundancy requirements in the electric system and onboard energy reserves.

Due to the high weight gain accompanied by energy storage, electrification prospects are assumed to enable short-distance flights initially. The Norwegian short-haul network has been pointed to as one of the most promising areas for electrification, with the Norwegian government stating a goal of electrifying the domestic aviation

sector by 2040 [46].

4.2 Goals and research questions

The main goal of this thesis is to assess the weight of the electrical system and present technological and regulatory challenges hindering its implementation. The thesis presents data on the short-haul network and conducts a weight analysis at the component level for the propulsion system of an all-electric aircraft. It is performed through a sizing procedure using Tecnam's P-Volt and Heart's ES-19 as references. The thesis will not include economic considerations but will present practical considerations caused by the transition to all-electric aircraft.

The research questions that arise from this are:

- How is the structure of the Norwegian short-haul network, and how is the flight pattern for short-haul flights?
- Is the prospects for electrification of routes on the network by 2026 plausible, or are the weight of the electric aircraft an issue preventing it?
- What are the weight effects of often omitted technological and regulatory aspects?

4.3 Contribution

The thesis thoroughly analyzes flights on the short-haul network through a data collection of 1500 flights of varying distances—the short-haul analysis results in a flight profile, including time regressions based on the flight distance. It also gives a complete overview of weekly flights on the network and considers important factors such as airport infrastructure and flight time. The work is inspired by Jux et al. [47], which used the same methodology to establish a standard mission profile for a regional aircraft. However, while they studied flights lasting approximately an hour, this thesis will use the same method for substantially shorter routes.

Gnadt et al. [41] gives a thorough analysis of the aspects of the design procedure of an aircraft. However, the article focus on 180-passenger aircraft, while this thesis focuses on smaller aircraft as the weight of a nine and 19-passenger aircraft is analyzed through a weight sizing algorithm. Gnadt et al. [41] also focuses more on the total system weight, while this thesis breaks it down to component level weights showing the weight attribution of each part of the electrical system. These weights can be used to find the most pressing issues when considering electrification. It also shows the effects different regulations such as reserve requirements and redundancy have on the aircraft. These requirements are present for any aircraft, and the impact of various regulations is estimated. Finally, this thesis presents the effects of battery losses and compares indirect and direct drive and the effects of different voltage levels. It shows the need to include all components and factors during the design procedure of an electric aircraft.

4.4 Thesis structure

Firstly, relevant aircraft dynamics and sizing equations are described in Section 5. Subsequently, Section 6 gives a detailed overview of the Norwegian short-haul network and looks at flight patterns and power requirements based on real-world data. The analysis concludes with a standardized power and time profile for flights on the network in Section 7. Section 8 describes components and important parameters for the design of the electric system on an all-electric aircraft. It also gives insight into state-off-the-art performance and current research efforts for these components. The section concludes with a possible design for the aircraft's electric system. Based on the design and reference aircraft presented in Section 9 a sizing algorithm for the weight of the electric propulsion system is developed. The algorithm gives an initial weight estimation for aircraft operating on a short-haul network. After that, different scenarios and requirements are applied, and their effects are shown in Section 10. The results are discussed and scrutinized in Section 11 before concluding in Section 12. Finally, efforts to improve the procedure and recommendations for further work are presented in Section 13.

5 Theory

In this section the aircraft fundamentals are presented. It will give an overview of the forces affecting the, and show the power required for propulsion. The calculations in the first section are based on Newtons laws, while the second part will show specific weight calculations for an all-electric aircraft.

5.1 Aircraft fundamentals

In Fig. 1 the free body diagram and the forces affecting the aircraft during a leveled flight are depicted. The forces affecting the aircraft are split into four different forces acting in opposite directions. These are weight, lift, drag and thrust.

The lift is mainly affected by the aerodynamic construction of the aircraft. The wings are the main contributor, contributing to the lift generation by utilizing a pressure and speed differential in airflow. The wings press air downwards as the aircraft moves, creating a difference in airflow above and under the wing. The airflow below the wings moves slower than the flow over the wing, which creates a pressure difference pushing the aircraft upwards, creating the lift. The lift force is always perpendicular to the direction of flight [48]. It depends on air pressure, the vetted area of the wings, and the speed of the aircraft, as shown in Eq. (1).

$$L = \frac{1}{2} \cdot \rho \cdot C_L \cdot S \cdot v^2 \tag{1}$$

The force counteracting the lift is the aircraft's weight, the product of the aircraft mass, and the gravitational force. It is important to emphasize that the lift and

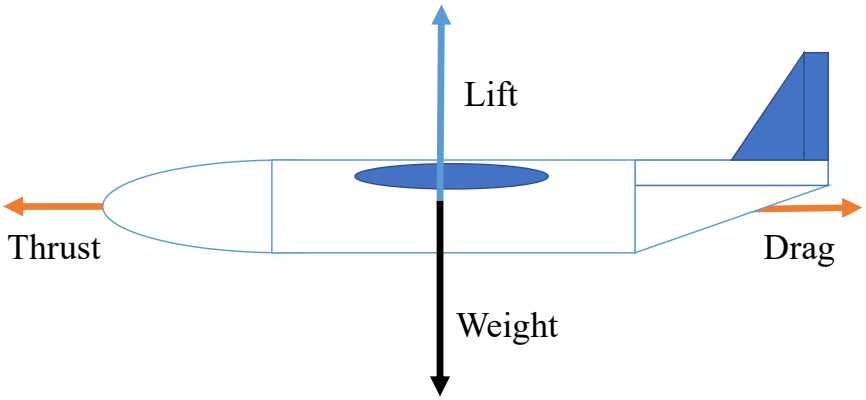

Figure 1: Free body diagram showing the forces acting on a levelled aircraft.

weight are not necessarily directly opposing. The lift force will always be perpendicular to the travel direction, while the weight will point directly towards the gravity center of the earth.

The propulsion force creates the forward motion of the aircraft. It is created in the motors and is used to create thrust and oppose the drag forces. The drag can be separated into two main parts; parasitic drag and lift-induced drag—the parasitic drag results from the form drag and the skin friction drag of the aircraft. The shape of the aircraft causes the form drag by, for example, creating eddy currents where multiple air flows gather. The skin friction drag is caused by the interface between the airflow and the aircraft. While the "skin" of the aircraft is smooth to the human eye, it is porous for air molecules. Hence, molecules closest to the aircraft, the boundary layer, stick to the aircraft. This effect increases the drag due to air being accelerated with the rest of the aircraft. These drag effects are called parasitic due to not producing any lift for the aircraft and thus only reducing the efficiency [49].

The lift-inducing drag directly results from the lift creation over the wings. Hence, it is necessary for flight. When air is deflected during lift production, it is displaced and creates vortexes at the wing's trailing edge, especially towards the wings' sides. These vortexes produce downwards facing forces called downwash. These forces cause the aircraft to experience reduced lift which can be translated into a drag force. Equation (2) shows an analytical expression for the drag force affecting the aircraft.

$$D = \frac{1}{2} \cdot \rho \cdot C_D \cdot S \cdot v^2 \tag{2}$$

It can be noted that the expression for drag and lift is similar, which results in Eq. (3). It shows that the lift and drag relation only depend on the coefficients of lift and drag.

$$\frac{L}{D} = \frac{C_L}{C_D} \tag{3}$$

This relation results in the lift-to-drag coefficient, an important metric for an aircraft. It is called the aerodynamic efficiency and describes the amount of lift to drag produced by the aircraft. In Raymer [50] an overview of standard L/D-ratios is shown where it varies between 15 and 20 for civil jets while it is around 14 for retractable propeller aircraft.

The following sections will give detailed derivations for the equations of motion affecting the aircraft in each phase of flight.

5.1.1 Cruise

The aircraft is assumed to have a constant speed and altitude during the cruise phase. Hence, the sum of the forces shown in Fig. 1 is zero. Hence, the propulsion force needs to counteract the drag, and the lift force will be equal and oppositely directed to the weight. For simplicity, any effect caused by wind is neglected.

Hence, the equations can be written as shown in Eq. (4) where the expressions from Eqs. (1) and (2) is inserted for the drag and lift force.

$$W = L = mg = \frac{1}{2} \cdot \rho \cdot C_L \cdot S \cdot v^2 \tag{4a}$$

$$F_{thrust} = D = \frac{1}{2} \cdot \rho \cdot C_D \cdot S \cdot v^2 \tag{4b}$$

Due to the proportionality of the drag and lift force described in Eq. (3), the expression can be rearranged as

$$F_{thust} = \frac{mg}{C_L/C_D}. \tag{5}$$

Hence, the cruising force is only dependent on the lift-to-drag coefficient and the mass of the aircraft.

5.1.2 Takeoff and taxi

During takeoff and taxiing, the aircraft is in contact with the ground, and equations used for modeling vehicle motion are used as a basis.

$$m \cdot a = F_{prop} - sign(v)(F_{tire} + D) - F_{slope} \tag{6}$$

The vehicle equation is shown in Eq. (6). The tire force is caused by friction between wheels and ground, while the tilting of the runway causes the slope force. Since the runway is flat, this force contribution is assumed to be negligible.

The friction force is a result of the normal force affecting the aircraft. This force is, in turn, the difference between the weight of the aircraft and the lift, as shown in Eq. (7)

$$F_{tire} = \mu_f(mg - L) = \mu_f(mg - \frac{1}{2} \cdot \rho \cdot C_L \cdot S \cdot v^2) \tag{7}$$

The equations can be rearranged into

$$F_{thrust} = m \cdot a + sign(v)(\mu_f(mg - \frac{1}{2} \cdot \rho \cdot C_L \cdot S \cdot v^2) + \frac{1}{2} \cdot \rho \cdot C_D \cdot S \cdot v^2). \tag{8}$$

The acceleration during takeoff is determined based on the length of the runway and takeoff speed of the aircraft, while the speed can be assumed constant during taxiing, simplifying the equation. During landing, the speed sign will be negative, which could be used for regenerative braking to return power to the aircraft.

It is difficult to establish the values of C_L and C_D since these data are not publicly available. However, assuming that the aircraft takes off as the normal vector becomes zero leads to Eq. (9).

$$N = 0 = \mu_f(mg - \frac{1}{2} \cdot \rho \cdot C_L \cdot S \cdot V_{takeoff}^2) \tag{9}$$

By assuming constant C_L, the equation can be solved for the constants in the equation resulting in Eq. (10), where the left hand side of the expression can be considered constant.

$$\frac{1}{2} \cdot \rho \cdot C_L \cdot S = \frac{mg}{V_{takeoff}^2} \tag{10}$$

The L/D-ratio is assumed to be constant during flight. Hence, the drag can be calculated as a proportion of the lift. This is shown in Eq. (11). As shown above, the lift can be calculated as long as the speed is known. However, this is a simplification due to the L/D changing during the different phases of flight.

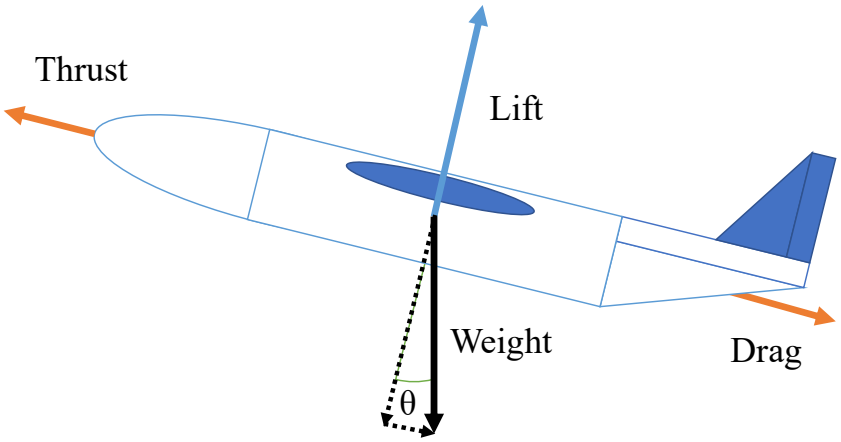

Figure 2: Free body diagram of an aircraft during climb.

$$D = \frac{L}{L/D} \tag{11}$$

5.1.3 Climb and Descent

During the climb, the aircraft accelerates while the speed decrease during descent. At the same time, the aircraft gains altitude during the climb and loses it in descent. Hence, the climb and descent phases of flight can be modeled similarly but with opposite motion. The high altitude of flight is due to reductions in air pressure which is advantageous for reducing power consumption during cruise. However, as the aircraft increases its kinetic and potential energy during the climb, the power requirements for the phase are considerable.

Figure 2 shows the forces affecting the aircraft during the climb. It is similar to the free body diagram during the cruise, but a component of the weight is added to the drag. This component further emphasizes the need for more power for the propulsion. By using a coordinate system referenced to the flight direction, the equations of motion during climb can be written as in Eq. (12).

$$ma = F_{thrust} - D - W\sin\theta \tag{12a}$$
$$L = W\cos\theta \tag{12b}$$

Equation (13) shows the same equation, where the drag force has been substituted by a weight expression based on the L/D-ratio.

$$F_{thrust} = ma + mg\sin\theta + \frac{1}{C_L/C_D} mg\cos\theta \tag{13}$$

Since θ describes the climb angle, the sine term is negative during descent. Hence the propulsion force during descent is lower than in the other flight phases. This relation is also evident when considering the kinetic and potential energy acquired in the climb phase.

5.1.4 Power and energy requirement

The power requirements for the phases are the product of the force and the aircraft velocity. In Eq. (14) the power equations for takeoff, climb/descent, and cruise are presented.

$$P_{takeoff} = (m \cdot a + sign(v)(\mu_f(mg - L) + D)) \cdot v \tag{14a}$$

$$P_{climb} = (ma + mg\sin\theta + \frac{1}{C_L/C_D} mg\cos\theta) \cdot v \tag{14b}$$

$$P_{cruise} = \frac{mg}{C_L/C_D} \cdot v \tag{14c}$$

Power is the most significant dimensioning factor for the aircraft's propulsion system. However, as power requirements vary for the different phases, the highest power requirement dimensions the system. This is expressed in Eq. (15).

$$P_{thrust} = max\{P_{takeoff}, P_{climb}, P_{cruise}, P_{descent}\} \tag{15}$$

On the other hand, the energy requirement is decided by the total power consumption during flight. Equation (16) shows the calculation where the integration variable is the flight time.

$$E_{total} = \int_0^{t_{takeoff}} P_{takeoff}\ dt + \int_0^{t_{TOC}} P_{climb}\ dt + \int_0^{t_{TOD}} P_{cruise}\ dt + \int_0^{t_{landing}} P_{descent}\ dt \tag{16}$$

5.2 Weight equations

The previous section shows a high dependency between the aircraft weight and the power requirements. This part will describe the weight estimation of a conventional aircraft and present the conversions necessary for an electric aircraft. It will also present the equations used in the sizing procedure in Section 9.

5.2.1 Aircraft weight

For a conventional aircraft, the weight calculation consists of three main parts. These are shown in Eq. (17) where the weight is separated into empty weight, fuel weight, and payload weight.

$$m_{tot} = m_0 + m_f + m_{pl} \tag{17}$$

The empty weight is the constant weight of the aircraft. It includes the aircraft structure, the interior, and technical equipment as the landing gear. However, the fuel and payload weight are variables changing for different missions. The amount of fuel is dependent on the length of the flight and the conditions, while the payload weight is the weight caused by passengers or other goods carried by aircraft. Additionally, the fuel weight for a conventional aircraft will reduce as the flight progresses due to fuel burn.

This effect is not seen in an electric aircraft. The battery will have constant weight throughout the flight. Unless the battery is changeable, the battery weight will also be independent of flight mission and conditions. Hence, the aircraft's total weight could be represented with the payload as the only variable weight. However, the empty weight will depend on the weight of the electric system. The analysis in this thesis is presented componentwise. In Eq. (18) this calculations for the total aircraft weight is shown where the weight for each component is denoted m_i.

$$m_{tot} = m_0 + m_{pl} + \sum_{i=1}^{n} m_i \tag{18}$$

5.2.2 EPS weight

The weight of the components in the electric propulsion system (EPS) is calculated based on the specific power of the components. It describes the power a component can handle per kilo of equipment. The power of the propulsion system found in Eq. (15) is the dimensioning power required by the propulsors. However, as losses occur upstream from the propulsors, they must be included in the calculations. This inclusion is shown in Eq. (19) where the calculation for the components in the EPS are shown.

$$P_{thrust} = \frac{m_{tot} g}{L/D} v_\infty \qquad P_{prop} = \frac{P_{thrust}}{\eta_{prop}} \tag{19a}$$

$$P_{gear} = \frac{P_{prop}}{\eta_{gear}} \qquad m_{gear} = 32.66 \frac{HP_{mot}^{0.76} rpm_{mot}^{0.13}}{rpm_{prop}^{0.89}} \tag{19b}$$

$$P_{mot} = \frac{P_{gear}}{\eta_{mot}} \qquad m_{mot} = \frac{P_{mot}}{p_{mot}} \tag{19c}$$

$$P_{inv} = \frac{P_{mot}}{\eta_{inv}} \qquad m_{inv} = \frac{P_{inv}}{p_{inv}} \tag{19d}$$

$$P_{CB,motor} = \frac{P_{inv}}{\eta_{CB,uni}} \qquad m_{CB,motor} = \frac{P_{CB,motor}}{p_{CB,uni}} \tag{19e}$$

$$P_{cable,1} = \frac{P_{CB,motor}}{\eta_{cable}} \qquad m_{cable,1} = \frac{P_{cable,1}/V_{DC}}{p_{cable}} L_{cable,1} \tag{19f}$$

$$P_{CB,bat} = \frac{P_{cable,1}}{\eta_{CB,uni}} \qquad m_{CB,bat} = \frac{P_{CB,bat}}{p_{CB,uni}} \tag{19g}$$

$$P_{conv} = \frac{P_{CB,bat}}{\eta_{conv}} \qquad m_{conv} = \frac{P_{conv}}{p_{conv}} \tag{19h}$$

The weight of the distribution system and the gear is slightly different from the rest of the components. Sizing of the gear is based on the works of Brown et al. [51], while the specific power of the cables is given in A/kg/m.

All losses are expected to result in heat generation. In a conventional aircraft, the heat is extracted through the engines, but since the electric propulsion system is closed, the excess heat needs to be handled by a thermal management system (TMS). The size and power requirements of the TMS depend on the amounts of excess heat produced in the EPS and the heat produced in the TMS circuit. The heat generation of the EPS is shown in Eq. (20).

$$\dot{Q}_{gear} = P_{gear} - P_{prop} = (\frac{1}{\eta_{gear}} - 1) P_{prop} \tag{20a}$$

$$\dot{Q}_{mot} = P_{mot} - P_{gear} = (\frac{1}{\eta_{mot}} - 1) P_{gear} \tag{20b}$$

$$\dot{Q}_{inv} = P_{inv} - P_{mot} = (\frac{1}{\eta_{inv}} - 1) P_{inv} \tag{20c}$$

$$\dot{Q}_{CB,motor} = P_{CB,motor} - P_{inv} = (\frac{1}{\eta_{CB,uni}} - 1) P_{inv} \tag{20d}$$

$$\dot{Q}_{cable,1} = P_{cable,1} - P_{CB,motor} = (\frac{1}{\eta_{cable}} - 1) P_{CB,motor} \tag{20e}$$

$$\dot{Q}_{CB,bat} = P_{CB,bat} - P_{cable,1} = (\frac{1}{\eta_{CB,bi}} - 1) P_{cable,1} \tag{20f}$$

$$\dot{Q}_{conv} = P_{conv} - P_{CB,bat} = (\frac{1}{\eta_{conv}} - 1) P_{CB,bat} \tag{20g}$$

The sum of the heat loss of each component is the total heat losses in the EPS.

5.2.3 TMS circuit weight

The size of the TMS depends on the heat losses. Additionally, the TMS introduces another power-consuming component. It will be more thoroughly described in Section 8.6, but a circuit powering the TMS is necessary. The size of the circuit can be calculated in the same way as the EPS weights, as shown in Eq. (21).

$$P_{inv,TMS} = \frac{P_{TMS}}{\eta_{inv}} \qquad m_{inv,TMS} = \frac{P_{inv,TMS}}{\eta_{inv}} \tag{21a}$$

$$P_{CB,TMS} = \frac{P_{inv,TMS}}{\eta_{CB,uni}} \qquad m_{CB,TMS} = \frac{P_{CB,TMS}}{\eta_{CB,uni}} \tag{21b}$$

$$P_{cable,2} = \frac{P_{CB,TMS}}{\eta_{cable}} \qquad m_{cable} = \frac{P_{cable,2}/V_{DC}}{p_{cable}} L_{cable,2} \tag{21c}$$

$$P_{CB,bat,TMS} = \frac{P_{cable,2}}{\eta_{CB,bi}} \qquad m_{CB,bat,TMS} = \frac{P_{CB,bat,TMS}}{p_{CB,bi}} \tag{21d}$$

$$P_{conv,TMS} = \frac{P_{CB,bat,TMS}}{\eta_{conv}} \qquad m_{conv,TMS} = \frac{P_{conv,TMS}}{p_{conv}} \tag{21e}$$

There will be heat losses attributed to these components as well. The heat losses are presented in Eq. (22).

$$\dot{Q}_{inv,TMS} = P_{inv,TMS} - P_{TMS} = (\frac{1}{\eta_{inv}} - 1)P_{TMS} \tag{22a}$$

$$\dot{Q}_{CB,TMS} = P_{CB,TMS} - P_{inv,TMS} = (\frac{1}{\eta_{CB,uni}} - 1)P_{inv,TMS} \tag{22b}$$

$$\dot{Q}_{cable,2} = P_{cable,2} - P_{CB,TMS} = (\frac{1}{\eta_{cable}} - 1)P_{CB,TMS} \tag{22c}$$

$$\dot{Q}_{CB,bat,TMS} = P_{CB,bat,TMS} - P_{cable,2} = (\frac{1}{\eta_{cable}} - 1)P_{CB,bat,TMS} \tag{22d}$$

$$\dot{Q}_{conv,TMS} = P_{conv,TMS} - P_{CB,bat,TMS} = (\frac{1}{\eta_{conv}} - 1)P_{CB,bat,TMS} \tag{22e}$$

The sizing of the TMS circuit is dependent on the size of the TMS. It is evident that the TMS depends on the size of the heat losses, and its sizing is based on two main metrics. The first, h_{TMS}, is the amount of power required by the fans and pumps of the TMS to remove heat. It is the amount of heat transferred per kg of TMS. This parameter can be regarded as a metric for the efficiency of the TMS, while p_{TMS} describes the specific power. The parameters for the TMS can be calculated as in Eq. (23).

$$P_{TMS} = h_{TMS}(\dot{Q}_{EPS} + \dot{Q}_{TMS} + \dot{Q}_{bat}) \tag{23a}$$

$$m_{TMS} = \frac{\dot{Q}_{EPS} + \dot{Q}_{TMS} + \dot{Q}_{bat}}{p_{TMS}} \tag{23b}$$

Low values for h_{TMS} and high values for p_{TMS} would be advantageous for the weight of the system.

5.2.4 Battery weight

The battery energy, power, and weight result from the requirements mentioned above. The power consumption of the battery is simply a sum of the power contribution of the TMS circuit and the EPS. On the other hand, the energy requirements are the sum of the power requirements throughout the flight in addition to any required reserves. A factor affecting the battery is the allowable discharge. This is decided by factor k_{bat} as shown in Eq. (24).

$$P_{bat} = \frac{P_{conv,EPS} + P_{conv,TMS}}{\eta_{conv}} \tag{24a}$$

$$E_{bat} = \int \frac{P_{bat}}{k_{bat}} dt + P_{cruise}\Delta_{res} \tag{24b}$$

The battery needs to handle the system's power requirements and store energy for the whole flight. The final weight of the battery results from a comparison between these requirements. The most demanding requirement is used to dimension the battery, as shown in Eq. (25).

$$m_{bat} = max\{\frac{E_{bat}}{e_{bat}}, \frac{P_{bat}}{p_{bat}}\} \tag{25}$$

The equations show the high interconnectedness of the system. The battery weight is dependent on the power requirements of the TMS circuit and EPS. When the requirements of the circuits increase, so does the weight of the battery. In turn, this increase the power requirements for the system, resulting in an even heavier TMS and EPS.

6 The Norwegian Short-Haul Network

An overview of the Norwegian short-haul network is analysed in this section. It gives an overview of the network and the requirements for aircraft operating on it with regards to range. The section also shows the prospect for electrification and lays the groundwork for the analysis based on the previously presented equations.

Figure 3: An overview of Norwegian airports [1]

6.1 Overview

This section will provide detailed information on the short-haul network's operation, capacity demands, and flight distances. It will also describe why the short-haul network is considered one the most likely areas for implementing all-electric aircraft.

The Norwegian short-haul network has been pointed out as a possible testing ground for electric aviation. The network consists of multiple airports located in northern and western Norway. The airports were mainly constructed during the late 1960s and early 1970s to increase mobility and reduce migration from rural areas. Due to the Norwegian geography in these areas, with mountainous terrain, fjords, and islands, transportation by plane is the only practical mode of travel.

The inspiration was found in Alaska, which was stated to have similar geographic challenges. They minimized the project's costs by constructing the airports with few features and with shortened runways. However, the shortened runways require specialized aircraft with the ability for short takeoff and landing (STOL) [52].

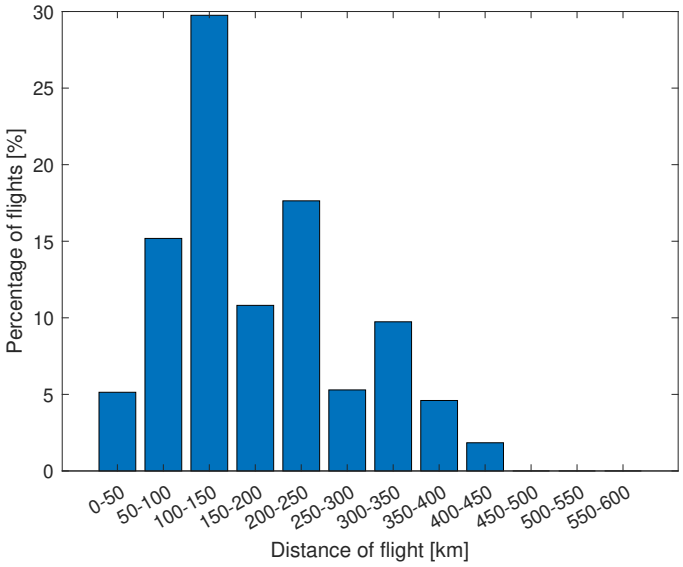

Figure 4: Distribution of flights by travel distance on the Norwegian short-haul network

Figure 3 shows an overview of Norwegian airports. The figure shows the high proximity of airports, especially in western and northern Norway, where the short-haul airports are located. Two airports are exempted, the airport at Svalbard, due to the long distance from the mainland, and Væreøya airport, which is closed for public transportation. The closing happened due to an accident in 1990 [53].

Lars Engerengen [52] gives an overview of the airports and the length of their runways. In total, the system consists of 25 short runway airports. The shortest, which will be the dimensioning runway for this thesis, is located in Leknes and have a runway of 799 meters. The small airports are mainly used to transport people to and from the regional airports. They are sometimes called bus routes due to the aircraft transiting through multiple airports to load and unload passengers during a single flight. This type of operation characterizes the network since it leads to many short-distance flights. The shortest is between Kirkenes and Vadsø, with an average flight time of 11 minutes according to Flightradar.com [5]. It is a publicly available site that tracks and collects data from flights worldwide.

The weakly frequency of each flight on the Norwegian short-haul network was collected using data available at the site. Some of these results are presented in Table 11. Figure 4 shows the distribution of the weekly flights by distance. Few flights surpass 400 km in flight distance, and the most frequent travel distance is 100-150 km. High frequency of flights between 50-100 and 150-200 km are also observed.

Figure 5 shows the cumulative distribution of the same data. A range of 150 km can cover 50% of the flights, and approximately 90% are covered for flight distances of 300 km.

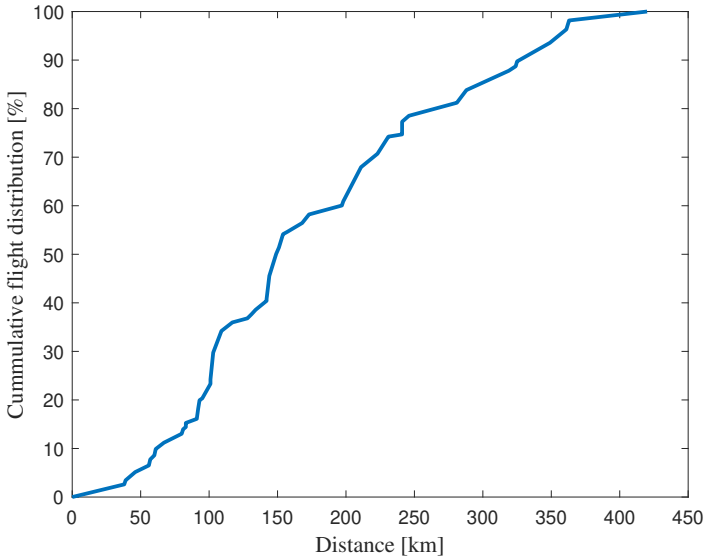

Figure 5: Cumulative distribution of flights covered by flight length

6.1.1 Operation

It is mainly four airliners operating domestically in Norway. These are SAS, Norwegian, Flyr and Widerøe. However, due to the specialized aircraft requirement and the relatively low capacity needs of the short-haul network, it is mainly operated by Widerøe. The company has used many years specializing in travels on the network [54]. The other companies mainly operate international flights and flights between the regional airports in Norway. Danish Air Transport (DAT) also operates a few distances on the short-haul network, but they only operate on airports with runways over 1000 meters [55].

Many of the routes on the short-haul network have few passengers, but the need for frequent flights. It makes them economically infeasible for a company to operate. However, it is vital for the population and government that these routes are operated, and the routes are part of the public service obligation (PSO). The Norwegian government subsidizes the PSO routes to ensure operation. The operator of the PSO routes is chosen in an auction where some preset demands need to be fulfilled. The cheapest operator meeting the requirements is chosen. It is comparable to the way other public transport operators are decided, for example, the operators of bus routes or the ferries in Norway [56]. The current concessions for the operation of the PSO routes last until 2024, and the operator is almost exclusively chosen based on the lowest monetary contribution from the government. If this factor does not separate two operators, the one adding the most capacity is chosen [57, 58].

6.1.2 Current fleet

Due to the short runways constructed for the short-haul network, specialized aircraft with STOL abilities are needed for operation. Initially, the Twin Otter DHC-8

Table 2: Overview of Widerøe's fleet [4]

Aircraft type	Number of aircraft	Capacity	Max cruise speed
E190-E2	3	110	890 km/h
DASH-8 Q400	10	78	667 km/h
DASH-8 300	4	50	501 km/h
DASH-8 100/Q200	26	39	482/518 km/h

operated on the network. It is a two-engine propeller aircraft with a capacity for 20 passengers [59]. As the Twin Otter was phased out, Widerøe found their replacement in the Dash-8 series produced by De Havilland [54]. The Dash-8s are used for the short-haul network and are turboprop aircraft with STOL abilities. The Dash-8 100/Q200 is the most frequently used aircraft on the short-haul network and are Widerøe's most common aircraft. In Table 2 an overview of the current Widerøe fleet is shown.

However, the Dash-8 100 has been in operation for a long time and is at the end of its lifetime. The high flight frequency for the Dash-8 100 means it is exposed to high amounts of stress, and as the aircraft is closing in on 20 years of operation, Widerøe is looking for replacements. However, there are no available replacement aircraft due to the need for STOL abilities. Thus, Widerøe has performed life-extending upgrades to the aircraft to operate them longer. It is still expected that the aircraft will be replaced during the 2020s [60].

6.1.3 Capacity

When considering the viability of electrification of the short-haul network, the flight's capacity need is essential. As previously mentioned, this is the deciding factor second only to price when deciding on the operators of the routes. The 1st generation electric aircraft will have lower capacity than the aircraft currently operating on the routes. It is due to a simpler certification process for aircraft with 19 or fewer passengers. For this category of aircraft, the certification process is performance-based instead of having to follow specified design details [61].

The cabin factor of an aircraft is the number of occupied seats to the total seats. This factor is a metric for calculating the actual capacity needed for a route. Keeping in mind that the short-haul network originally was operated by smaller aircraft could mean that the current aircraft is over-dimensioned. The cabin factor for specified routes is not publicly available, but the total cabin factor for all Widerøe flights in 2018 was 58.1% [62]. However, this number does not separate on routes. For a Dash-8 100, this would mean that 22-23 seats are occupied on average. Since many of the routes on the short-haul network need governmental subsidies, it is expected that the cabin factor on these routes will be lower.

6.2 The prospects for electrification

The Norwegian short-haul network is a good prospect for electric aviation. Due to the short distances, aircraft do not need to be equipped with large energy storage. This is very advantageous due to the low specific energy of batteries. The scarce population with a high frequency of airports can allow small aircraft with low capacity. As the 1st generation of electric aircraft will have a capacity lower than 20 passengers, it could replace the currently operating Dash-8 100. These require replacement, and since few alternatives are available, an electric aircraft with STOL abilities could be an attractive solution. The replacement of aircraft rarely happens due to the long lifetime of aircraft (¿20 years). An opportunity for replacing the smallest conventional aircraft with electrical aircraft will not occur soon if this chance is not taken.

The short-haul routes are currently operated mainly by a single airliner. That makes it easier to implement electric aircraft as multiple airliners do not need to be willing to take the step. Only Widerøe needs to be convinced. Additionally, many of the routes on the short-haul network are part of the PSO, allowing the government to influence the requirements for operation. Despite environmental concerns not being a part of the latest concessions, the government can attach these requirements in the next auction. The Norwegian government has already imposed these requirements for new ferries and city buses [63]. It should also be noted that the Norwegian government has started the process. In March 2020, Avinor (a state-owned company in charge of Norwegian airports) and the Norwegian Civil Aviation Authority published a report outlining the road toward all-electric aviation in Norway. It was given on request of the Norwegian Ministry for Transportation [64]. It is also a stated goal that all domestic flights should be all-electric by 2040 [46]. Widerøe has also shown initiative and has announced a partnership with Rolls-Royce and Tecnam for the development of Tecnam P-volt, an all-electric 9-passenger aircraft [65].

As previously mentioned, the environmental advantages are highly dependent on electricity generation. The Norwegian power generation is mainly based on renewable energy sources such as hydropower and wind [66]. It removes the emissions from the power generation, and it would make the electric aircraft run on green energy. However, as Norway is a part of the European power grid which uses fossil sources for generation, the picture is more nuanced. Anyhow, renewable power generation is pointed out as one of Norway's main advantages in the electrification of the aircraft industry.

6.3 Challenges

Despite the advantages presented above, there are multiple challenges associated with the operation of the Norwegian short-haul network. Some are general for electric aviation, while some are specific for Norwegian airspace.

6.3.1 Weather conditions

The coast of Norway is frequently experiencing extreme weather conditions, especially in western and northern parts. Rainfalls, snow storms, and high winds make it a demanding area for air travel. The temperatures are also regularly below zero degrees Celsius, with the icing being a critical concern. Any aircraft operating on the network thus needs to be sturdy and able to operate in the demanding environment. Due to harsh weather conditions, diversions are also a common phenomenon. This phenomenon can affect the need for onboard energy storage reserves.

6.3.2 Energy reserves

Due to the weight and fuel consumption caused by over dimensioning the fuel loading of the aircraft, the airliners try to keep it as low as possible. However, due to uncertainties, rerouting, and other scenarios, carrying an energy reserve onboard is necessary. Due to the high weight addition caused by increasing the capacity of the batteries, this is a considerable concern for the implementation of all-electric aircraft.

For each flight, the airliner calculates the assumed fuel consumption based on data regarding the aircraft and the weather conditions. It also calculates the energy needed for taxiing. This energy is dependent on the airport size, but on the small short-haul network in Norway, this is expected to be low. However, for larger airports it can be substantial [67]. Slight deviations from the calculated fuel consumption are expected and could be caused by weather changes. Therefore, it is recommended that the aircraft have a 5% buffer of fuel for such events.

Weather and other operational issues could cause the aircraft to be redirected to a secondary airport. The diversion consists of a secondary climb, cruise, and loitering phase that must be accounted for when dimensioning the fuel loading. The alternative airport choice is important when calculating the fuel required for this event. It can be argued that the high proximity of the airports in the short-haul network should leave this reserve low. However, the aircraft is usually diverted to one of the larger regional airports for safety measures.

The main issue for the aircraft is the demand for final reserve fuel. It describes fuel reserves that need to be unused throughout the flight. It is only there as a final reassurance if unexpected events occur and the aircraft finds itself in a state of emergency. The requirement is for 30 minutes of cruise during visual flight rules (VFR) and 45 minutes during instrument flight rules (IFR). IFR is used when the conditions make the pilot unable to see the landscape, for example, during night flights or when experiencing fog or other bad weather. In general, if an aircraft displays lower reserves than the requirements mentioned above after flight, an investigation is conducted [68, 69, 70].

These rules will make aircraft unnecessarily heavy and hinder electric aircraft, especially on short routes where the main proportion of the energy onboard is allocated for reserves. To enable electric flight, it may be necessary with specialized rules for

Table 3: Flight WF970 [5]

Route	Distance	Average time
Hammerfest-Berlevåg	198 km	33 min
Berlevåg-Båtsfjord	39 km	12 min
Båtsfjord-Vardø	57 km	16 min
Vardø-Vadsø	56 km	13 min
Vadsø-Kirkenes	38 km	11 min

the electric aircraft to reduce these demands. As new regulations have been adopted for small aircraft design, they could also be adopted for fuel requirements.

6.3.3 Multiple routes per flight

Due to the short distances for the short-grid network, it is usual that the aircraft conduct multiple flights per day. A single flight can include multiple airports where the aircraft only land for a short period to allow new passengers to board before flying to the next airport. It allows the aircraft to be refueled with the necessary fuel for each lap of the flight. Hence, the weight attributed to the fuel loading is less at shorter routes. However, for an electric aircraft, the capacity and weight of the batteries would be dimensioned by the longest flight. They do not possess the same capability of dynamic dimensioning the energy carrier since battery's weight is independent of the state of charge (SOC). This effect would lead to over-dimensioned battery packs on short laps if the route include longer laps.

This consideration is exemplified in Table 3 where the complete route of flight WF970, operating between Kirkenes and Hammerfest, is shown. The distance between Hammerfest and Berlevåg is thrice that of Vadsø-Kirkenes. If the same battery is used for all the distances, it would include thrice the required capacity for the shortest routes. Hence, the battery would be heavier than necessary, reducing the advantage of the electrical aircraft.

An additional concern with the stopovers is the turnaround time. During the turnaround, the aircraft is refueled, which, for a conventional aircraft, is a quick process that only requires refilling the tanks. This process could be a challenge for the electric aircraft due to the slower recharging of the batteries. Charging technology has improved recently, and fast-charging has become standard for electric vehicles. However, it still requires some time to recharge them, and the energy requirements for aviation are more significant than for vehicles. The current stopover time is around 15-20 minutes, and if the electric aircraft is unable to achieve similar results it could lead to delays and less capacity for the routes. A proposed solution is replaceable batteries. The batteries would then be charged at the airport and be available once the aircraft lands. This solution would also solve the above mentioned issue with overdimensioned batteries. However, multiple security factors are involved, and most projects focus on recharging the batteries. The aircraft infrastructure for allowing quick charging also poses a challenge due to the high power requirements for fast-charging [71].

Table 4: Format of collected data

Timestamp	UTC	Callsign	Position	Altitude	Speed	Direction
1651482507	2022-05-02T09:08:27Z	WIF932	”69.676331,18.914303”	1200	107	14

7 Short-haul analysis

An analysis of flights on the short-haul network is performed to find a standard flight profile rooted in actual flight data. These are based on the equations of motion and the data presented in the previous sections. Additionally, this section will present a power distribution of the flights during the different phases of flight as done for a regional aircraft in [47]. However, this thesis will try to generalize the expressions, making them viable for all distances on the short-haul network. It is solved by implementing a time regression based on climb, cruise and descent duration.

7.1 Data collection

The analysis of the short-haul network is performed on the basis of data collected from Flightradar.com. The data were collected in the time period from January to April and resulted in data on 1500 flights. Table 4 shows the format of the collected data.

The quality of the data found at Flightradar varied. Many flights had incomplete datasets where parts of the flight were missing. It was also significant differences in the sampling rate for the data points, especially during takeoff. Low sampling rates during takeoff resulted in low acceleration during takeoff, while the more heavily sampled datasets showed the opposite. A set of requirements were applied to the data. These requirements were meant to ensure that the data were consistent. The requirements are listed below.

- Frequent sampling during takeoff
- Includes takeoff, altitude(0) = 0
- Includes landing, altitude(end) = 0
- Completes route, no diversion
- Primarily constant cruise altitude

An additional requirement of zero initial speed and zero end speed was applied during the initial data collection. It was applied to find the power and energy requirements for taxiing. However, it proved hard to find data satisfying these requirements. An attempt was also made to collect flights from all routes on the short-haul network. Unfortunately, many of the routes had insufficient data and had to be omitted. Figure 6 shows the flight distances of the collected data against

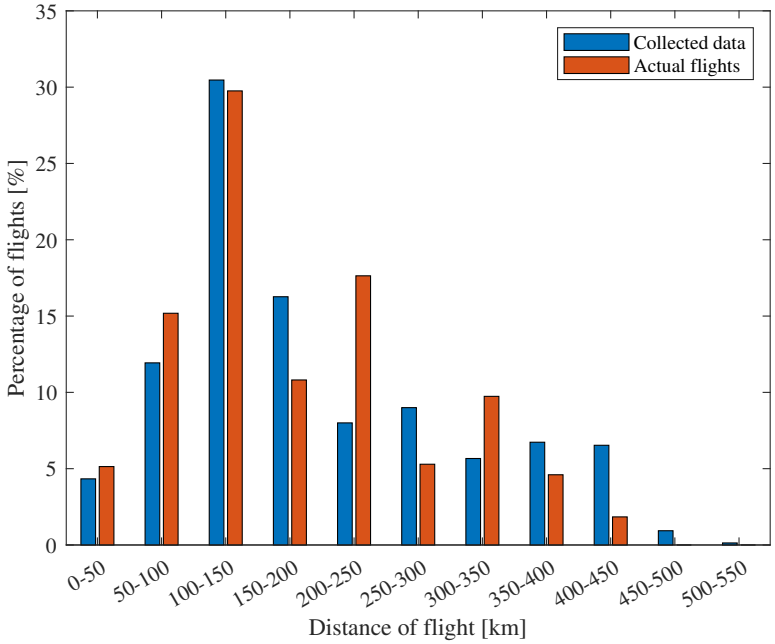

Figure 6: Comparison of flight distance of collected data and data of planned flights on the short-haul network

the actual flights presented in Fig. 4. The collected distribution shows some deviation at the short distances but is more significant as the flight distance exceed 150 km. The largest difference is for the 200-250 km segment, and the longest distances are over-represented in the collected data. It is also noted that the collected data has distances exceeding the longest distance on the short-haul network. These discrepancies occur because some of the collected flights include loiters and detours, resulting in longer travel distances compared to the ideal direct flight between the airports.

Figures 7 and 8 shows an example of the altitude, speed, and power profile for a flight on the short-haul network. It shows a peak in power at takeoff and stabilizes. The power falls as the aircraft reaches the top of climb (TOC) and stabilizes at a lower level. Lastly, the power falls to zero as the aircraft approaches its destination. However, a small spike is observed as the aircraft stabilizes its speed after 2000 seconds before falling to zero as the aircraft lands.

7.2 Flight profile

The flight profile is based on the collected flights. A generalized flight profile is created by using regression analysis on the data points from the flights. Power calculations are also performed on the data by using subsequent data points and using the equations presented in Section 5.

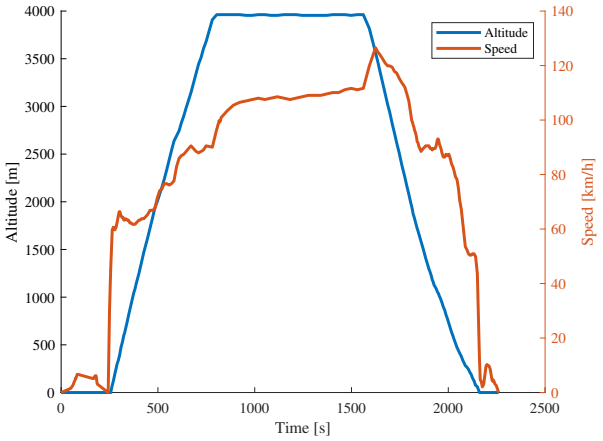

Figure 7: Altitude and speed profile in example flight

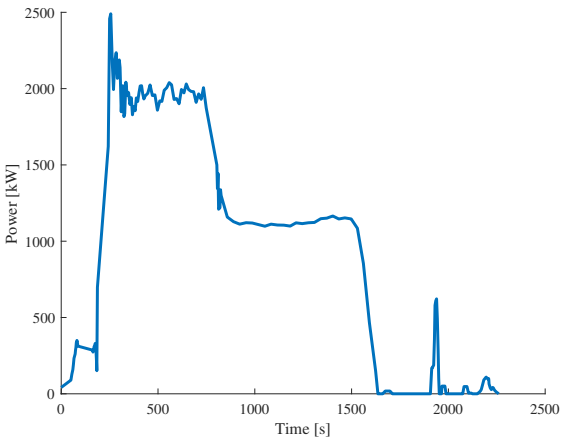

Figure 8: Power profile in example flight

7.2.1 Takeoff

The takeoff data showed huge discrepancies. The tracking of the flights often began at the moment of liftoff, and when starting prior, the sampling frequency was low. Hence, the data collected for the takeoff phase was unreliable and showed a considerable variation in both times spent during takeoff and power consumption. It is natural with some variation, but the takeoff time varied from 1 to 100 seconds, where neither of the extremes is possible. Instead, the time spent during takeoff was estimated by using the shortest airfield as a dimensioning factor. The aircraft needs to handle takeoff on 800-meter runways to enable operation on the short-haul network. An analysis of the takeoff speed of the aircraft showed a takeoff speed of approximately 180 km/h. It was some inconsistencies in the results, but the most reoccurring was between 170 and 190 km/h, which is in accordance with technical data [72]. Equation (26) shows the calculation for the time spent during takeoff where the acceleration is assumed constant, and the acceleration starts from a standstill. An 800-meter airfield and a takeoff speed of 180 km/h give an average takeoff time of 32 seconds.

$$t = \frac{d}{V_{avg}} = \frac{2d}{V_{takeoff}} \tag{26}$$

The power requirements of the takeoff phase are assumed as the maximum power output of the motors. This assumption is discussed in multiple papers assessing the power consumption of an aircraft [47, 73, 74]. It results in 32 seconds of full power for the takeoff phase.

7.2.2 Cruise altitude

The standard march altitude is around 10 km for long-distance, regional flights. The altitudes on the short-haul network are substantially lower but vary by flight

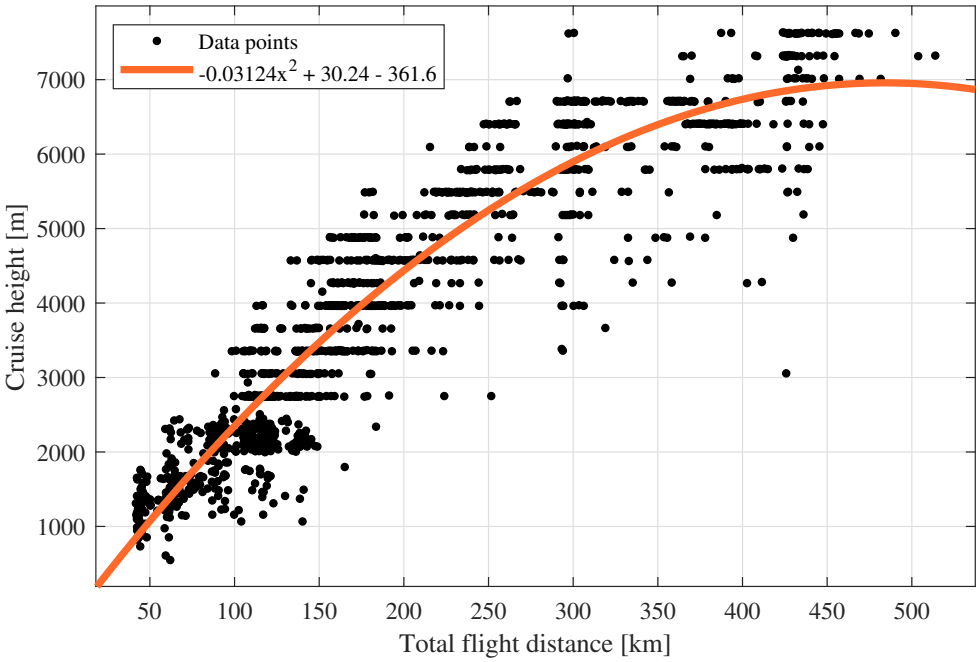

Figure 9: Altitude as a function of flight distance

distance. This variation is shown in Fig. 9 where the cruise altitude is shown against the flight distance. The figure shows multiple standardized levels where multiple aircraft are located at the same altitude. Some outliers are also observed, especially for long flights that operate at a low cruise altitude. This trend is probably a result of long loiters. The loiter extended the flight distance, but the planned trip was substantially lower, which resulted in the low altitude. The relation is almost linear up to around 300 km, where the altitude starts to stabilize. The highest flights are found at around 7600 meters which is the service ceiling of the Dash-8 100 [72]. For aircraft able to operate at a higher ceiling, it could be expected that the cruise altitude would increase further. The expression for the regression line shown in the figure shows the previously mentioned trends, but it is important to observe that it peaks at 475 km. Hence, the expression is invalid for distances exceeding 475 km as the altitude would stabilize, not decrease.

7.2.3 Climb

The climb phase is dependent on the flight altitude. As the altitude increases, so does time spent on climbing. This relation is shown in Fig. 10 where the data points and regression line of the time spent in the climb are shown as a function of the flight distance. The regression line has a negative sign for the squared part of the expression. Hence, it will have a decreasing rise in climb time as the distance increase.

The climb is a power-demanding process. The aircraft both accelerates and climb, using power to counteract gravity. It is observed in Fig. 11 where the peak of the frequency is between 63 and 80% of maximum power.

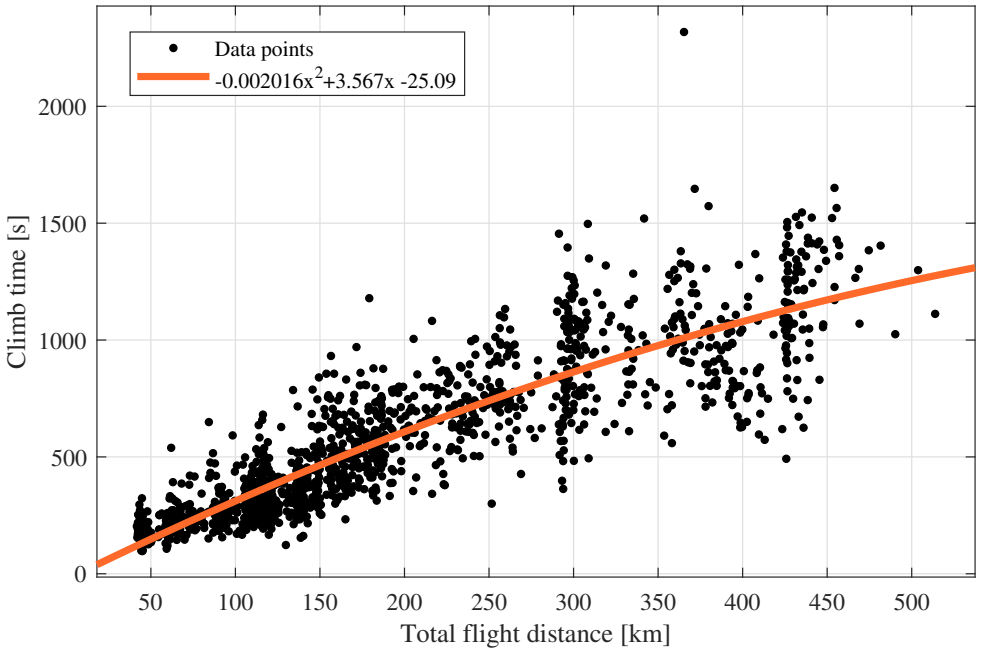

Figure 10: Climb time as a function of flight distance in km

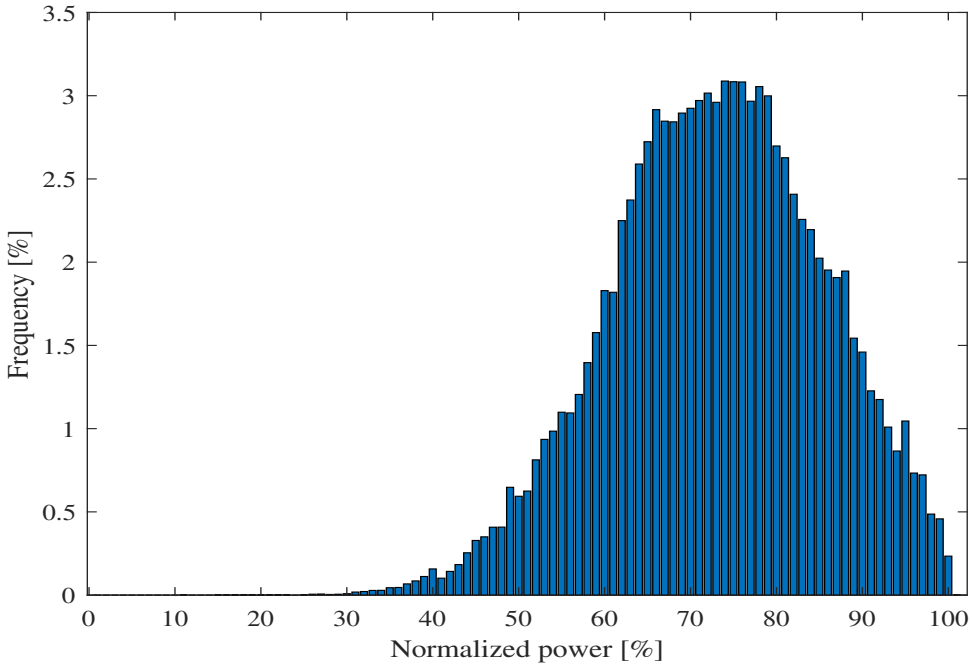

Figure 11: Power distribution during climb

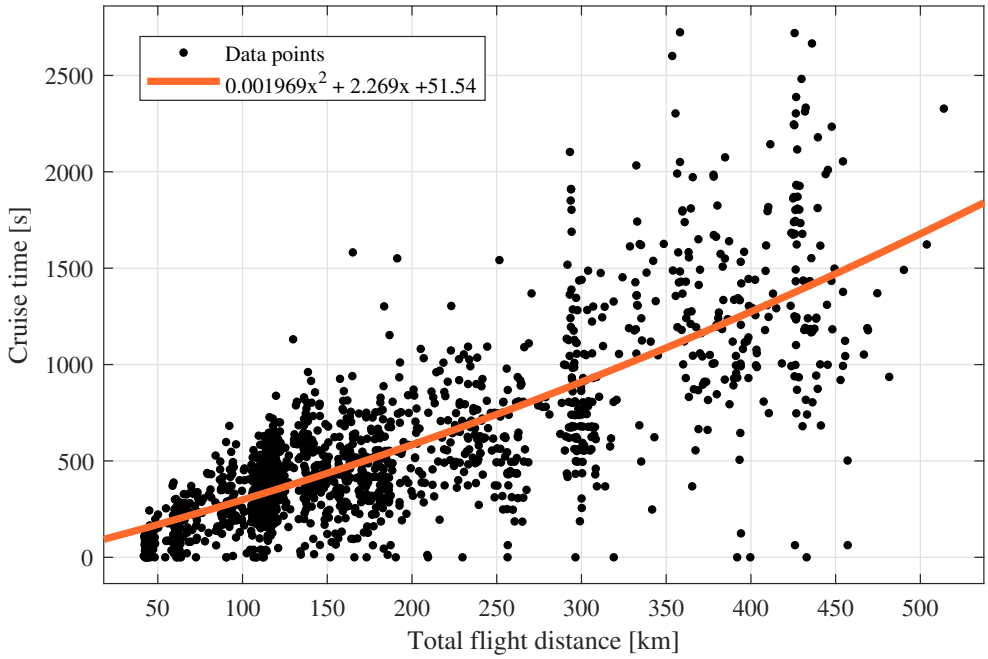

Figure 12: Cruise time as a function of flight distance in km

7.2.4 Cruise

Figure 12 shows the time spent in cruise during flight. This flight phase shows the largest variation, and multiple outliers are observed. The main trend is that the cruise time increase as the distance increase. This trend is following the trends for climb time. As less time is spent climbing to higher altitudes, the time spent on cruising needs to increase.

Multiple data points are at zero cruise time. This phenomenon is common, especially for the shortest distances. It is not uncommon for short flights to only consist of a climb and then descent towards the destination. For the longer flights, this is more unlikely and could result from inaccuracies in the analysis.

The power distribution during the cruise is shown in Fig. 13 where it is shown to be substantially lower than the climb phase. The distribution is normalized around a peak power of 43% of the maximum power.

7.2.5 Descent

The final phase is the descent phase. As shown in Fig. 14 it follows the same trend as the climb. However, the descent time is higher than the climb time. It is due to the aircraft gliding towards the destination at a lower angle than used for the climb. During the climb, the sole goal is to reach cruise speed, while the descent phase can be used to save fuel by optimizing the descent angle. Patròn et al. [75] mentions that the continuous descent approach (CDA) is found to be an optimized method for the descent which results in noise and fuel reduction. It also mentions that this

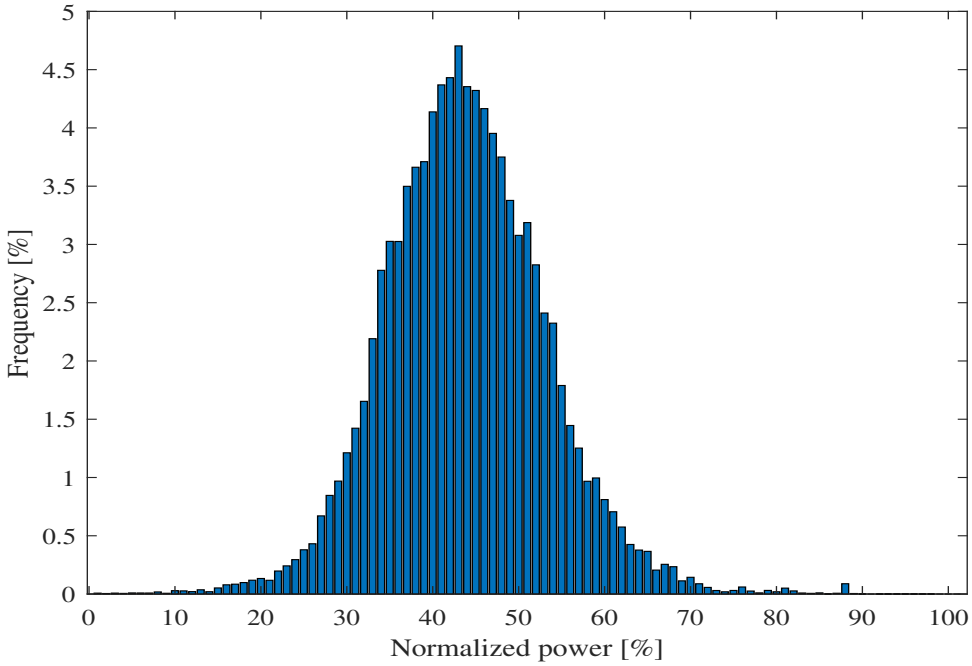

Figure 13: Power distribution during cruise

is only practically available for low-capacity airports due to safety reasons, making it applicable for most airports on the short-haul network.

Since the aircraft can use the potential energy it has built up during the climb in the descent phase, the power consumption can be minimized. Figure 15 shows this, and the highest power frequency is by far the zero power requirement. The aircraft is then gliding through the air, not utilizing the power of the propulsors. These findings could mean that most flights on the short-haul network already utilize CDA.

The prospect of regenerative braking is not included in this thesis, resulting in negative power not contributing to power generation for the aircraft. However, it could be viable for the aircraft's propellers to work in braking mode during the descent phase. They could then recharge the batteries as done in electric vehicles. Unfortunately, this increase the demands of the electric propulsion system and is less efficient than optimizing the descent trajectory [76]. It could, however, be an opportunity for future designs but would be a trade-off with a more complex electric propulsion system [67, 77].

7.2.6 Summary

A generalised power distribution of the flights are shown in Fig. 16. The figure's x-axis is time but is not enumerated due to the varying time of the phases as discussed in the previous sections. The time spent in climb, cruise, and descent is shown in Eq. (27) respectively, where x is the total flight distance in km.

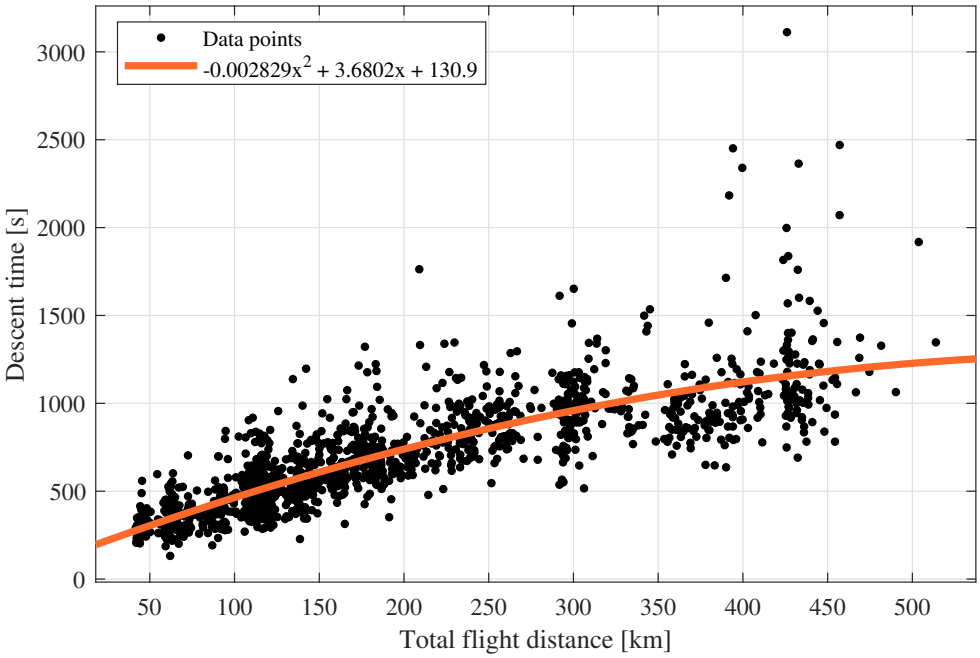

Figure 14: Descent time as a function of flight distance in km

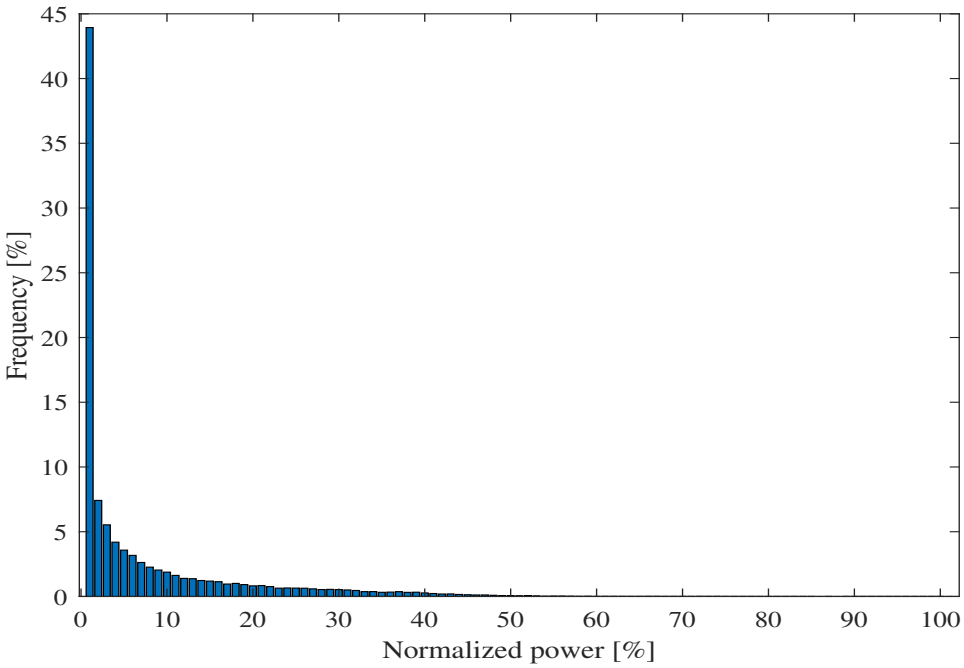

Figure 15: Power distribution during descent

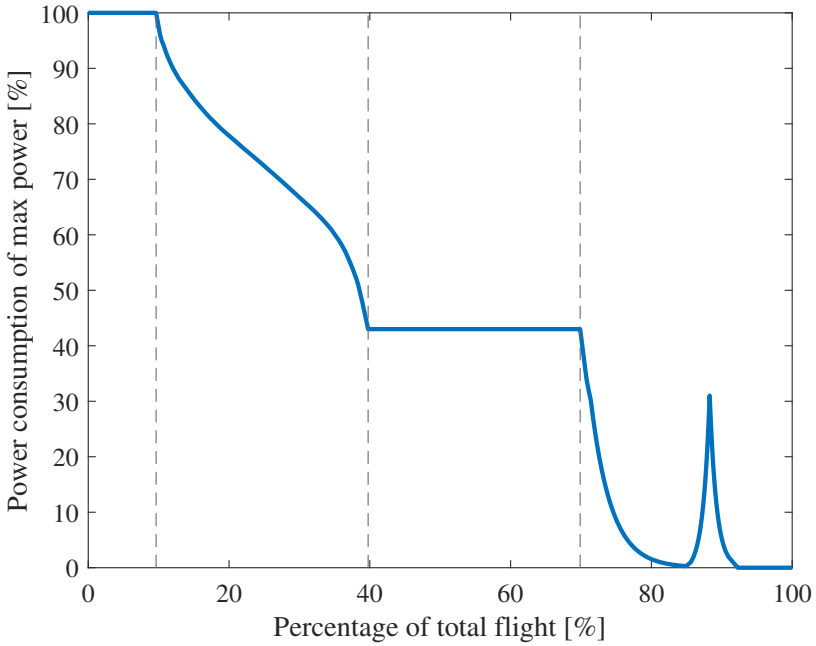

Figure 16: Generalized power profile for the short-haul network

$$-0.002016x^2 + 3.567x - 25.09 \tag{27a}$$
$$0.001969x^2 + 3.369x + 51.54 \tag{27b}$$
$$-0.002829x^2 + 3.6802x + 130.9 \tag{27c}$$

The power consumption during takeoff is modeled as full power for 32 seconds. The moment after takeoff is at maximum power in the climb phase, but it falls gradually until the aircraft stabilizes at cruise altitude. The cruise phase is modeled at a constant power of 43% due to the normalized curve around 43 shown in Fig. 13. The power then falls quickly as the aircraft descends towards the destination. However, a spike is observed towards the end of the descent. This spike occurs due to a stabilizing in altitude or acceleration as the aircraft approaches the destination. The final spike of the descent reaches 30% of maximum power. Comparing the generalized power profile to Fig. 8 shows a similar waveform, but the example profile is more stable during the climb.

8 Design of electric circuit

To operate an all-electric aircraft, the architecture and design of the system is of high importance. This section presents the components required for the powertrain of an aircraft operating on the Norwegian short-haul network. It includes the design and a short description for the operation of the components. A short discussion on current technology and main technological hurdles is also presented. Future

design possibilities and technology projections will be discussed before a finalized design used in the sizing process is presented. Top-level considerations, such as distribution topology, voltage level, and redundancy issues, will also be presented. Multiple sections are heavily influenced by work performed in the project foregoing this thesis in [78].

8.1 Distribution system

The distribution system is the section of the architecture connecting all the main components. This section describes the considerations applied to the system and the choices in topology.

8.1.1 DC vs AC

In recent years the interest in DC distribution has increased substantially. With the use of DC grids in the electrification process for ships, the technology has evolved [44].

An all-electric aircraft have some design freedom compared to conventional aircraft. It can result in the use of multiple propulsors through distributed propulsion. However, the need for a safe and controllable system is of high importance. Due to the high complexity of an AC system, as it requires synchronisation, a DC distribution system is most commonly considered for aviation purposes [42, 79, 43]. By using a DC system the motors are uncoupled and can operate independent of each other. It can result in better dynamic control during transient events as gusts of wind, especially as the electrical motors have quicker response than conventional engines. The need for redundancy will also increase the complexity of the distribution system. It will require multiple interconnected energy storage units and distribution circuits. The increased complexity could require the use of a DC distribution.

Despite, the advantages of simpler control for a DC system, studies as Loder et al. [80], show that a DC distribution leads to lower efficiency in the system. This could lead to higher power levels for components upstream of the distribution grid, causing a weight penalty for the system. However, this is not the findings of the Loder et al. [80]. They instead show that the a DC distribution could result in weight savings (at least with high operating voltage), compared to an AC system. The savings are partly caused by reduced conducting materials in the DC-system [44].

The research mentioned above performed analysis on a hybrid-electric aircraft creating power in generators. The generators produce AC power and it can be the reason for the reduced efficiency in the DC system. However, a battery delivers DC power which would further emphasize the use of DC distribution [41]. The same consideration applies to fuel cells which is considered as energy storage in future designs [81].

Though superconducting AC distribution grids might still be an option [38] it is not considered for this paper due to the necessary technological advances required to

enable superconduction.

The cables used for aircraft are made from aluminum alloy or nickel-plated aluminum and can have a throughput of 228 kW [82]. The area of the conducting material is limited by the current density it can carry, while the isolating material is dependent on the voltage level of the distribution. In Teichel et al. [82] they state a current density for the conducting material of 3.9 A/mm^2. It results in a total weight estimation of 2.7 kg/kW per kilometer of cable when the insulation weight. Jansen et al. [42] choose a value of 170 A/kg/m. This value is between technology readiness level (TRL) 4 and 5 on according to Armstrong et al. [43]. They use 50 A/kg/m for TRL 5-6 and 250 A/kg/m for TRL 3-4. Generally, the efficiency of the distribution system is considered high, showing a performance at 99.6% [42].

8.1.2 Voltage level

Another important factor is the voltage level of the circuit. In general, higher voltages tend to lead to more compact electrical devices, and weight reductions [27]. It also reduces the size of the copper in the wires due to lower currents. These reductions are advantageous as they reduce the weight of the components. However, as the voltage increases so does the risk of discharges. A discharge occurs when a dielectric material breaks down and can cause damage to the components and create short-circuits. In short circuit events, large currents are generated. These currents cause heat generation and can lead to breakdown of the electrical components. In worst-case scenarios, it can shut down the electrical power system.

The danger of discharges means that the requirements for the cable insulation is vital. The power electronic converters and the electric motors also need to handle the high voltages. It could lead to an increased need for physical separation of different parts and components, which could result bulkier components.

An additional issue for operation requirements for an electric aircraft is the pressure drop due to the altitudes of flight. Figure 17 shows that the breakdown voltage is dependent on the separation distance between the materials and the air pressure. As the pressure decreases, the breakdown voltage also decreases, increasing the probability of a partial discharge. It means that the requirements for physical separation and insulation increase with decreasing pressure. Paschen's law also shows that a minimum breakdown voltage is required independent of the pressure and separation. This level is 327 V [76] and breakdown voltage will not occur for voltages below this threshold. It is an unrealistically low value when considering the aircraft's power ratings, which will be in the MW figures. The need for large currents would cause heating and would not allow for the compact and efficient systems needed.

The voltage level of electric aircraft has been kept at a standardized level of $\pm$135 V to ensure safe operation within the threshold mentioned above. However, with the implementation of the more-electric aircraft seen in the Boeing-787, a higher level was where a higher voltage level of $\pm$270 V was chosen [83, 73].

High voltage levels will reduce the cabling weight but increase the need for reliable insulation. For converters and electrical motors, it could allow for a more compact

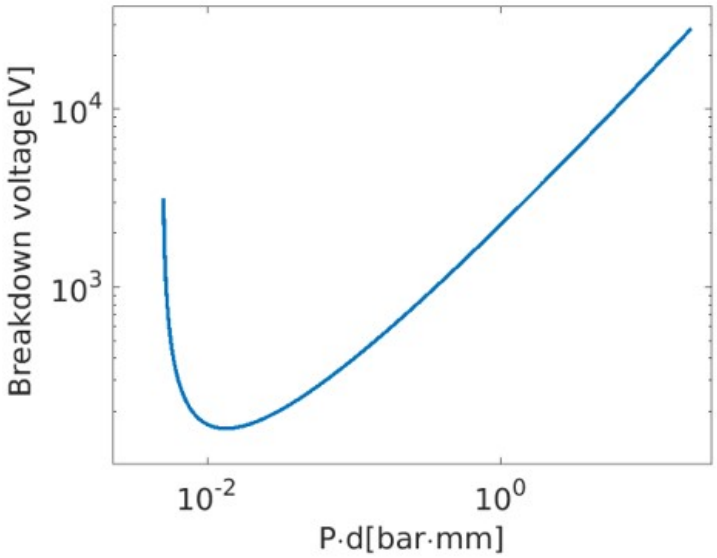

Figure 17: Paschen's law shows the relation between air pressure, separation distance and breakdown voltage [2]

design, especially since the current density of the field windings of the electrical machine could be reduced. However, it could lead to more extensive separation needs for the components and could increase the wear of the components. The voltage level is thus a trade-off between compact design, safety, and technology readiness.

For the NASA N3-X, a cryogenic cooled DC distribution with a voltage rating of 3000 V is chosen [43]. However, it is a large aircraft, and lower voltage levels are expected for smaller aircraft. A pragmatic voltage level in the area of 1000 V can be sufficient for the short-distance flights considered for this thesis [83, 38, 84]. A power level of 1000 V is, for example, chosen for the STARC-ABL project conducted by NASA [85]. However, the NASA Maxwell project, which is expected to have its maiden flight in 2022, uses a more modest distribution voltage between 400 and 525 V [86], which puts it in the area of the voltage level of the Boeing-787.

8.1.3 Safety/Redundancy/Reliability

There is a need for redundancy of the electrical power system on the aircraft. Safety is of the utmost importance since the consequences of faults can be catastrophic. As the wear of the components increases throughout their lifetime, the electrical grid is likely to experience faults. Cano et al. [44] includes a description of the failure rates of the components of the electrical propulsion system and shows the allowable failure rates for different design assurance levels (DAL). For catastrophic failures, failures that will cause a crash and death denoted level A in the DAL, the probability of failure needs to be less than 10^{-9} per flight hour. Faults reducing the operativeness of the aircraft also have stringent demands attached. For B and C level faults the possibility needs to be kept below 10^{-7} and 10^{-5} per flight hour respectively. As faults in the electrical system is expected, these faults needs to be

handled and cannot result in failures on the top three DALs.

It shows that the reliability of the components is essential. However, it also shows the need for redundancy for the electrical propulsion system. Even at crucial components, a single failure cannot lead to a shutdown of the electrical system. The design implication is a need for backup solutions for most components.

The most detailed redundancy designs found in the literature are for the N3-X system. It is a superconducting system operating at a very high voltage. Hence it would experience large currents if a fault occurred. In Jones et al. [87] they compare different distribution topologies to investigate the redundancy issue. An H-bridge connection is chosen for the architecture, where each power source is connected to multiple distribution grids. Each motor is further connected to two grids ensuring operation with total power loss. This configuration is more thoroughly described in [80].

Hence, the battery pack needs to be divided into at least two separate modules as short-circuiting a single battery pack leaves the aircraft without power. Additionally, it shows the need for a secondary distribution system. This system will cause additional weight on the system but will make it more reliable and ensure that failures do not leave the aircraft without the power necessary to finish the flight or make a controlled emergency landing.

The redundancy requirements for the motors depend on the number of propulsors. Single-engine operation is required in a conventional aircraft consisting of two turbines or propellers. If a motor loses power, the remaining engine needs to handle the power requirement of the aircraft. However, if the aircraft operates multiple motors, the loss of a single motor is not as detrimental. This effect could encourage distributed propulsion system, as the requirements for each motor would decrease.

8.1.4 Subsystems

Aircraft are currently trending towards more use of electrical power with the focus on More Electrical Aircraft (MEA). In this trend, subsystems previously using pneumatic, hydraulic, or mechanical energy are transferred to using electrical power [73]. These subsystems can include taxiing, avionics systems, pumps, actuation systems, environmental control systems, and wing ice protection systems.

Boeing-787 introduced a no-bleed air system. Usually, the air is tapped from the engines leading to decreased efficiency of the engines. By using a no-bleed system, the Boeing-787 used electrical power instead of compressors for the process [67]. Electrifying the onboard systems could yield substantial weight and energy savings compared to conventional aircraft, and in Yildiz [88] he quotes NASAs predictions of 9% fuel reduction and 10% less empty weight with MEA. It is also expected that the system would be more reliable as mechanical interconnections are removed.

The power requirements of these subsystems contribute to the total power consumption of the aircraft, and for an all-electric aircraft, it increases the energy requirements of the battery. In total, the subsystem requires around 10% of the total power

consumption of the aircraft according to Zhang et al. [89].

8.2 Energy storage

Energy storage is one of the most limiting factors when converting from conventional to electric aviation. Aviation needs large amounts of energy stored due to high continuous power output. It also needs to deliver large amounts of power, especially during takeoff and climb. Hence, the most important factors for energy storage are the specific energy and the specific power. Efficiency is also of high importance, and of course, safety issues must be addressed.

Conventional turboprop aircraft utilize the high specific energy of jet fuel for energy storage. Jet-A, the most common jet fuel, has a specific energy of 11.900 kWh/kg [24]. Despite the high specific energy, fuel is still a substantial part of the aircraft weight, with fuel weight fractions ranging from 40% of TTOW for large, long-range aircraft, to around 20% for smaller regional aircraft [90, 91, 92, 93, 94, 95]. Batteries and other renewable energy storage cannot compete with jet fuel's specific power. Hence, the need for new energy storage technologies with the high power density and high energy density is important.

This thesis will only focus on three different battery compositions. However, multiple other compositions and technologies are considered for energy storage and could be of interest for future projects. These include different metal-air batteries as zinc-air, aluminum-air, Solid-state batteries with lithium anode, hydrogen fuel cells, flywheels and supercapacitors [81, 96, 37, 97, 98].

A battery's main components are an anode and a cathode separated by an electrolyte as depicted in Fig. 18. The battery utilizes the electrochemical potential difference between the anode and cathode to generate power [99]. The cathode is the battery's positive pole, and during discharge, it takes up ions which are electrically loaded atoms. Electrons are forced through an electrical connection between the anode and cathode, creating the current utilized by electrical applications. The separator separates the anode and the cathode and is a non-conducting material that enables ions to pass through but forces the electrons through the electrical load [100]. This process is reversed when recharging the battery. The material choices for the different components decide the specifications of the battery cell.

A battery consists of multiple connected battery cells. Series connections of the batteries increase the output voltage, while parallel connections increase the capacity [101]. The cells are usually arranged in a casing that controls the battery cells' moisture, temperature, and other conditions. The battery management system (BMS) is also responsible for the security measures for the batteries [76]. The casing contributes to the total weight of the battery pack and accounts for 20-30% of the total weight of modern batteries [37, 19].

Two important parameters for batteries are the state of charge (SOC) and the depth of discharge (DOD). The first describes the battery's immediate charge to the maximum charge. It is of importance due to the dynamic behavior of batteries.

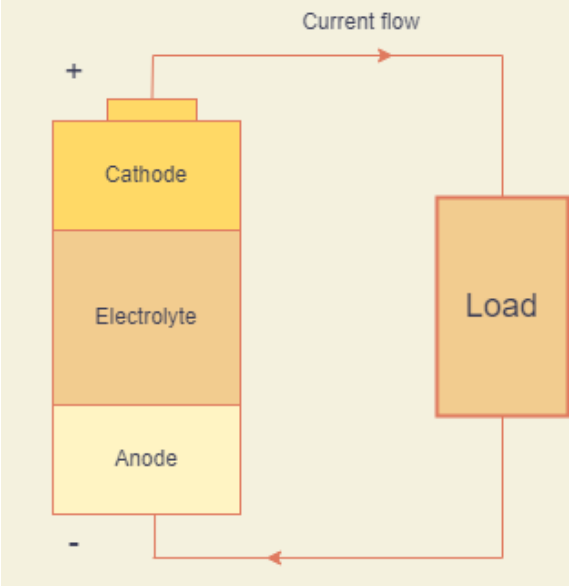

Figure 18: Simple diagram of a battery during discharge.

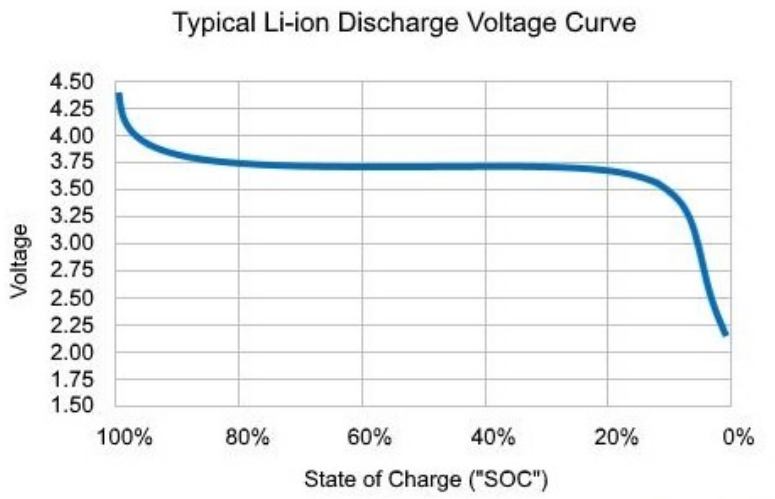

Figure 19: Typical Li-ion Discharge Voltage Curve [3].

Though often assumed constant, the voltage output during discharge of the battery will depend on the SOC [99]. Figure 19 shows a typical Li-ion discharge voltage curve, and it is observed that the voltage at the terminals of the battery reduces during discharge.

Depth of discharge (DOD) is the amount of battery discharge where 100% describes a fully discharged battery, while fully charged batteries have a DOD of 0%. Deep discharges occur if the DOD is too high. The threshold for deep discharge is different for different battery compositions, but occurs at around 80% DOD for Li-ion batteries [76]. Deep discharges can severely reduce the life cycle of batteries. It means that 1/5th of the Li-ion battery's energy storage is unavailable if the life cycle is to be preserved.

Another important factor for batteries is the operating temperature. As batteries

operate outside their optimal temperature, the efficiency reduces. Jafari et al. [102] shows the assumed discharge capacity for a Li-ion battery at different temperature ranges. The capacity decreases by 5% as the temperature diverges from the optimal temperature of 25°C to 60°C. In addition to inefficiencies when operated outside of optimal conditions, safety issues need to be handled. Batteries can experience thermal runways if operated outside of safety boundaries. A thermal runaway occurs when a fault in one battery cell cascades to the rest of the battery pack and can cause heating and fires [103].

The heat production of the battery will increase with aging. As the battery ages, the internal resistance increase creating more heat [102]. It will also decrease the battery's output power as more power is lost to the resistance. In addition, as the battery life is extended, the total power capability of the battery decrease [45]. The battery cannot hold the same charge as when it was installed. This effect results in further reductions in the battery's capacity unless they are changed rapidly, which would increase the cost attributed to the battery extensively. The battery's life cycle endurance depends highly on the use, with both maximum state of charge, depth of discharge, and the power during operation affecting the result. A reduction of 25% over a year of operation can be expected [104]. As the power of the battery increase, the probability of thermal runway also increase [105], and with the high power demands for aviation, this is a concern.

8.2.1 Lithium-ion

Today's most used and mature battery technology is the Lithium-ion (Li-ion) battery. It is used in many applications due to the high energy and power density and the long life cycle when compared to other mature battery technologies [106]. Li-ion batteries do not describe a specific material composition but are a general term for batteries using lithium ions traveling between anode and cathode. The most common composition consists of a graphite anode, a lithium cathode, and liquid organic carbonate electrolytes [107].

Though Li-ion cells have high specific power and energy, it does not meet the requirements of the aviation industry. Different sources estimate different specific energies, but they are within a interval between 200-265 Wh/kg [24, 41, 108, 109]. A white paper by the US Department of Energy states that battery technology needs to reach levels around 500 Wh/kg before single-aisle flights are possible, which would demand a doubling of the specific energy compared to current levels. For larger aircraft, this is increased to surpass 1000 Wh/kg [110]. These levels are unlikely for Li-ion batteries due to the theoretical maximum level of current Li-ion compositions of 396-607 Wh/kg on cell level [41]. Even if the theoretical values can be reached on a battery level, the weight addition of casings would place the batteries below the threshold value. In NASA projections towards 2045, growth in the specific power of Li-ion batteries to around 390 Wh/kg is expected. It includes the casing of the battery [37]. By 2030 they predict slightly lower values with around 320-333 Wh/kg.

The specific power of modern Li-ion batteries is approximately 1200 W/kg and is not deemed the limiting factor compared to the specific power [41]. However, as

technology improves Gnadt et al. [41] assumes that specific energy will increase at a higher pace than the specific power. It is due to the specific energy increasing with volume, while specific power increases with the surface area of the battery.

Since the probability of Li-ion batteries fulfilling the specific energy requirements of electrical aviation is low, research focuses on new battery compositions. Two interesting battery compositions are Lithium-Sulfur and Lithium-Air due to their high specific energy potential.

8.2.2 Lithium-Sulfur

While Li-ion batteries use lithium as the cathode material, using Lithium-metal as the anode material could be more advantageous [111]. One of the most intriguing technologies is a Lithium anode combined with a Sulfur cathode. It has a high theoretical specific energy of around 2500 Wh/kg and shows great capacity [112]. Sulfur is also non-toxic, abundant, and thus a cheaper and more available material compared to, for example, cobalt currently used in Li-ion batteries [112, 113].

However, multiple hindrances have made the industrialization of Li-S batteries slower than many expected. Nevertheless, the technology is in development and is approaching the market [112]. One of the main issues has been cyclic stability. Recharging the batteries has been deemed hard due to material issues, and in Ueno [114] they show a power retention rate for a Li-S battery of 60% after 600 cycles. Hence, the battery discharged 60% of its capacity during no-load operation after being recharged 600 times. Another issue is the safety of the batteries. Dendrite formations occurring in Lithium-metal can lead to short-circuiting of the battery, which again can cause thermal runaway [115]. However, this is present in all forms of Lithium batteries and is also one of the main risks in commercialized Li-ion batteries.

Additional concerns are volume fluctuations occurring during a discharge [113] which will be an issue for packaging but could also separate conducting parts leaving the battery unusable. The batteries are currently experiencing low electrical conductivity due to the formation of partial sulfur intermediates [113, 116]

Despite the difficulties with the implementation, it is still viewed as the next generation of Li-batteries. In Dever et al. [37] it is projected that there will be available Li-S batteries at around 350 Wh/kg by 2030 and that it can increase to as much as 640 Wh/kg by 2045. Schefer et al. [27] on the other hand, estimates Li-S batteries with 500 Wh/kg by 2030. Companies further substantiate this as Oxis Energy and Lyten, which are start-up companies trying to commercialize Li-S batteries. Oxis stated in early 2021 that they were able to produce Li-S batteries with a specific power of 450 Wh/kg and a cycle life of at least 250 [117]. They were also stating rapid improvements in performance with the potential 550 Wh/kg by 2023 and 600 Wh/kg by 2026 [118]. However, an ominous sign for the company was a struggle with funding, and in 2021 it was placed under administration. Lyten, on the other hand, claims a specific energy of 900 Wh/kg ready for production in 2025/2026 with a cycle life of over 1000 charges [119, 120].

8.2.3 Lithium-Air

Lithium-Air batteries use oxygen as cathode and lithium-metal as the anode and are usually referred to as Li-O_2 batteries. There are two main categories, depending on the choice of electrolyte. The electrolyte is either aqueous or non-aqueous. They both have high theoretical specific energies with 3505 Wh/kg and 3582 kW/kg, respectively [41]. The non-aqueous solution has an advantage when it comes to volumetric density [111]. However, these levels are unrealistic due to the lightweight of lithium, which makes any additional components, such as electrolytes and battery structure, severely increase the weight [121]. However, to exceed the expected values of Li-ion batteries, only 15% of the theoretical value needs to be achieved.

There are challenges regarding both types of Li-O_2 batteries. The Lithium-metal anode is present in both types, and the issues are similar to those for the Li-S batteries. In the same manner, as the Li-S batteries, the Li-O_2 batteries also suffer from limited cell life due to decomposition of the electrodes and electrolyte [122]. Hizarci et al. [116] also show a capacity loss of 25% after only 50 discharge cycles.

Li-O_2 batteries will require large amounts of air or oxygen intake. This air can be collected from the ambient, but since moisture and dirt would be damaging to the battery, filters controlling the airflow are required [121]. It would also require fans and other components that would add to the weight of the battery management system. This issue can be circumvented by carrying the oxygen on board and supplying it directly to the battery. However, this would still increase the weight of the system due to the weight of oxygen storage units and the distribution system for the oxygen [37]. Hence, a comparison of the two concerns is required to find the most lightweight solution. Gallagher et al. [123] estimates that with the subsystems needed for reliable operation, only 384 Wh/kg is achievable.

Another issue is that Li-O_2 has low specific power [121]. Hence, it would struggle with providing enough power during peak power operation. Girishkumar et al. [121] proposes that the problem can be solved by using Li-ion batteries for the supply of power during these periods.

A concern when regarding aviation is that during flight, a Li-O_2 battery would increase in weight [37]. It would be lightest during takeoff, which is an advantage, but during the reduction of oxygen, the weight would increase, making the aircraft heaviest during landing. That would increase the strain on the landing gear and possibly increase the weight of the equipment. A dynamic weight model for the battery weight is needed to account for this effect. However, it needs to be stated that an increase in weight is more optimal than the decrease experienced with conventional fuel. The most power-consuming phase is at the beginning of the flight, and minimizing the weight during this phase is advantageous. The power consumption is a lot lower in later stages of flight and would not be a severe cause of concern. However, it could affect aborted landing processes.

Despite the concerns mentioned, it is still optimistic views on developing high specific energy Li-O_2 batteries for aviation. Both Dever et al. [37] and Schefer et al. [27] expect viable batteries by 2030 with specific energy of 360-500 Wh/kg. It might be

Table 5: Specific energy for state of the art batteries and projections towards 2045

Battery composition	2020	2030	2045	Theoretical maximum
Li-ion	200-265	320-333	390	607
Li-S	-	350-500	640	2500
Li-O_2	-	360-500	900	3582

as high as 900 Wh/kg by 2045 [37].

8.2.4 Summary

Li-ion batteries dominate modern battery technology. They have high specific energy and power compared to other mature battery technologies, but their use in aviation is limited due to the high energy consumption. It is expected that there will be improvements in Li-ion batteries in the following years, but it is not predicted to meet the requirements of the aviation industry. Therefore, new battery compositions are needed, and two proposed compositions are the Li-S and Li-O_2. Both show higher specific energy potentials than Li-ion, though there are technological obstacles to overcome before they are ready for market. Table 5 summarizes data for the different battery types and shows predictions for 2045.

Safety and reliable operation are central to the implementation of the batteries. Each battery will have battery management systems to handle this. It will increase the weight of the batteries, making them unable to reach the theoretical maximum values for specific power and specific energy.

8.3 Electric motors

The electric motor has seen a growing interest and has become dominant within the automotive sector in Norway [124]. Due to this increase, it has seen considerable improvements in power density and specific power and is now approaching a level where it is feasible for aviation.

Compared to conventional internal combustion engines, there are numerous improvements with the electric motor. ICEs use thermal combustion to create the propulsion force. The engine's thermodynamic efficiency is lower than that of an electric motor. In Strathoff et al. [23], it is stated that generic piston engines have a peak efficiency of around 35%, while Lin et al. [125] uses an efficiency of 40%. On the other hand, the electric motor is assumed to have an efficiency of more than 95%. Some sources state efficiencies in as high as 99.5% [41, 24]. For a vehicle carrying the energy storage on-boards, the increase in efficiency means that less energy needs to be stored on the vehicle, reducing the weight.

The electric motor has fewer moving parts compared to conventional motors. It also has fewer parts in contact since the electromagnetic force works across airgaps. These factors reduce the mechanical stress and increase the reliability of the motor.

It can reduce the need for maintenance, hence increasing the operational time of the aircraft. The increased operational time will allow for more flights and will benefit the airlines economically [109, 126]. The reduction in moving parts could also reduce the noise produced by the aircraft.

The efficiency of the combustion engines is highly dependent on the size of the engines and the rotational speed. The efficiency reduces with smaller sizes, which is why two large ICE are being used almost regardless of the size of the aircraft. In [41] it is stated that small aircraft using combustion engines will have a thermal efficiency as low as 25% while the electric motor would be unaffected by the size decrease.

The efficiency of a conventional engine also reduces when the rotational speed diverts from the optimal. This effect means that the operational range of the propellers is small for conventional aircraft [23]. They are usually fixed in speed, and any change in torque is done by adjusting the angle of the propeller blades. These effects are not as apparent for an electric motor, which could enable variable speed propellers. There are some efficiency losses by increasing the RPM of the motor, and the efficiency is usually higher for large motors than for smaller ones. However, these effects are minor compared to ICE's and thus give more flexibility to an electric aircraft than a conventional aircraft. In addition, due to the dependence on oxygen for the combustion process, the efficiency of combustion engines is negatively impacted by altitude [76]. This effect is not present in the electric motor.

8.3.1 Motor Topology

There are several different arrangements for electric motors used for different purposes. However, they all convert electrical power to mechanical power using electromagnetic forces. The primary separation is between DC and AC motors, but there are numerous subcategories under each of these. Sirimanna et al. [127] and Anderson et al. [128] examine relevant motor topologies for aviation. They conclude that the most viable motor topology is the permanent magnet synchronous motor (PMSM) due to its high power density and efficiency, critical for the electric motor. The authors also state that the brushless DC motor (BLDC) show similar performance and could be more efficient at higher specific power. Despite other research articles pointing towards axial flux permanent motor (AFPM) [129] showing the highest specific power, the PMSM is the most frequent motor choice in the literature [37, 125, 67, 130].

In Dever et al. [37] considerations for future improvements for specific power is discussed. It points to more high-conducting conductors utilizing carbon nanotube conductors (CND), leading to an 84% decrease in weight compared to copper. Other possible advancements are material improvements for magnets, insulation materials, and magnetized bearings [37]. Another possibility is to reduce the use of iron. The use of air gap windings would remove the teeth of the stator since the need for slots is removed. A Halbach array is also considered weight saving as the iron yoke of the rotor can be removed [131].

A significant limitation of the electric motor is the thermal limitations. The high power requirements and low weight make heating a cause of concern. In Sirimanna et al. [127] all designs were limited by their thermal conduction. The main area of concern is the heating of the field windings. Especially the end-windings. In addition to experiencing high heat generation in this area, the wires increased temperature increases the resistivity of the windings, further increasing the losses and heat generation [37]. Higher temperature also affects the magnets making them less efficient [132]. The need for efficient cooling is therefore of great importance. The heating concerns mainly occur in the high-power phases of flights. The most critical point of operation is during take-off and climb; less cooling capacity is needed during cruise and descent. Hence, it is attractive with a motor that can be temporally overloaded. It would mean that the motor size could be reduced as heating would be of less concern during the initial phases. In Yi and Haran [133] they experiment with the use of phase-shift materials. It is a material that can work as a thermal capacitor and store or absorb large amounts of heat. They find that for a 20 minutes take-off with approximately double the power of a cruise, a weight reduction of 44% could be achieved by phase-shift materials.

8.3.2 Direct drive vs gearing

Equation (28) shows the relation between power, torque, and speed of the PMSM. It shows that by either increasing the torque or the rotational speed of the motor, the power can be increased. The torque, however, is dependent on the motor size and is proportional to the volume of the motor [89]. Since increasing the torque yields a larger motor with increased weight, it is not viable to increase the specific power. However, increasing the speed can be done without alterations to the size [127]. It is mainly dependent on the frequency of the applied current to the stator windings. It can, in theory, increase the specific power of the motor proportionally to the speed increase. Therefore, high power density motors tend to operate at high rotational velocity [21].

$$P_{motor} = T_{motor} \cdot \omega_{motor} \tag{28}$$

It would be advantageous for the motor to operate at high speed. Unfortunately, the aircraft's propellers have speed limitations, which in direct drive operations also limit the speed of the motor. The tip speed of the propeller can be calculated as shown in Eq. (29). In Anderson et al. [128] it is stated that new research limits the tip speed of propellers to 0.8 Mach which is around 280 m/s. The limitation occurs due to the high speeds of the air flowing through the propeller. When the speed of the airflow reaches and exceeds 1 Mach, it creates shock waves behind the propeller, which significantly reduces the efficiency of the propeller [134]. However, the equation shows that the speed can be upheld if the radius of the propeller is reduced. That can be achieved by increasing the number of motors. However, propellers tend to operate between 800 and 1500 rpm, and they become more efficient as they become larger and more slow-moving [135].

$$V_{ts} = \omega_{motor} \cdot r \tag{29}$$

A solution is to attach a gear between the motor and propeller. It would decouple the speed of the propeller from the speed of the electrical motor. The speed of the motor is thereby not directly affected by the maximum tip speed. However, adding a gear also brings negative attributes. It reduces the efficiency of the transmission system and increases the weight. Mechanical gears also experience mechanical stress, which leads to more maintenance and increases operational cost [21]. It, for example, needs a lubrication system due to the high-speed and high-pressure operation [136]. These additions will further add to the weight of the gearbox. The gearbox weight can be estimated as shown in Eq. (30) based on historical data from [51]. The constant K_g is set to 32.65 per future prognosis from the article.

$$W_{gearbox} = K_g \frac{hp_{motor}^{0.76} \cdot rpm_{motor}^{0.13}}{rpm_{prop}^{0.89}} \tag{30}$$

An alternative is magnetic gearing, as discussed in Scheidler et al. [136]. A magnetic gear does not have mechanical components changing the rotational speed but instead uses magnets for the gearing. The contact points in mechanical gears are thus removed, and it secures more reliability, is quieter, and does not require the same level of maintenance. In [137] they successfully test a magnetic gear in an Audi A8 Quattro, and magnetic gears have also been tested for wind power and marine technologies [138]. Despite a successful demonstration of a magnetic gear for aviation in Wong et al. [139] the technology is still at a low TRL level, especially for high-power and high-torque operation. For that reason, only mechanical gearing is considered in this thesis.

An additional consideration when choosing an operational speed for the motor is the mechanical stress on the rotor. It will depend on whether the motor has an inner or outer stator. However, speeds over 10 000 rpm are viable for electric motors and should not be a limiting factor [128, 132].

Due to the high weight of the energy storage for electric aviation, the efficiency of each component is an important metric. For the electric motor, the efficiency is usually a trade-off with the power density [140]. As the speed increases, frequency-dependent losses increase, and these produce heat, which leads to lower efficiency [89].

Hence, when deciding between direct and indirect drive it is necessary to perform a cost analysis between the savings in the motor weight and the weight additions of a gearbox. The addition of the gear will can also lead to increased losses in the circuit which must be accounted for. An additional consideration is the operational costs attributed with the mechanical strain on the gearbox and the weight caused by the lubrication system. Anyhow, most of the current research emphasizes leaving out the gearbox and using a direct drive.

8.3.3 Electric motor performance

The technology development within electric motors for aviation is high, and new concepts are presented regularly. Multiple established companies are working on developing more power-dense and more efficient motors. In addition, the landscape of start-ups trying to beat them to it is wide. Some of the currently available motors and some promising developments will be presented in this section.

EMRAX, a Slovenian-based company, offers motors in the range of 52-348 kW motors with a dry power of around 5 kW/kg at nominal power and a peak specific power of around 10 kW/kg. The efficiency is 92-98% and is used in electric gliders, and trainers [141]. In 2015 Siemens presented a motor with a rating of 260 kW at a specific weight of 5.2 kW/kg, which at the moment was the highest specific power available [142]. Newer announcements claim a specific power of 5.9 kW/kg at an even lower operating speed for the SP200D. They have also announced the SP2000 with a specific power of 10 kW/kg and produce 2000 kW of propulsion force. Wright Electric has also announced the testing of a 2 MW motor with the same specifications for power density [31]. These specifications can be backed up by research articles predicting potential motor designs in the range of around 10 kW/kg [143, 89].

A concoction of electric motors is presented in Table 6, where many still are in the design process and verified data is unavailable. It is also important to mention that most of these motors are specified with dry weight. It means that cooling liquid is exempted and would increase the weight if included [140]. It can also be noted that the only motors with a power output in the range needed for larger aircraft are the Wright Electric motor and Siemens' SP2000, which claim an output power nearly tenfold that of their competitors. The speed range of the motors is also of interest as most of them operate at relatively low speed. It suggests that they are designed for direct drive. The only exemption is the H3X motor, but they also present a planetary gearbox with a 1:4 ratio weighing 3 kg having an efficiency of 99%. It place them in the same range as the rest of the motors [144]. That is a substantial improvement compared to the analytical expression Eq. (30) which results a gearbox weighing 4.2 kg. However, it is in the same weight range. The speed of the motors may still be too high to operate the propeller directly, and might need to be around the speed of the Siemens SP200D. That would either reduce the specific power substantially or include the addition of a gear. However, as smaller propellers allow for high rotational speed, the use of distributed propulsion could allow the motors to operate at the rated speed.

Despite the improvements in the electric motor, the Department of Energy in the US has estimated that an electric aircraft motor needs to have a power density of 20 kW/kg in order to be competitive with the conventional aircraft [21]. Neither of the ones presented in Table 6 meets this requirement. NASA instead considers a 13 kW/kg motor with an efficiency above 96 percent as sufficient and is currently conducting several research programs focusing on it as presented in Jansen et al. [152]. Two parallel programs are conducted to create a motor with the intended power density. In collaboration with the University of Illinois, they are creating a 1 MW motor PMSM with >96% efficiency, and a 2.7 MW induction motor (IM) with

Table 6: State of the art electric motors for the aviation industry

Company	Model	Nominal power	Specific power	Efficiency	Nominal speed
EMRAX	348	210 kW	5.1 kW/kg	92-98%	3600-4500 rpm [141]
Magnix	Magni5	265 kW	5.2 kW/kg	95%	1200-2300 rpm [145, 146]
Siemens	SP200D	204 kW	5.9 kW/kg	95%	1300 rpm [142]
Siemens	SP2000D	2000 kW	7.6 kW/kg	-	6500 rpm [142]
MGM COMPRO	REB30	25-30 kW	4.9 kW/kg	-	4000 rpm [147]
YASA	P400R	160 kW	5.67 kW/kg	-	4000 rpm [148]
Magnax	AXF250-X	130-140 kW	4.2 kW/kg	-	- [149, 150]
H3X	HPDM-250	200 kW	13.33 kW/kg	94.5-95.7%	20 000 rpm [144]
Wright Electric	-	2000 kW	10 kW/kg	-	- [31]
Safran Group	ENGINeUS	500 kW	-	94%	4500 rpm [151]

the same power density and efficiency is in development at the University of Ohio [152].

8.4 Converters

The aircraft's onboard electrical system consists of multiple voltage levels and includes DC and AC operations. To enable the operation of the electrical system, highly reliable, efficient, and high-power converters are needed. For the electric propulsion design in this paper, the most crucial converters are the DC/AC-converter, often referred to as an inverter, and the DC/DC-converter. Modern converters are power-dense and efficient, but the need for high-power equipment, compact design, and the challenging environment in an aircraft means that new designs and technology are necessary [27].

8.4.1 DC/DC

The purpose of the DC/DC-converter is to control the power flow from the battery. It is vital to ensure the battery's safe operation and deliver the required power drawn to the EPS and TMS. Due to the dynamic behavior of the battery during discharge, a boost converter is needed to ensure a constant voltage level on the DC bus. A second standardized voltage level of a 28 V bus is used for secondary sources. It would require a buck converter able to reduce the voltage level in the transition between the DC busses.

The main difference between DC/DC converters is between isolated and non-isolated converters. In an isolated converter, it is a galvanic separation; hence it is safer than non-isolated converters. The most common topology for the isolated DC/DC converter is the dual active bridge using soft (zero-voltage) switching techniques [153, 83]. Other topologies such as the active-bridge active-clamp converter and active neutral point clamped can be considered as they show better power density and efficiency [154, 155]. However, in Channegowda et al. [156] they argue that isolated converters add a considerable weight penalty and instead suggest the use of non-isolated converters. They suggest that a multilevel boost converter yield the

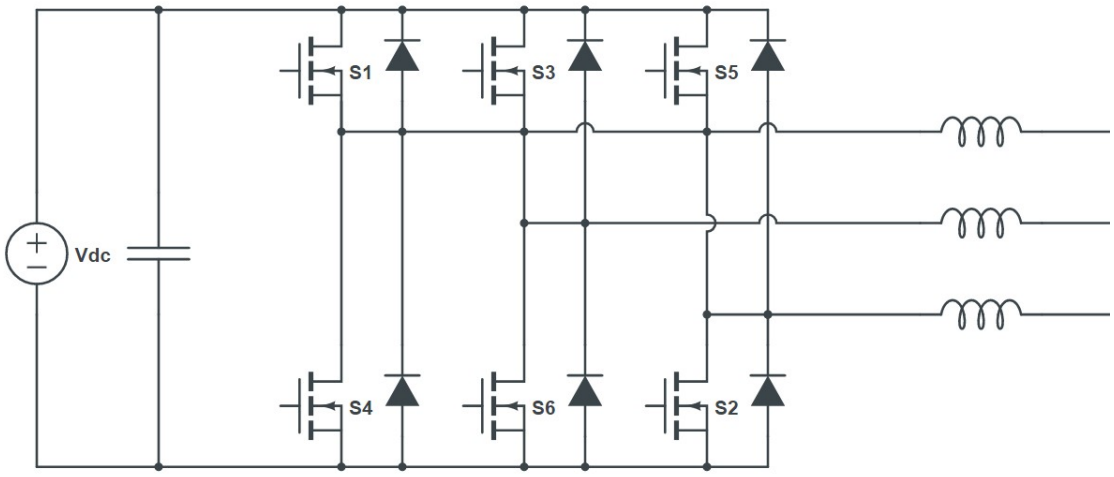

Figure 20: Schematic of a three-phase inverter.

highest specific power.

8.4.2 DC/AC

The DC/AC is mainly used for inverting and controlling the signal from the DC bus to the propulsors. Some subsystems will also run on AC and will need additional inverters [83]. If a pump is needed for the thermal management system, it would also require an inverter in the same manner as the propulsors. The inverters for the propulsion units control the operating speed of the motors by adjusting the frequency of the sinusoidal signal they are fed, as shown in Eq. (31).

$$f_{el} = \frac{p}{2} \cdot f_{mech} \tag{31}$$

By controlling the output signal, the speed of the motor, and the current fed to it, the motor is controlled [157]. The most common topologies for the inverter are either a classic 2-level inverter as depicted in Fig. 20 or more complex multilevel structures where the voltage is split into sections. This method is used to construct a more sinusoidal output signal [108].

8.4.3 Considerations

The primary attribution to losses in a converter is the losses in the switch, consisting of conduction losses and losses during switching [27]. Conduction losses occur when the switches are "on." Current flows through the switch, and the losses are ohmic losses caused by the internal resistance in the switch. On the other hand, switching losses occur due to a change of state for the switches. During switching, it is a finite

time when the voltage across the switches and the current through them are nonzero [37]. Therefore, the switching losses depend on the duration of the switching and the amplitude of current and voltage. By decreasing either, the switching losses will decrease.

The size and weight of the inverter are dependent on the switching frequency. By increasing the frequency, the size decreases. However, as switching increases so does the switching losses [158]. Another factor in the size and weight is the capacitor and the inductors. The capacitor keeps the DC voltage constant while the inductors are put on the AC side to reduce the ripple currents. These components will have an impact on the weight of the system and thus reduce the specific power of the power electronics [27].

For the choice of converters, it is important to consider whether they need to be uni- or bidirectional. Bidirectional converters are heavier than unidirectional but allow for more modes of operation. The DC/DC converter connected to the battery needs to be bi-directional [73]. It would allow for battery recharging, and despite some manufacturers considering battery swapping, recharging seems to be the most favored choice. For the inverters, it is not given what the correct choice of operation is. In electric cars, braking is used for recharging the batteries. Similarly, it is viable to use the descent part of the flight, where the propellers are braking and thus recharging the batteries. This use would call for bi-directional inverters for the motors. However, the use of bi-directional inverters would add too much weight [76].

Research focuses on new materials, especially wide-bandgap technology such as SiC and GaN in the IGBTs and MOSFETs [27]. These materials have a wider range of operation, which can reduce the size of the switches, and with lower losses, the size of the heat sink can be reduced [37]. New topologies and switching methods can reduce the losses; for example, topologies producing fewer harmonics, which in order will increase the efficiency, are also a possibility for improved power electronics [155].

One of the main issues, especially for the DC/DC converters, is the lack of high-power converters with low losses. A challenge is, for example, the need to handle high voltages with a compact design [27]. Keshmiri et al. [155] shows an isolated DC/DC converter design with a power density of 11.7 kW/kg for a 5 kW converter. The efficiency is above 96% using WBG materials. However, the power level is far below the required. Tarisciotti et al. [154] shows a converter operating at 20 kW, but this reduce the power density to around 2.5 kW/kg. They also omitted the weight of a thermal management system and the PCB board, which would yield an even lower power density. The efficiency is in the same range for both converters. However, this is better than currently available DC/DC converters for aviation which have power densities in the range of 0.92-1.25 kW/kg [83].

Inverters have had longer maturity in the market and operate at higher power with higher efficiency. However, as MW level compact inverters currently are unavailable, NASA is conducting a series of projects aiming for the construction of a 1-2 MW class inverter [152]. They have a performance goal of 99% efficiency and specific power of 19 kW/kg but operate with an optimistic scenario of 25 kW/kg and efficiency of 99.5% [42].

Table 7: Summary of converter SOA and future projections

	Efficiency [%]			Specific power [kW/kg]		
	2021	**2030**	**2045**	**2021**	**2030**	**2045**
DC/AC	93-99	98	99-99.5	5-12	16.44-20	24.66-50
DC/DC	96	98	99-99.5	0.92-5	16.44-20	24.66-50

Wheeler et al. [108] states that current converter designs for aerospace applications are at roughly 5 kW/kg. It includes filtering and thermal components and is conservative when compared to Dever et al. [37] who claims a state-of-the-art technology with 8.22 kW/kg with a 93-95% efficiency. A specific power of 8 kW/kg is backed up by Armstrong et al. [43], while Zhang et al. [159] demonstrates a 1 MW inverter with a power density of 12 kVA/kg and an efficiency of 99%. In Deshpande et al. [160] they show the design of a module of a three-phase inverter rated for 100 kW peak operation. It showed a power density of 27.7 kW/kg and 98.2% efficiency.

The future predictions of Wheeler et al. [108] are, however, more optimistic. They state that high-level TRL converters are capable of specific power at around 20 kW/kg within 2026 and that it is realistic to reach 50 kW/kg in a not too long time horizon. These values are lower in Dever et al. [37] where the specific power is expected to increase to 16.44 kW/kg and 24.66 kW/kg in 2030 and 2045, respectively. The efficiency is assumed to improve to 99% by 2045. Table 7 summarizes the data presented in this section, where the NASA data is included in the 2045 prospects.

8.4.4 Summary

The power demand in the aviation industry has led to a need for high-power converters with high efficiency. This demand requires new technology is required. Especially for DC/DC converters who currently operate at low power levels and have relatively low power density. New materials such as SiC are promising for lowering losses, and new topologies and more efficient packing could improve the performance. These advances lead Gnadt et al. [41] to assume that DC/DC and DC/AC converters will operate at the same power density shortly. As it has been hard to find a specified prognosis separating the converter types, and the most promising DC/DC converters seem to reach the same power density levels as the inverters, the same assumption is made in this thesis.

8.5 Circuit Breakers

Safety is of the utmost importance for the electrical system onboard an aircraft. Faults can occur in the components or the distribution grid, which can cause short-circuits and high currents disabling the electrical system. The fault resistance of the system must be upheld, and a single fault cannot cause the electric system to shut down. In order to prevent this shutdown, multiple circuit breakers are required. These are placed in the power system to isolate a section or component experiencing

a fault. Circuit breakers can be divided into AC breakers and DC breakers. Due to the nature of the electric power system in aircraft, both types are utilized. However, the emphasize of this thesis is on DC-breakers as AC subsystems are omitted.

AC circuit breakers use the zero-crossing of the current in an AC system to break the current. This method enables lightweight design, and high power breakers are commercially available. It is partly due to AC distribution being the most common distribution in electrical grids. However, the high power necessary for aviation could be an issue. Additionally, the altitude poses issues due to the increased possibility of partial discharges in the electric circuit.

In the DC distribution grid chosen in this thesis, zero crossing of the current is unavailable. Hence, other methods are needed to break the current. Multiple circuit breaker topologies and technologies are considered for the purpose. In Schefer et al. [27] four different topologies for breakers are discussed. These include the vacuum interrupter, solid-state circuit breaker (SSCB), CBs with arc chamber, fuses, and hybrid CB. It is pointed out that vacuum interrupters cannot be used for DC operation due to their inability to block DC currents. It also shows high weight gains compared to other technologies. The rest of the technologies handle DC operations, and the hybrid circuit breaker is the most promising technology. However, the readiness of the technology is low, and SSCB could show the same promise with new materials for power electronic converters. This section describes the operation of the different topologies and their advantages and disadvantages.

8.5.1 Mechanical Circuit Breakers

Mechanical switches are based on AC switching and can only switch during zero or low current conditions. This condition can be achieved in multiple ways. It can, for example, set up an opposing arc which will negate the original arc occurring as the switch opens. Another opportunity is to increase the resistance of the circuit and thus reduce the current [161]. The mechanical switch is highly effective during regular operation, exhibiting small conduction losses. However, as they experience arcing when breaking the circuit which can be hazardous. This effect might exclude it from being viable for operation in an aircraft unless the robust safety measures are applied. The safety measures could be penalized by weight additions. The mechanical switch also has slower reaction time than its competitors. The fault current increase until the circuit is broken, and to avoid high overcurrents, the reaction time of the breakers is needs to be kept short.

8.5.2 Solid State Circuit Breakers

A solid-state circuit breaker uses semiconductors during operation. Multiple switching devices are connected in series, and multiple switching topologies can be used [162]. Due to the high switching frequency of the devices, the reaction time of the SSCB is shorter than the mechanical switch. However, it has high conduction losses during no-fault operation, resulting in significant losses for the distribution grid. It is also expensive due to the high amount of switching devices. SSCB is mainly

used for medium to low-voltage applications, and in 2020 ABB presented an SSCB designed for ships. It could operate with 2100 V and rated currents around 3000 A [161]. This rating would enable it to the use onboard the aircraft. Despite showing power levels in the class necessary for the aviation industry, it does not mean that it is ready for implementation. The harsh environment in the aircraft and the high importance of weight and size contributed to the aircraft are more challenging demands than in a ship. However, Beheshtaein and Cuzner [163] presents a possible design for DCCB onboard NASA's N3X with the specifications of 6 kV and 2.083 kA with an efficiency of 99.94%.

Conduction losses could be substantially lowered, for example, by using wide-bandgap technology such as SiC or GaN. In that case, it could allow SSCBs to be used in an all-electric aircraft [164]. SSCBs are also prone to heating issues and hot spots and require extra cooling circuits, which would increase the weight and size of the system [27].

8.5.3 Hybrid Circuit Breakers

The hybrid DCCB combines the technologies of an SSCB and a mechanical switch. It consists of three main branches; the first is the primary conduction branch consisting of a mechanical switch in series with power electronics. However, the amount of power electronics is substantially lower than in the SSCB. This reduction leads to lower conduction losses during regular operations. It is, however, higher than the ones experienced in the mechanical switch. A more considerable amount of switching devices is placed in a parallel branch. These are used for breaking the circuit. The final branch has a voltage limiting device consisting of variable resistors [165]. The use of power electronics makes the device react quickly, and it does not experience the same arching as the mechanical switch. It can also be packed more compact and lightweight than the SSCB. However, an issue contributed to the hybrid DCCB is price, as they are expensive to manufacture. Another issue is the need for shorter reaction time. The hybrid CB use a utilize a mechanical switch in its main circuit. It limits the reaction time of the circuit breaker. Other types of switches are considered, such as Thomson coil and piezoelectric actuators [164] which could result in quicker reaction. Improved commutation time between the conducting and breaking branch would also be advantageous.

Currently, it seems as if the hybrid DCCB is considered for use in HVDC grids since conduction losses are detrimental. For the MVDC grids in an electrical aircraft the reaction time of the breaker is more vital. Some conduction losses are allowed as long as the reliability of the system is kept.

8.5.4 Summary

As shown in Table 8 most of the found research examples are SSCBs. Hybrid circuit breakers are still in their infancy, and experiments showing weight and power density are hard to find. Due to the short response time of the SSCB, this is probably the most viable for the aircraft. The mechanical breakers are too slow, and it could also

Table 8: Current and future projections for DC and AC circuit breakers

Technology	Specific power	Efficiency	Comment
SSCB	67.5 kW/kg	99.2%	Unidirectional[166]
SSCB	34 kW/kg	99.2%	Bidirectional[166]
SSCB	14-200 kW/kg	-	Depend on TRL[43]
DC mechanical switch	12-93 kW/kg	-	[43]
AC CBs	220-260 kW/kg	-	[43]
SSCB	44 kW/kg	99.7%	[41]
SSCB	200 kW/kg	99.77%	[42]
SSCB	200 kW/kg	99.9%	[80]

Table 9: Clearance time for different CB technology [6]

Technology	Clearence time
Mechanical CB	15 msec
SSCB	0.6 msec
Hybrid CB	3.4 msec

be the case for the hybrid version. In Table 9 the reaction times of the different technologies are shown [6]. With improved clearance time for the hybrid breaker it could be viable in future designs. The range in power densities and efficiency varies, but they generally show high perfomrance parameters.

8.6 Thermal Management System

For a conventional aircraft, the heat is mainly created by fuel combustion. The heat produced by the process is then released directly to the ambient with the exhaust of the engine [108]. An electrical system, on the other hand, is a closed system where the electric components need to be protected from dirt, and moisture [167]. Hence, the system can not utilize air directly from the ambient and needs a thermal management system (TMS) to handle any excess heat. It needs to be a closed loop system and all the produced heat needs to be safely transferred away from the components [168].

The temperature management system (TMS) of the electric propulsion system is crucial both to avoid damaging the components and keep the system's efficiency high. As previously mentioned, the operating temperature of the converters and motors is essential for their performance. High temperature can cause damage to the components if the temperature exceeds the maximum allowable value. In a worst case scenario these faults can cause fire or malfunctions of the components. Low temperatures are beneficial for the converters, motors, and wires, whereas the battery is the most crucial component of the heating system. It is more sensitive to operating temperatures, and in high operating temperatures, the likelihood of thermal runaway increases [74].

In addition to increasing the efficiency of the components, lower temperatures can

lead to a more compact design which leads to higher specific power. This benefit has made cryogenic cooling an area of interest for future aircraft development [169]. However, there are challenges with weight and power requirements for the cryogenic system due to the low-temperature requirements [170].

8.6.1 Cryogenic cooling

Electric aviation has a large power consumption. Large currents are transmitted in the power system, which leads to ohmic losses in the components [169]. A possible solution is the use of superconducting electrical machines that possess the ability of high efficiency, and high specific power [171]. However, superconducting materials require low temperatures in the range of 20-60 K [76]. Temperatures in this range are called cryogenic temperatures and require a TMS to enable such low temperatures. Most literature points to a reverse-Brayton cryogenic cooler as the technology for such cooling [172, 169]. However, the technology has not reached maturity due to the high additional weight and power consumption [169, 170, 168].

Despite the immaturity of the technology, it is viewed as necessary for large aircraft, and NASA is currently working with the technology for their N3-X program [76]. It is supposed to have its maiden flight by 2040, which requires substantial technological advances. One of these can be to use hydrogen fuel cells both as energy storage and as a medium for the cryogenic cooling process. This technology is examined further in Hartmann et al. [167].

8.6.2 Non-cryogenic cooling

Though the interest in cryogenic cooling has increased, it still needs significant technological advances to be viable for aviation. It makes non-cryogenic cooling important for modern technology. There are multiple methods for heat extraction, which can be categorized as either convection, conduction, or radiation. Popescu et al. [173] presents modern technology within these categories and states that making use of all the methods gives the best thermal effect for modern motors. These can include passive heat sinks, liquid, spray cooling, and active cooling with heat pumps [174]. In Anderson et al. [128] they use liquid cooling on the stator and air cooling on the rotor. They state that it should be sufficient for safe operation. However, thermal management was the limiting factor for all motor designs in the paper. Better cooling techniques could enable even more lightweight and compact designs.

Chapman et al. [174] states that a typical heat exchanger topology for an aircraft is a ram air-based TMS. The system utilizes ambient air in convection with a coolant through a heat exchanger. A ram fan is placed inside a ducted channel in order to maintain the speed of the air [167]. The speed of the air is maintained to avoid creating unnecessary drag. Chapman et al. [174] concluded with a design that used an air-oil cooler for the generator while an air-air cooler was used for the inverter. Kellermann et al. [175] also examine a ram air-based TMS where they optimize it

Table 10: Base values for thermal management system

Parameter	Value
h_{TMS}	0.14
p_{TMS}	0.83 kW/kg

for a 180-passenger single-aisles hybrid-electric aircraft. The result is a TMS that only adds 0.19% to the total power consumption of the aircraft.

For future projections Hartmann et al. [167] summarizes five TMS studies and makes projections for the performance of a TMS in 2035 based on these. The system in the article is a fuel cell system allowing for operation at higher temperatures. It enables a better effect for the TMS since the temperature difference is one of the main factors for heat extraction. Batteries need to operate at lower temperatures leading to substantially lower efficiency for the TMS. This also shows that the most critical operation for the TMS is during takeoff and climb when the power requirement is high. The temperature difference between the ambient and the components are lowest [74]. However, improvements are expected due to more efficient materials and transmission systems [37]. In addition, Freeman et al. [168] suggests that the high-temperature side of the cooling process can be used for auxiliary purposes such as anti-icing, heating of the cabin, and cooking in galleys. That would increase the efficiency of the TMS further.

The values for TMS performance are chosen from Rheaume et al. [176], another project utilizing a ram air-based TMS. The values are shown in Table 10. These values are similar to the findings in Gkoutzamanis et al. [74] who designs a ram air-based cooling system for a hybrid-electric commuter aircraft with a p_{TMS} at 0.79 kW/kg. However, if redundancy issues are considered, they find a 21.3% increase in weight.

8.6.3 Design

Figure 21 shows the design for the electric system in this thesis for an aircraft operating with four motors. The figure are meant to illustrate their approximate placement in the circuit and the connections between the components. The size of the components are not illustrative of their actual size, it is for example, expected that the volume allocated to the battery would be greater. The same electrical system structure applies to the electrical system in a two-propeller aircraft where the only difference is the number of motors.

The figure shows that the battery is connected to a DC/DC-converter. It will keep the DC distribution grid at a constant voltage and handle recharging of the battery. It will also ensure safe operation of the battery. The converter is connected to the distribution grid, but is protected by a DC circuit breaker. This is to ensure that the battery and converter is undamaged if a fault occurs on the distribution grid. This also applies to the rest of the components. The TMS is modelled in the back of the aircraft. This is to take into account the length of the aircraft, but is not

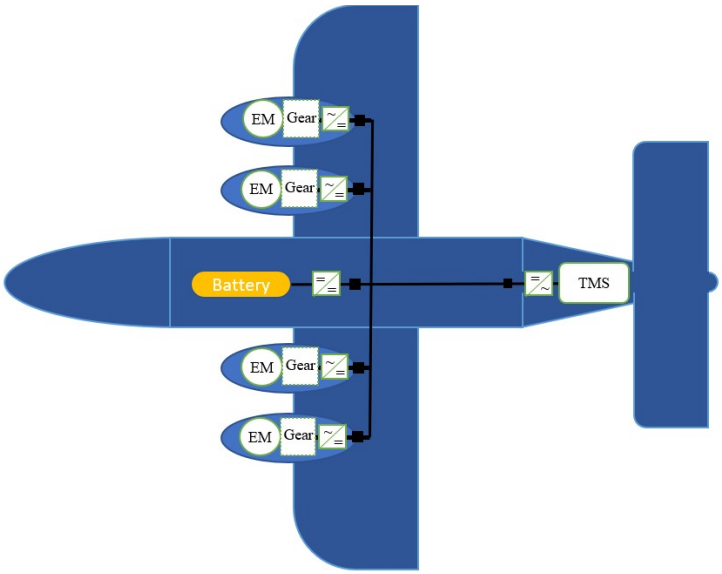

Figure 21: Example design of the electric system onboard a four-motor electric aircraft

necessarily the actual placement of the system. The TMS is connected by a inverter to the distribution grid. It is due to the power consumption of the pumps and fans in the TMS is expected to run on AC.

For each of the motors present on the aircraft the need for inverting the electrical power as for the TMS. The gear is optional and will be further discussed in later parts of this thesis. Anyways, the propellers are connected to the motor, either through direct drive when the gear is omitted, or indirect when the gear is a part of the system.

The propellers are not working as air brakes and thus no power is generated in them. Hence, AC breakers were not included on the motor side of the inverter. A thorough analysis of the dynamics of the power system is not a part of this thesis and should be further analysed. The choice to omit ACCBs are based on the work by Cano et al. [44].

Figure 22 shows the same electric way to display the electric system is shown in Fig. 21. This shows the system as a single line diagram, and separates the system into the EPS and TMS circuit. The battery, DC/DC converter and battery breaker are shared by both circuits, and will be sometimes be referred to as the battery circuit. However, the contribution to these components can be separated for each of the circuits.

9 Sizing

The section describes the sizing procedure based on the previously presented design. Firstly, it gives an overview of the case studies. Subsequently, the sizing algorithm is presented before the scenarios conducted on the short-haul flights are explained.

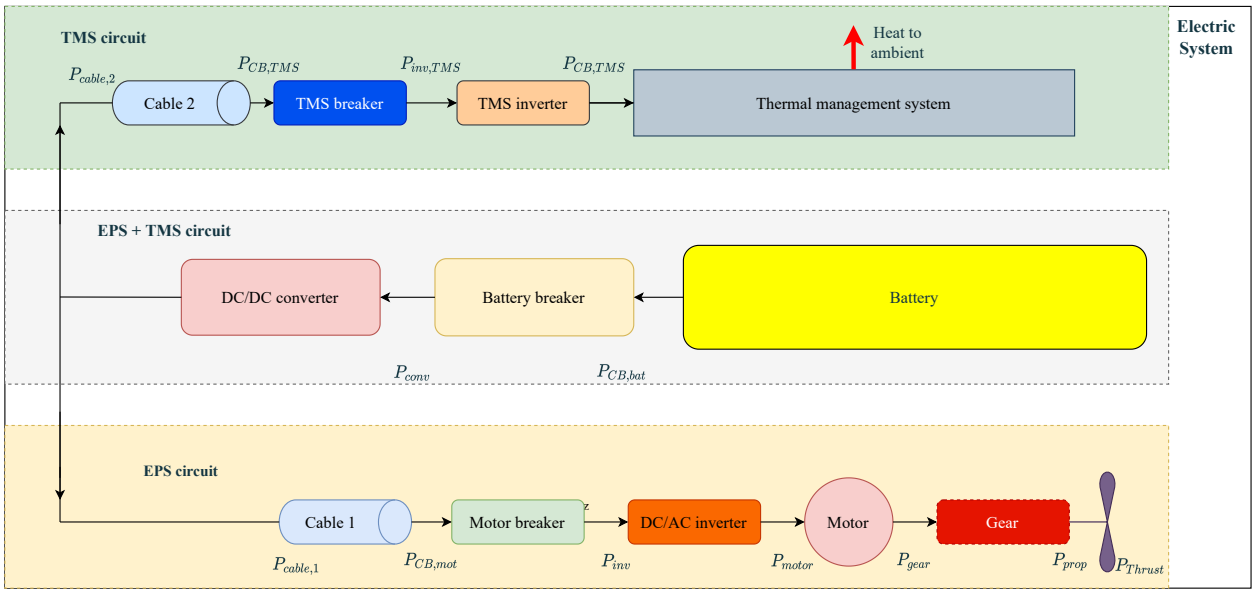

Figure 22: Overview for the electrical system onboard the aircraft. The system is separated into an EPS and TMS circuit while the battery, DC/DC converter and battery breaker is shared by the circuits.

9.1 Case studies

Figure 23 shows the routes and the aircraft chosen for the case study. The flights are in the shorter range for the short-haul network, with the longest being Tromsø-Hammerfest with a big circle distance of 211 km. However, the short routes are chosen since they are expected to be electrified earliest. All the routes are currently being operated by Dash 8-100s used for the flight analysis in Section 7.

Table 11 gives an overview of the number of weekly flights on each of the reference distances. They show a high frequency which partly is the reason for choosing them. The trip between Tromsø and Hammerfest is the most frequent route on the short-haul network with its 92 weekly trips. The rest of the routes are the most frequently traveled routes in their respective range.

As they are highly frequented an electric aircraft would operate 20% of all flights on the short-haul network by electrifying these routes alone. However, if all routes shorter than Tromsø-Hammerfest were operated by electric aircraft it would result in the electrification of 66% of the short-haul network. The shortest route of the short-haul network between Kirkenes and Vadsø is included as it possesses the minimum energy requirements. Hence, it is the lowest threshold necessary for enabling all-electric flights.

9.1.1 Tecnam P-Volt

The reference aircraft chosen are the Tecnam's P-Volt and the ES-19 produced by Heart Aerospace. They are both turboprop aircraft enabling STOL. Neither of the aircraft is in operation, but both are expected to fly commercially by 2026 [35, 14].

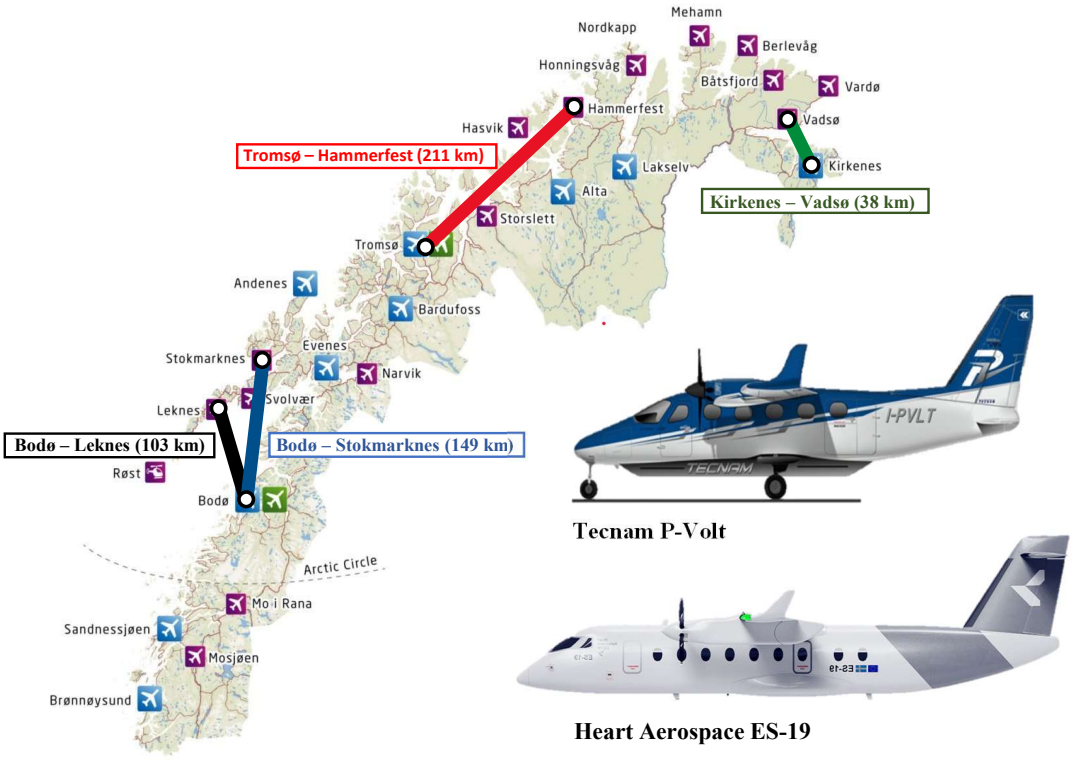

Figure 23: An overview of the reference aircraft and the chosen flight distances

Table 11: Case study flight distances and weekly frequency

Flight route	Distance	Weekly flights
Kirkenes-Vadsø	38 km	34
Bodø-Leknes	103 km	72
Bodø-Stokmarknes	149 km	59
Tromsø-Hammerfest	211 km	92

Table 12: Specifications for 9-passenger commuter aircraft [7, 8, 9, 10]

Model	MTOW	Empty weight	Wingspan	Length	Engine power	Cruise speed
Pilatus PC-12	4740 kg	2810 kg	16.28 m	14.4 m	890 kW	537 km/h
Tecnam P2012 Traveller	3680 kg	2286 kg	14	11.8	560 kW	360 km/h
Eviation Alice	7484 kg	-	19.2 m	17.4 m	1280 kW	464 km/h
Tecnam P-Volt	4086 kg	2177 kg	14 m	11.8 m	640 kW	222 km/h

The Tecnam P-Volt is based on Tecnam P2012 traveller and is a joint project where Rolls Royce delivers the electric propulsion system. It is of particular interest due to Widerøe being one of the partners in the project, announcing their intent to purchase and operate it on the short-haul network [35]. The aircraft will fit nine passengers in addition to two pilots and is expected to have a range of 157 km [177]. This range enables it to fly three of the four routes chosen for the case scenario. Table 12 shows the aircraft's specifications compared to similarly-sized aircraft.

In the table, the aircraft is directly compared to its conventional engine counterpart, the P2012 Traveller. They have the same outer diameters, but the MTOW of the P-Volt exceeds the P2012. It is likely due to the battery weight and applies despite a reduction in empty weight. However, the P-Volt is the lightest compared to the rest of the aircraft.

Alice is another all-electrical aircraft currently in development and presents a novel design. They claim higher performance metrics than the P-Volt, with a range of 400 km and a cruise speed over doubled that of the P-Volt. The range is likely the reason for the high weight discrepancy. Alice's high weight and speed also increase its installed power which could affect the weight.

9.1.2 ES-19

The ES-19 is a 19-passenger aircraft produced by the Swedish start-up Heart Aerospace. They are operating from Gothenburg and have successfully conducted a demonstration with a subscale version of the aircraft. It has four motors, and despite not being a retrofit, the Heart team claims that the aircraft is built on tried and tested design [178]. They claim a maximum range of 400 km, which is substantially higher than the P-Volt and would enable them to operate most of the routes on the short-haul network. The use of four motors ensures the STOL abilities despite high weight of the aircraft.

In Table 13, the aircraft has been compared to other 19-passenger aircraft. The empty weight of the ES-19 is substantially reduced compared to the other aircraft. Despite the weight reduction, the MTOW is higher, and the cruise speed is significantly lower. It is the same tendency as seen for the P-Volt.

The wingspan of ES-19 is also increased significantly, at least when considering that the aircraft length is amongst the shortest. It could be required to fit four propellers on the wings. The power specifications for the motors are unavailable. However, the correlation between weight, cruise speed, and motor rating should put the aircraft in the range of the Beech King or the Jetstream. The company expects to be certified

Table 13: Specifications for 19-passenger commuter aircraft [11, 12, 13, 14, 15, 16]

Model	MTOW	Empty weight	Wingspan	Length	Engine power	Cruise speed
Beech King 1900D	6950 kg	4730 kg	15.85 m	14.37 m	760 kW	480 km/h
Jetstream 31	7688 kg	4360 kg	17.67 m	17.63 m	954 kW	425 km/h
Fairchild D228	6400 kg	3740 kg	16.97 m	16.56 m	530 kW	350 km/h
Heart Aerospace ES-19	8600 kg	3600 kg	23 m	14.5[1] m	-	330 km/h

[1] Estimated based on the similarity in size between the ES-19 and Beech King as showed in [180].

and has signed multiple agreements of intent—the latest with the American airliners United and Mesa for 100 aircraft each [179].

9.2 Sizing algorithm

The sizing is performed using an analytical sizing algorithm. Through an iterative process, the aircraft's weight, power, and energy requirements are calculated. In Fig. 24 a flow chart of the algorithm is depicted.

The input data for the algorithm is threefold. The mission specifications include important metrics for the reference aircraft: dimensions, empty weight, passenger count, and cruise speed. It also utilizes the ratio between cruise and takeoff and the time regressions presented in Section 7. The time regression determines the time spent in each flight phase based on the mission's length specified in the case scenario. The performance for the components presented in Section 8 is also included as input data. Lastly, decisions on the voltage level of the distribution, aerodynamic efficiency of the reference aircraft, and several initialization are needed.

The interconnections of the sizing algorithm results in two iteration loops. These are shown in Fig. 24. The inner loop sizes the TMS circuit while the outer loop is used for sizing the EPS. The algorithm assumes an initial power requirement based on the input data. This power requirement is recalculated at each iteration due to weight increases as the power requirement increase. Convergence is acquired if two subsequent iterations' power level is within a threshold. The threshold is set to 1 for all scenarios. When converging, the result is the weight of each component, the power level, and the aircraft's energy consumption.

Whenever convergence is not acquired, the power and energy requirements of the EPS components are recalculated. The thermal dissipation of the EPS circuit is also calculated. Based on the heat dissipation, the TMS sizing is performed. However, as the power requirement of the TMS increase, the losses in the TMS circuit increase, leading to an even larger TMS. The iterative TMS sizing loop handles this. It recalculates the power requirement of the TMS and the power in the components until it converges.

The weight of each component is then calculated, where the battery, DC/DC converter, and battery breaker result from the sum of both the TMS and EPS contribution. However, of the iteration limit is reached, the algorithm terminates without convergence. If the limit is not reached, the process repeats.

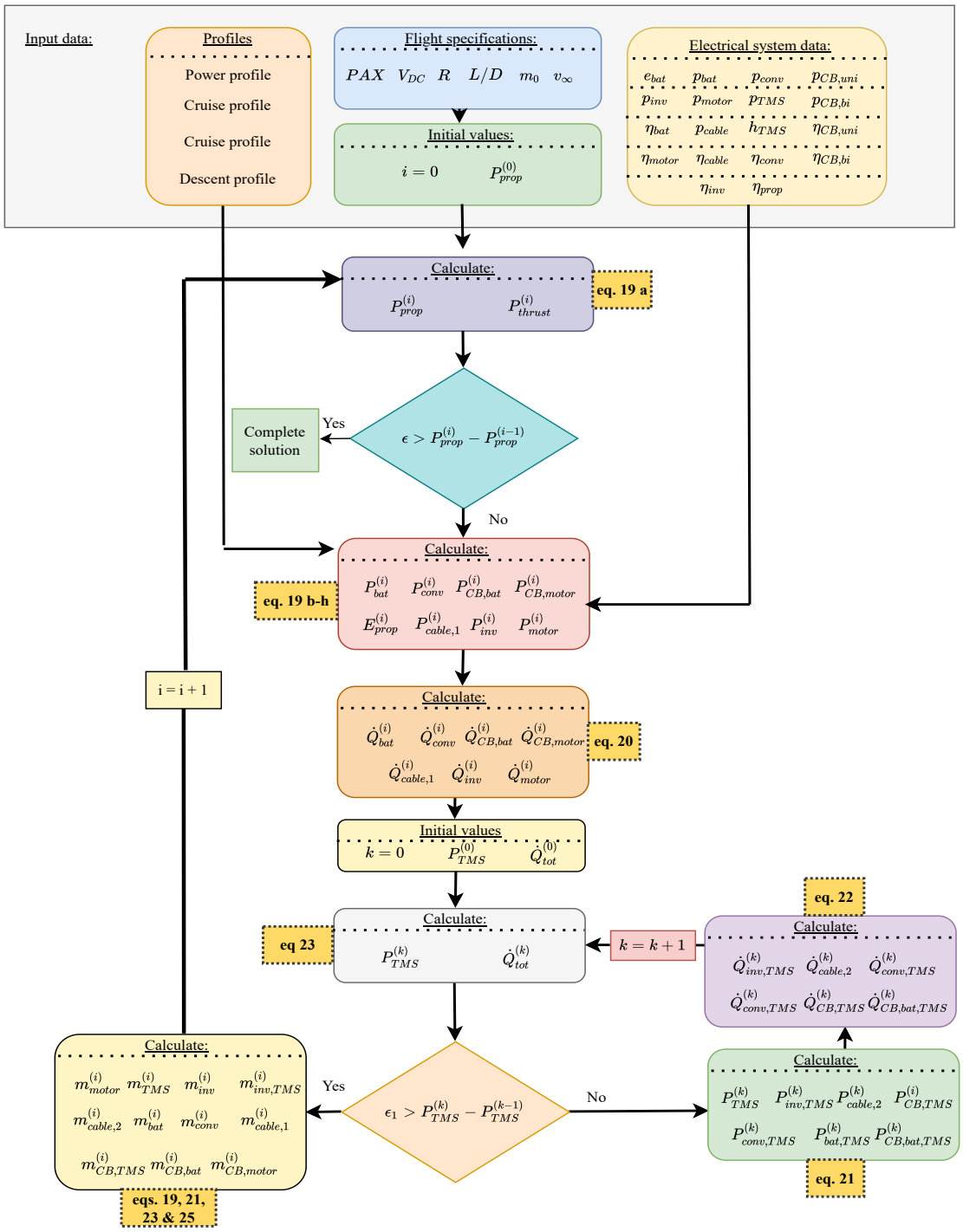

Figure 24: Flow chart of the sizing algorithm

9.2.1 Assumptions and simplifications

Several assumptions and simplifications are embedded in the algorithm. These are shortly touched upon in this section.

Firstly, the L/D-coefficient is assumed to be constant throughout the flight. It is also assumed to be the same for both of the reference aircraft. The coefficient is part of the propulsion calculation, and it would have a significant impact if it were changed. The estimation is set to 15, which is per the data in [50].

Turboprops generally use fixed-speed propellers. They can adjust their pitch to adjust the efficiency of the propeller. Low pitch is efficient at low velocities, while coarser pitch results in high efficiency at high velocities. By utilizing the optimum pitch at a given speed, the propeller efficiency can be assumed constant for the majority of the flight [181].

The components in the circuit are expected to scale linearly with the power requirements. It results from basing the sizing on specific power. They are also sized according to the downstream requirements and their losses. Hence, the components are unable to handle power levels exceeding this. This power level could be too low, and a manufacturer would likely include a margin in case of higher power requirements.

As mentioned in Section 8.2, the SOC of the battery is vital for the cycle life. Hence, the SOC is prevented from falling below 20% throughout the sizing algorithm. This level is per the presented literature.

In Section 7 the reference aircraft is the Dash 8-100. The regression lines for the time spent on the flights are thus an analysis based on the speed and climb rate of the Dash 8-100. It has a cruise speed of 445 km/h, which is faster than the cruise speed of the P-Volt and the ES-19. Hence, the speed difference needs to be accounted for as longer flight time will require more stored energy. The relation between the cruise speed of the Dash 8-100 and the electric aircraft was used to account for the different cruise speeds. This relation was multiplied by the regression models for the time in Section 7, which increase them. However, as the takeoff requirements are the same, this phase was exempted. As a result, as the time is increased, the climb rate falls. This fall could affect the aircraft's power requirements, but is not considered, and the short-haul analysis' power profiles are used for all scenarios.

9.3 Test scenarios

9.3.1 Base case

The base scenarios are chosen to find the viability of operation on the short-haul network with current technology. A minimum amount of requirements are attached, and the cases serve as a reference as more constrains are introduced. In Table 14 the performance parameters of the base case scenarios are presented. These are based on the data presented in Section 8.

Table 14: Base case parameters

Component	Specific power	Specific energy	Efficiency	Heat dissipation
Battery	1200 kW/kg	200 Wh/kg	100%	-
Motor	5.9 kW/kg	-	95%	-
DC/AC inverter	9.0 kW/kg	-	96%	-
DC/DC converter	2.5 kW/kg	-	96%	-
Unidirectional DCCB	67.5 kW/kg	-	99.2%	-
Bidirection DCCB	34.0 kW/kg	-	99.2%	-
TSM	0.83 kW/kg	-	-	0.14 kW/kW
Cable	100.0 A/kg/m	-	99.6%	-
Propeller	-	-	89%	-
TMS circuit	-	-	90.3%	-
EPS circuit	-	-	76.4%	-

The battery is assumed to have an efficiency of 100%, since BMS is expected to handle any excess heat, thereby, fulfilling the battery's safety requirements. However, the BMS will reduce the specific power and specific energy of the battery as the casing will weigh the battery cells down. Battery chemistry utilizing Li-S or Li-O_2 is envisioned to improve the battery's specific energy significantly. However, these technologies are still in development and are not commercialized. Therefore, the battery composition chosen for this thesis is a Li-ion battery with cell-specific energy of 250 Wh/kg and specific power of 1500 kW/kg. As these values are at the cell level, the performance is reduced with the inclusion of the BMS. It is expected to increase the weight with 20% according to [41, 19] resulting in the performances in Table 14.

For a reference motor, the Siemens SP200D is chosen. It exhibits high power density at a low RPM, and the efficiency is in the same range as the other presented motors. The low RPM enables direct drive, making it ideal for testing the effects of gearing. The gearbox is omitted in the base case scenario, and the power density and efficiency are modeled as constants.

The power electronic converters must include a DC/DC-converter for the battery and a DC/AC-inverter for the motors. The performance of both types of power electronics is set close to the average of the 2022-values in Table 7. This choice applies to both efficiency and specific power. The DC/DC-converter needs to be bidirectional as it needs to handle the recharging of the battery. It is not necessary for the inverters as regenerative braking is not included.

The same consideration applies to the DC breakers. The battery breaker needs to enable bidirectional flow, while the TMS- and motor breakers only need unidirectional power flow. Table 7 shows a significant variation in breaker performance even within the same topology. It is expected that the breakers in the electric aircraft will be SSCBs as they exhibit the fastest response, which ensures safe operation during faults. For the modeling, the parameter performance presented in Valente et al. [166] is used. They separate unidirectional and bidirectional breakers, and their performance values are in the middle of the range presented.

The TMS values are based on the ram air system presented in Rheaume et al. [176]. However, huge uncertainty is attributed to the parameters due to the need for customized TMS for individual aircraft. The propeller operates at a constant efficiency of 89% [181] and the voltage level of the DC distribution is set to 1000 V. The cable efficiency is found in Jansen et al. [42] while the current-carrying capability is set to 100 A/kg/m. It is a doubling compared to the capability for TRL 5-6 presented in Armstrong et al. [43]. However, as the article is from 2012, it is expected that significant improvements have been made in the past years.

In the table the efficiencies of the EPS and TMS circuit is presented. It is a result of the downstream losses and for the EPS it results in a low efficiency barely above 75%. This is due to the inclusion of the propeller efficiency and would be close to 85% without it. The TMS circuit shows a higher efficiency as it consists of fewer components and thus experience fewer losses.

9.3.2 Scenario 1 - Cruise

Many papers trying to establish the required improvements, range, and weight of an electrical aircraft often base their work on Breguets range equation. This methodology was used in the preliminary work for this thesis in [78]. Hepperle [24] also uses the equation to estimate aircraft performance. A shortcoming of this equation is the assumption of constant cruise throughout the flight. Hence, the power requirements during takeoff and climb are ignored, leading to an under-dimensioned electric system. As the components in the circuit are sized by their specific power, neglecting the high power requirement in the takeoff will impact the system severely. The base case is compared to only including cruise in this scenario.

9.3.3 Scenario 2 - Voltage levels

The cable weight is dependent on the voltage level of the DC grid. The effects of the voltage level are tested by sizing the aircraft at different voltage levels. 1000 V was chosen for the base scenario, but this might be high due to the concerns with partial discharges due to reductions in air pressure. The highest voltage level used in modern aircraft is 540 volt. However, for future projects, voltage levels towards 3000 V are considered. As 540 V has been implemented successfully, this is the lower range. For the highest threshold the 3000 V envisioned for the NASAs N3-X is used.

9.3.4 Scenario 3 - Addition of gear

The Siemens SP200D allows for direct drive of the propeller. However, adding a gear could improve the system as it could enable a more compact and lighter motor. This hypothesis is tested in this scenario with the inclusion of a gear in the electrical drivetrain. The motor's weight is weighed against the additional weight caused by the inclusion of the gear. Table 15 shows the different gear ratios assessed in the

Table 15: Scenario 2 - Gear ratios

Gear ratio	Gear efficiency	Specific power	Rotational speed	Motor efficiency
2	98%	10.8 kW/kg	2600 rpm	95%
4	98%	23.6 kW/kg	5200 rpm	95%
8	98%	47.2 kW/kg	10400 rpm	95%

scenario and the impact it has on the specific power of the motor. The specific power is expected to increase linearly with the gear ratio as the motor speed increases at the same rate. The modeling of the gearbox weight is performed following Eq. (30).

9.3.5 Scenario 4 - Battery heat loss

The base case assumes a battery efficiency of 100% due to the inclusion of a BMS increasing the weight and handling safety issues. However, this is a simplification, and the battery will have inefficiencies. The inefficiency is partly caused by the battery's internal resistance and will add heat losses to the circuit. The TMS must handle these losses because the battery performance depends on the temperature. Hence, it will increase the size and power consumption of the TMS. Gnadt et al. [41] estimate a battery efficiency of 95.9% which is used for this scenario.

9.3.6 Scenario 5 - Redundancy

As shown in Section 8.1.3, the need for safe operation is critical. A single fault cannot interrupt the whole propulsion system. Figure 25 shows a proposed design of the electrical system where redundancy is included. It separates the battery into two sections which are connected by an H-bridge as proposed in [73]. This connection enables both batteries to deliver power even if a fault is experienced on the distribution grid, which is necessary to sustain the original range. Moreover, it means that the batteries do not need to double the capacity, which would be detrimental to the aircraft's weight. However, if a fault occurs in either of the batteries, the capacity loss is acceptable and would require the aircraft to land at the closest airport. It is also the reason for including two separate distribution grids.

Each distribution grid needs to accommodate maximum power flow, which means that the components also need to enable the same flow. As shown in the figure, the redundancy requirement leads to an increased number of CBs. In total, 12 new breakers are added. Two of them are added to the battery circuit and enable bidirectional flow. The rest are added either to the motors or TMS and are unidirectional. Another DC/DC-converter is also added between the distribution grids.

Although the large amount of CBs added, most of these are connected in parallel with the already included CBs. These will not affect the system's efficiency, whereas the one connected in series with the motor or TMS CB will make the efficiency slightly lower.

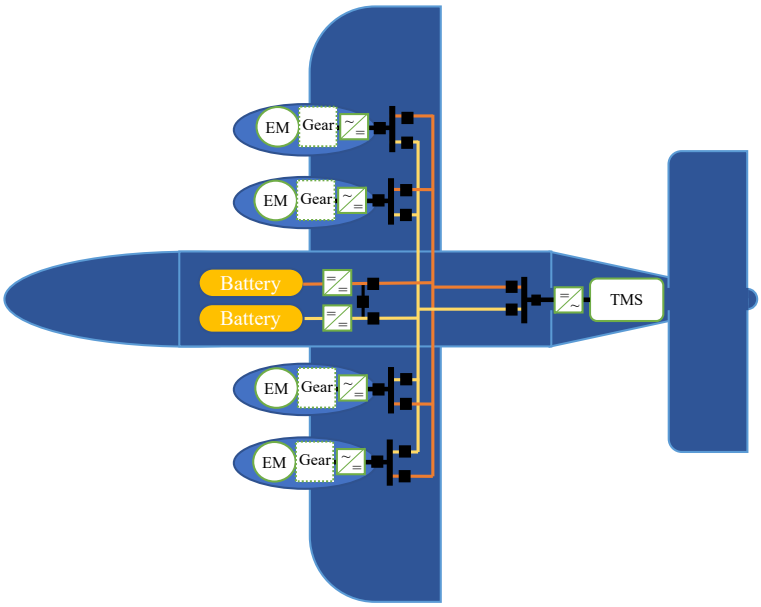

Figure 25: Electric schematic with redundancy for ES-19. The black boxes are DCCBs

TMS redundancy is included by increasing its weight by 21.3%. This increase is per the works in [74].

Two different methods for adding the redundancy were tested to tested. The first adds the extra components to the base case's result, while the second includes them before the sizing procedure. It will show whether adding the components after the sizing is sufficient or if the additional weight of the components affects the system to a more significant extent.

9.3.7 Scenario 6 - Energy reserves

The regulations of the FAA and EASA have strict requirements for the fuel reserves on board the aircraft. In the base case, these requirements are omitted but will have a large impact on the aircraft's weight due to the increased capacity required for the battery. The scenario is conducted for four reserve requirements. These are summarized in Table 26. The minimum requirements for the flight are 30 minutes in VFR conditions and 45 minutes under IFR conditions. Additionally, it is added extra capacity to enable loitering and rerouting. These are added as extra reserves in the scenario and consist of energy reserves of 5% of the total cruise distance and 15 minutes extra to allow for rerouting.

Table 16: Energy reserve requirements

VFR	IFR	Full VFR	Full IFR
30 min	45 min	45 min + 5% of distance	1 hour + 5% of distance

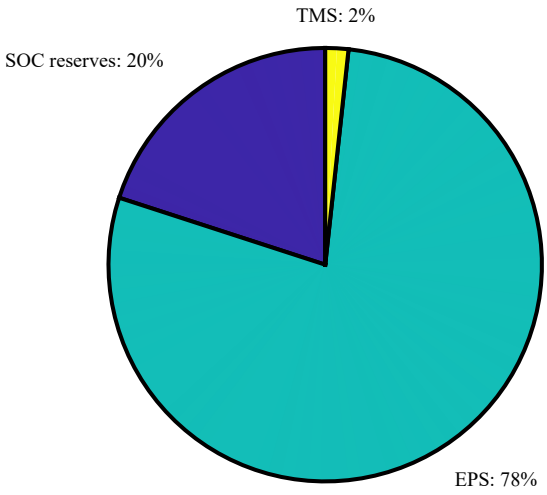

Figure 26: Contribution to the battery weight by the TMS circuit, the EPS circuit and the weight reserved to remain at 20% SOC. The contribution from the TMS circuit is constant throughout the base cases.

10 Results

This section contains the results of the scenarios presented in the previous section. It also contains a short analysis of the results. However, the impacts of them are more thoroughly discussed in the section following this.

10.1 Base case

Figure 22 shows that the battery, DC/DC breaker, and battery CB are supplying the propulsion units and the TMS. In Fig. 26 the battery weight are separated into three parts. The weight added by the EPS and TMS energy requirements and the energy reserved to keep the SOC at 20%. It shows that the TMS only is accountable for 2% of the battery capacity. This relation is constant in the base cases and also applies to the DC/DC converter and battery CB.

10.1.1 Kirkenes-Vadsø

Figure 27 a) shows the distribution of weight for the P-Volt for the 38 km flight between Kirkenes and Vadsø. The most significant contributor is the empty weight

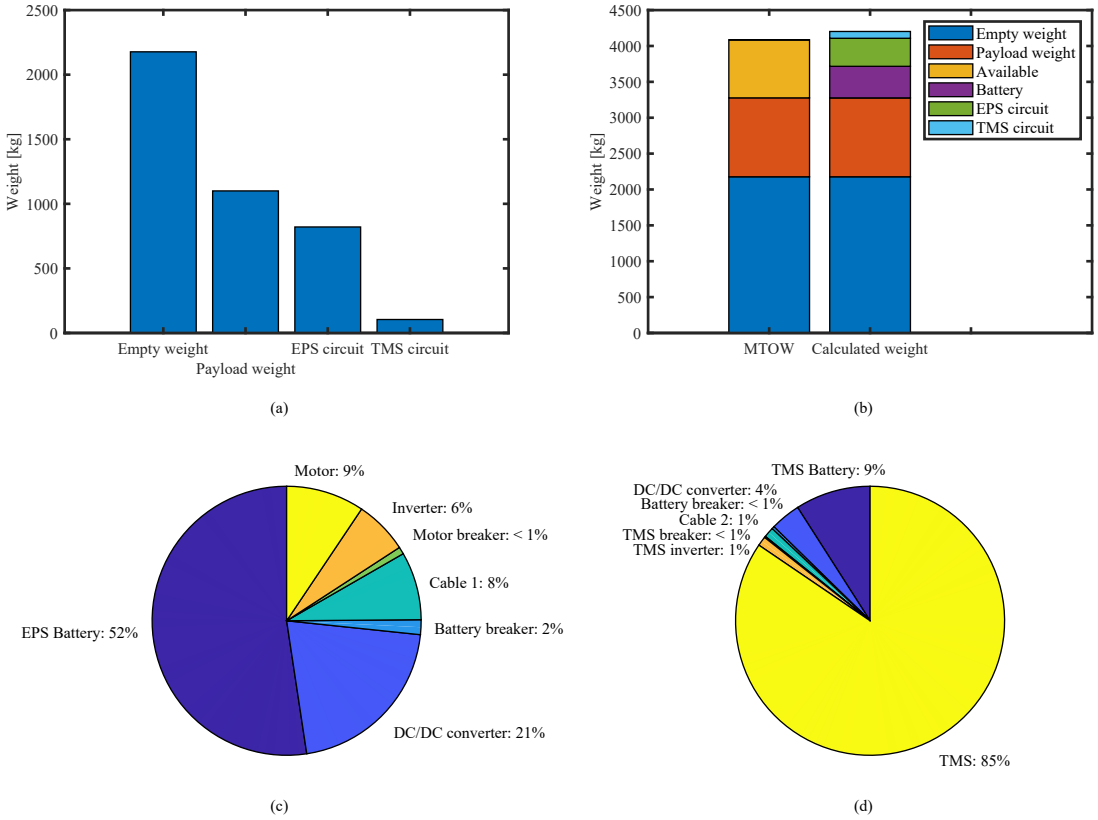

Figure 27: An overview of weight and weight distribution for P-Volt between Kirkenes and Vadsø (38 km). Figure a) shows the weight addition by each weight group. In b), the MTOW of the aircraft is shown against the calculated values. It shows the share of the weight contributed by the battery, while c) and d) shows the weight distribution of the EPS circuit and the TMS circuit respectively.

accounting for approximately half of the total weight. The other half is mainly added by the payload and EPS circuit. The weight of the TMS circuit is minor compared to the other components as it adds less than 100 kg. In b) the same figure data is shown stacked. The battery weight is separated from the circuit as it is a significant contributor to the weight, and it shows that the electric system adds more weight than is available for the P-Volt. However, it is with a slim margin, and small reductions in payload weight would put the electric aircraft weight within the MTOW.

The large proportion of the electric system weight allocated for the battery is shown in b) but is underscored in c), where the weight distribution of the EPS is shown. The battery adds more than half of the total EPS weight, and the DC/DC converter required for the battery system adds another 21%. By including the bi-directional CB used to protect the battery makes the battery circuit accountable for 75% of the total EPS weight. The final 25% are used by the motor, inverter, and distribution cable while the weight of the motor CB is negligible.

In d), the same figure is shown for the TMS circuit. The TMS is the primary contributor accounting for 85% of the weight. The battery and the DC/DC converter are the second and third contributors, while the rest of the TMS circuit barely adds any weight, in total less than 3%.

The same figures are shown for the ES-19 in Section 10.1.1. Compared to the P-Volt, a more significant proportion of the weight is attributed to the EPS circuit. While the payload was the second largest contributor to the total weight for the P-Volt, it is the EPS in the ES-19. It is because of the higher weight of the ES-19 compared to the P-Volt. Therefore, it has a higher propulsion power demand which increase the power ratings for the components. As the components are dimensioned by the specific power, the weight will increase accordingly.

However, despite the relative weight increase of the EPS, the weight is just exceeding the MTOW, as shown in b). It only exceeds the MTOW of the aircraft by 70 kg. It is less than the weight added by a single passenger and makes it reasonable that the aircraft is capable of operating at the distance.

The distributions are shown in c) and d) are similar to those presented for the P-Volt. The battery circuit accounts for a slightly smaller fraction of the EPS. The decrease of the battery circuit is solely transferred to the cable due to the need to carry a substantially larger current. The TMS circuit is unaltered from the one presented for the P-Volt.

10.1.2 Bodø-Leknes

In Section 10.1.2 the distribution of the weights shows an increase in the EPS circuit weight. It surpasses the payload weight and is the second-largest contributor to the weight. By comparing it to the MTOW, the calculated weight exceeds the limit by only accounting for the battery weight. Hence, the weight of the EPS and TMS further increase the discrepancy. The attribution of the battery weight is shown more clearly in the distributions where the battery takes up a substantially more

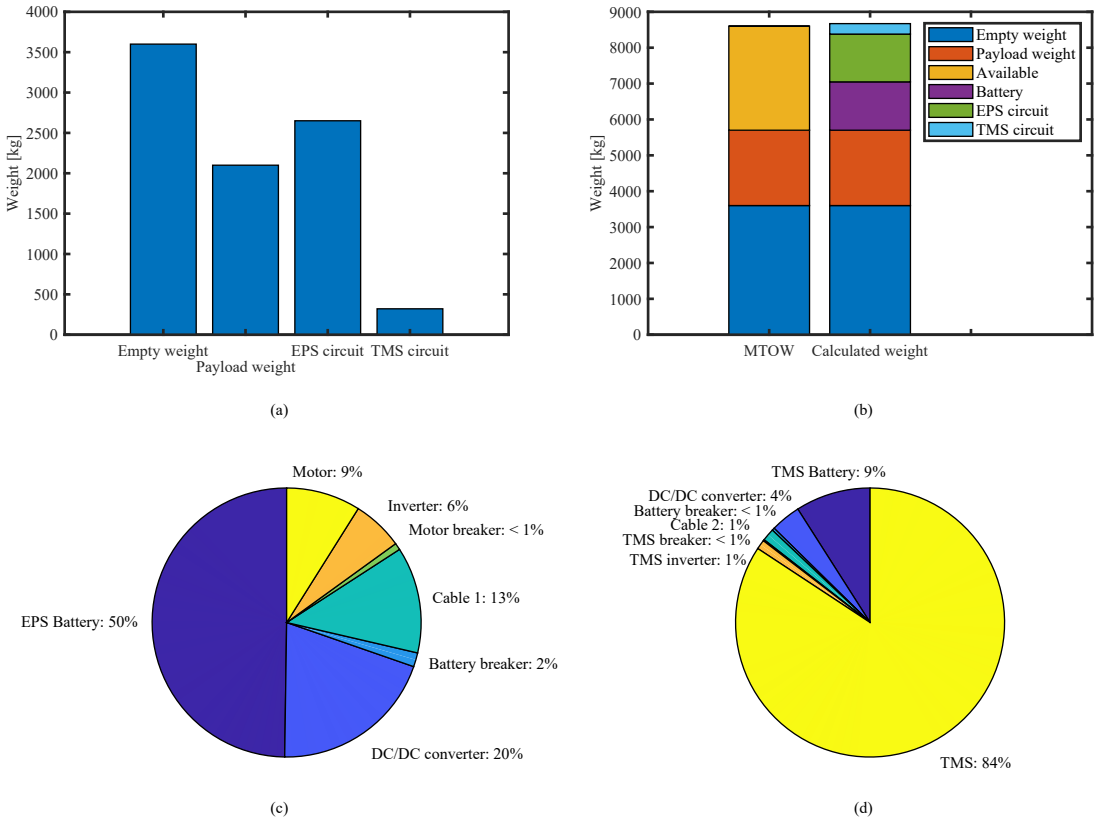

Figure 28: An overview of weight and weight distribution for ES-19 between Kirkenes and Vadsø (38 km). Figure a) shows the weight addition by each weight group. In b), the MTOW of the aircraft is shown against the calculated values. It shows the share of the weight contributed by the battery, while c) and d) shows the weight distribution of the EPS circuit and the TMS circuit respectively.

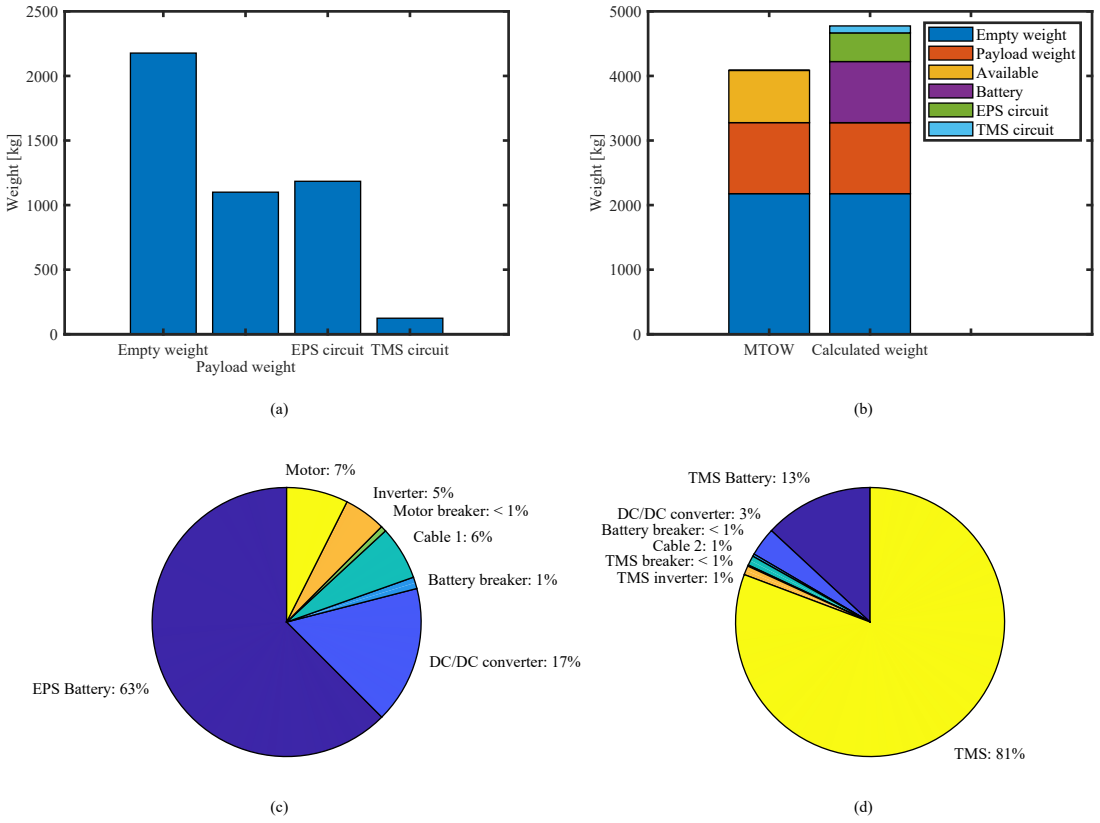

Figure 29: An overview of weight and weight distribution for P-Volt between Bodø and Leknes (103 km). Figure a) shows the weight addition by each weight group. In b), the MTOW of the aircraft is shown against the calculated values. It shows the share of the weight contributed by the battery, while c) and d) shows the weight distribution of the EPS circuit and the TMS circuit respectively.

significant portion of the EPS. At the same time, it has increased its portion of the TMS circuit.

The change for the ES-19 is less evident than for the P-Volt. However, the weight of the EPS has increased, further increasing the discrepancy between the calculated weight and the MTOW. This weight has been more evenly distributed in the system with only minor changes in the distributions.

10.1.3 Bodø-Stokmarknes

As the distance increase, the trendlines become more evident. The EPS constitutes an increasingly significant portion of the aircraft weight, where the battery is the most influential parameter. It is shown by the EPS circuit weight being substantially higher than the payload weight in Fig. 31, while it was approximately the same for

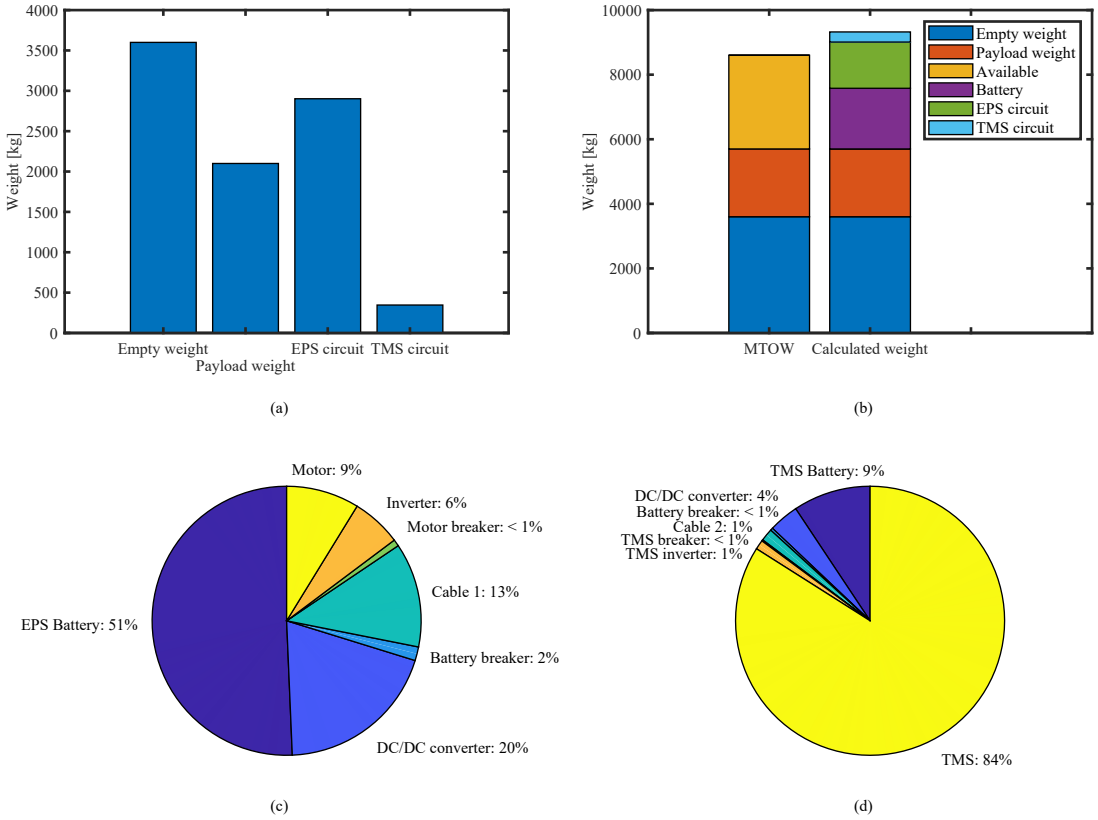

Figure 30: An overview of weight and weight distribution for ES-19 between Bodø and Leknes (103 km). Figure a) shows the weight addition by each weight group. In b), the MTOW of the aircraft is shown against the calculated values. It shows the share of the weight contributed by the battery, while c) and d) shows the weight distribution of the EPS circuit and the TMS circuit respectively.

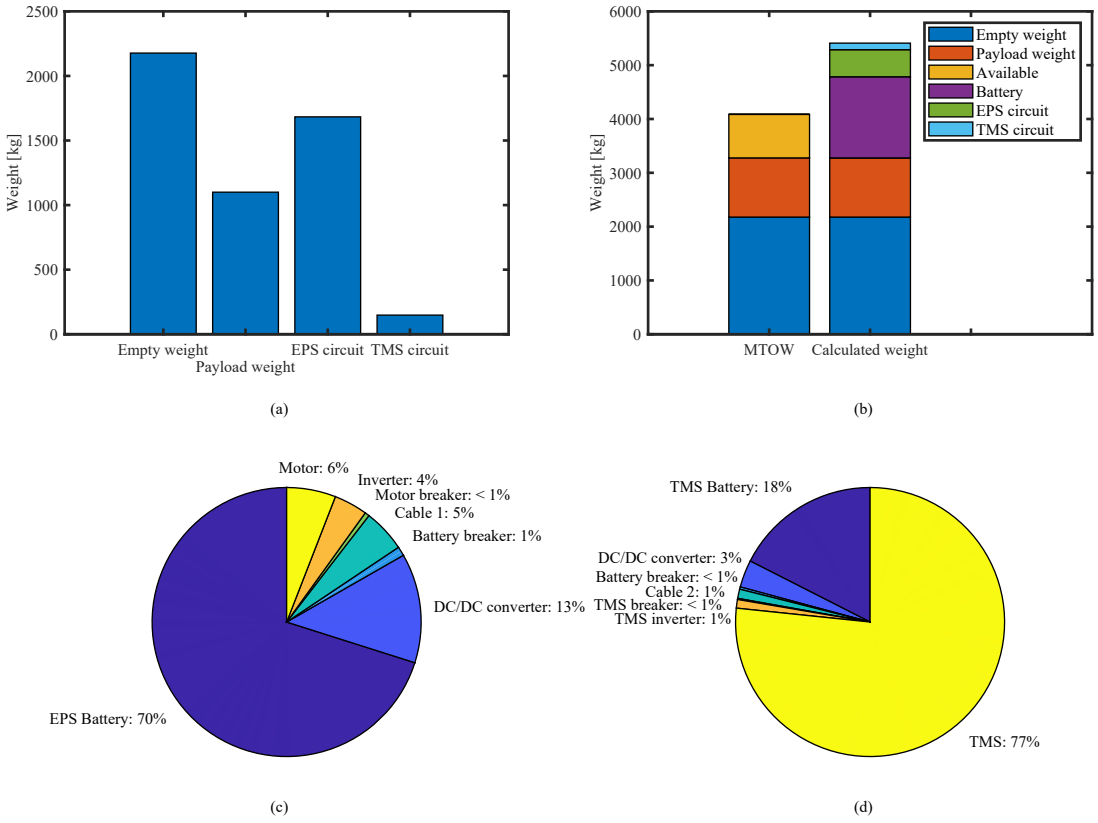

Figure 31: An overview of weight and weight distribution for P-Volt between Bodø and Stokmarknes (149 km). Figure a) shows the weight addition by each weight group. In b), the MTOW of the aircraft is shown against the calculated values. It shows the share of the weight contributed by the battery, while c) and d) shows the weight distribution of the EPS circuit and the TMS circuit respectively.

the distance between Bodø and Leknes. While the battery takes up a more significant portion, the importance of the other parameters reduces; however, their weight does increase, just not at the level of the battery.

Section 10.1.3 shows that the weight gains of the EPS in the ES-19 is more evident than for the P-Volt. Between Bodø and Stokmarknes, the EPS weight exceeds the aircraft's empty weight. Hence, the electric system's weight exceeds the material weight of the aircraft structure. Most of this is attributed to the battery as shown in b), where the battery weight exceeds the available weight. While the composition change of the EPS between Bodø-Leknes was similar to the composition between Kirkenes and Vadsø. However, for the distance between Bodø and Stokmarknes, the weight distribution alters with a more significant part being allocated for the battery. The same trend is seen in the TMS.

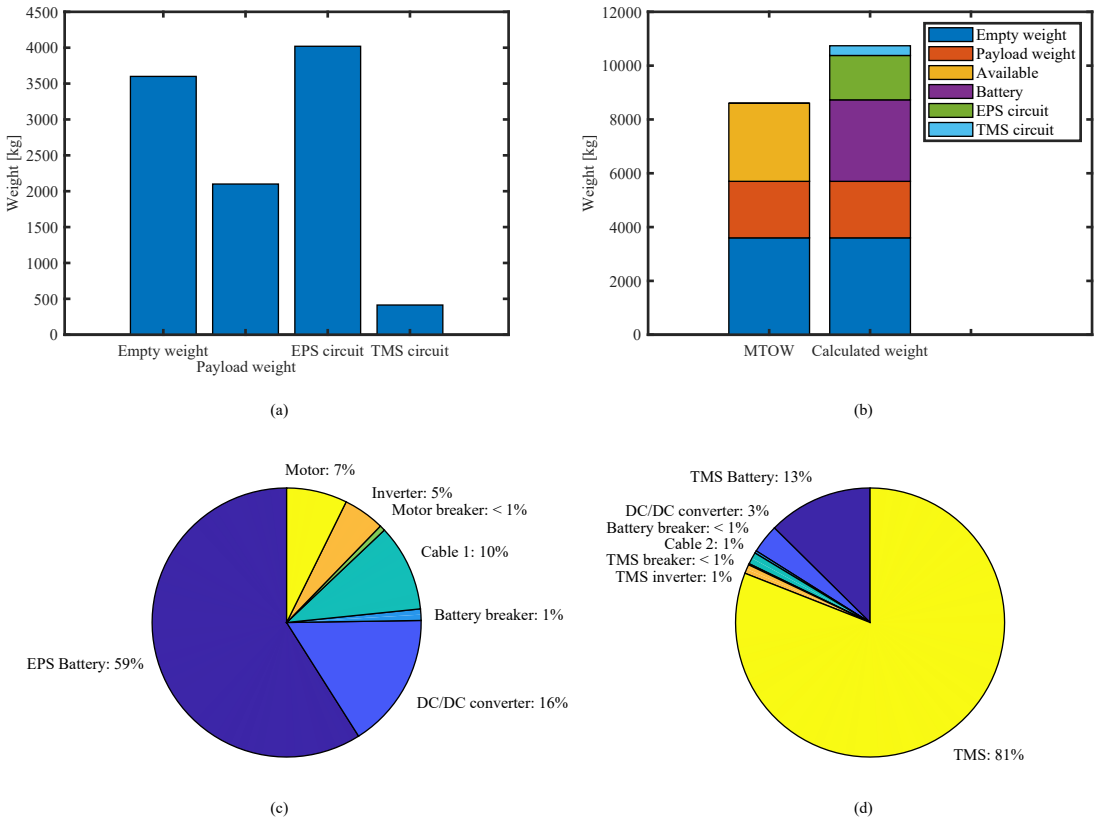

Figure 32: An overview of weight and weight distribution for ES-19 between Bodø and Stokmarknes (149 km). Figure a) shows the weight addition by each weight group. In b), the MTOW of the aircraft is shown against the calculated values. It shows the share of the weight contributed by the battery, while c) and d) shows the weight distribution of the EPS circuit and the TMS circuit respectively.

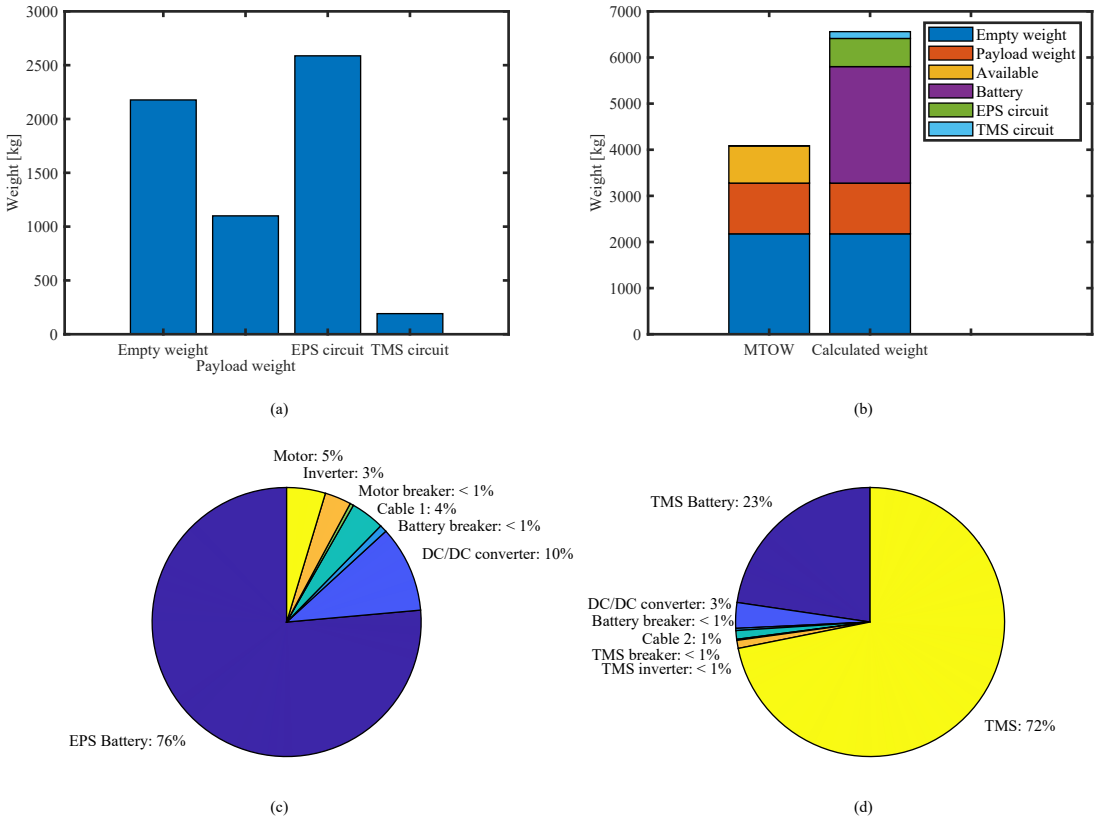

Figure 33: An overview of weight and weight distribution for P-Volt between Tromsø and Hammerfest (211 km). Figure a) shows the weight addition by each weight group. In b), the MTOW of the aircraft is shown against the calculated values. It shows the share of the weight contributed by the battery, while c) and d) shows the weight distribution of the EPS circuit and the TMS circuit respectively.

10.1.4 Tromsø-Hammerfest

The longest flight distance between Tromsø and Hammerfest also shows the most significant battery weights. Figure 33 shows that the battery is solely responsible for 3/4th of the EPS weight. Less than 15% of the EPS weight is seized by the motor, inverter, and cable. Figure b) also shows this tendency, with the battery being the most significant contributor, even accounting for the empty weight. In the TMS circuit, the TMS still accounts for majority of thee weight. However, the proportion of the weight attributed to the battery is increased to almost a quarter. The rest of the TMS circuit is negligible since it only accounts for 5% of the total TMS circuit weight, which is only a minor contributor to the total weight. The total calculated weight is increased to around 6500 kg, which exceeds the MTOW by around 2500 kg.

The ES-19 is also experiencing weights exceeding its MTOW. The EPS circuit weighs around 6500 kg, thus accounting for around 50% of the total aircraft weight. Sec-

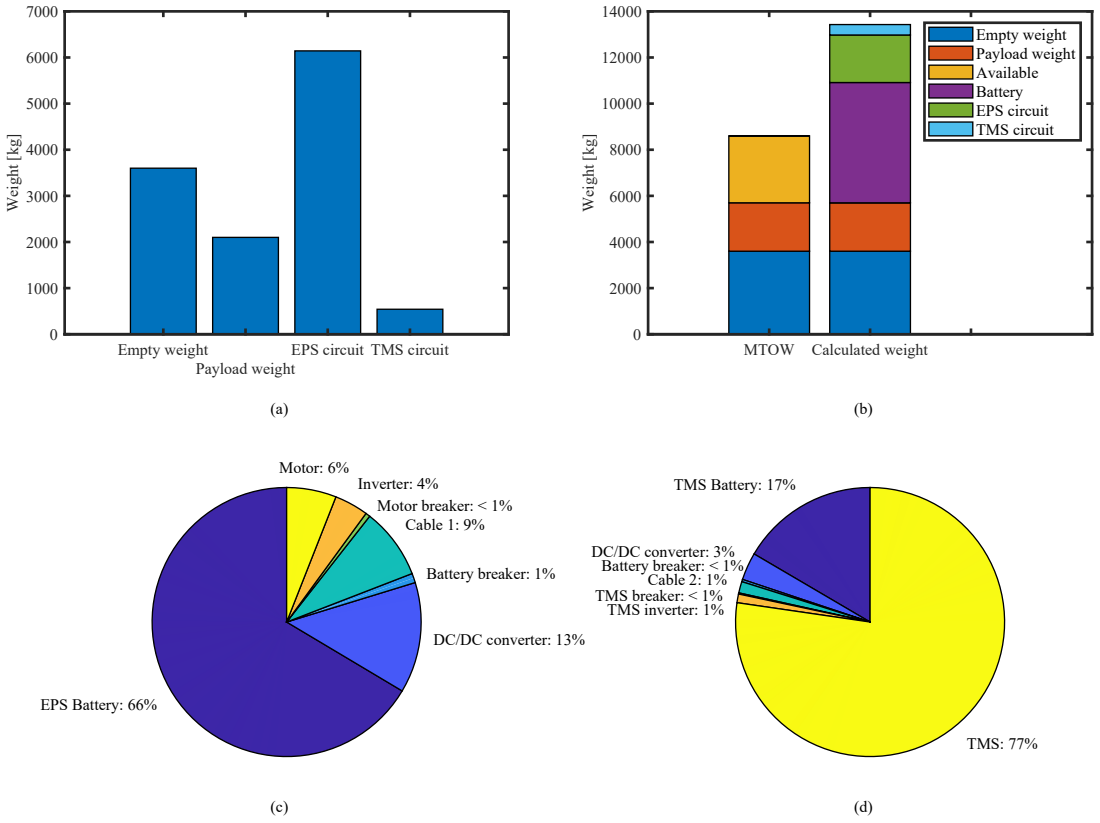

Figure 34: An overview of weight and weight distribution for ES-19 between Tromsø and Hammerfest (211 km). Figure a) shows the weight addition by each weight group. In b), the MTOW of the aircraft is shown against the calculated values. It shows the share of the weight contributed by the battery, while c) and d) shows the weight distribution of the EPS circuit and the TMS circuit respectively.

tion 10.1.4 shows that the battery accounts for most of the weight but that it is responsible for a smaller portion of the EPS than the P-Volt. The cable weight is still substantial and accounts for 10% of the EPS weight. This weight is around the same as the contribution of the motor and inverter combined.

10.1.5 Summary

The parameter values for the P-Volt are compared in Table 17. The flights are compared to the shortest flight between Kirkenes and Vadsø. It shows the trends mentioned above where the most significant change is the battery's capacity increases, increasing battery weight. The other components scale at the same rate and result from the increased propulsion power. It results from the use of specific power for the sizing procedure. An important caveat to the table is that it does not express each component's power rating and weight. The P-Volt has two motors

Table 17: Parameter values for the P-Volt for each distance. For the comparison the shortest flight were used as reference

Component	**Kirkenes-Vadsø (38 km)**	**Bodø-Leknes (103 km)**		**Bodø-Stokmarknes (149 km)**		**Tromsø-Hammerfest (211 km)**	
Symbol	Value	Value	Change	Value	Change	Value	Change
P_{prop}	394.1 kW	447.8 kW	13.6 %	507.4 kW	28.7 %	615.3 kW	56.1 %
P_{TMS}	10.2 kW	11.6 kW	13.6 %	13.2 kW	28.7 %	16.0 kW	56.1 %
P_{bat}	527.4 kW	599.2 kW	13.6 %	679.0 kW	28.7 %	823.4 kW	56.1 %
E_{bat}	68.6 kg	189.1 kg	175.6 %	301.5 kg	339.4 %	505.1 kg	636.1 %
m_{tot}	4202.2 kg	4774.5 kg	13.6 %	5409.7 kg	28.7 %	6560.6 kg	56.1 %
m_{bat}	439.5 kg	945.7 kg	115.2 %	1507.5 kg	243.0 %	2525.3 kg	474.6 %
m_{conv}	175.8 kg	199.7 kg	13.6 %	226.3 kg	28.7 %	274.5 kg	56.1 %
$m_{CB,bat}$	14.9 kg	16.9 kg	13.6 %	19.2 kg	28.7 %	23.2 kg	56.1 %
$m_{cable,1}$	67.2 kg	76.4 kg	13.6 %	86.5 kg	28.7 %	104.9 kg	56.1 %
$m_{CB,motor}$	7.1 kg	8.0 kg	13.6 %	9.1 kg	28.7 %	11.1 kg	56.1 %
m_{inv}	52.7 kg	59.9 kg	13.6 %	67.9 kg	28.7 %	82.3 kg	56.1 %
m_{mot}	77.2 kg	87.7 kg	13.6 %	99.4 kg	28.7 %	120.5 kg	56.1 %
$m_{cable,2}$	1.3 kg	1.4 kg	13.6 %	1.6 kg	28.7 %	2.0 kg	56.1 %
$m_{CB,TMS}$	0.2 kg	0.2 kg	13.6 %	0.2 kg	28.7 %	0.2 kg	56.1 %
$m_{inv,TMS}$	1.2 kg	1.3 kg	13.6 %	1.5 kg	28.7 %	1.9 kg	56.1 %
m_{TMS}	88.2 kg	100.2 kg	13.6 %	113.5 kg	28.7 %	137.7 kg	56.1 %

which means that the total propulsion power generated by each motor is halved and only needs to produce around 300 kW.

Table 18 shows the same parameters for the ES-19. It exhibits the same trends, but the increases occur slower than for the P-Volt. The rate of increase is lowest for the short distances, and as the distance increase, the rate quickens. This increase is most evident for the increase from 149 km to 211 km, where the capacity needs of the battery are doubled despite only increasing the distance by 62 km. It shows the high range dependency for the sizing procedure and illustrates that the shortest routes show the greatest prospects for electrification.

10.2 Scenario 1 - Cruise only

Table 19 compares the flight time of the aircraft to the original flight time used by the Dash 8-100. The table shows two comparisons; the first is the base case presented in the previous sections. The second is with only cruise applied, where the power and time profiles found in Section 7 are omitted, and the speed of the aircraft is assumed to be the cruise speed for the entire flight. Thus, the only factor affecting the flight time is the cruise speed.

The table shows that the P-Volt generally uses twice the original flight time due to the low cruise speed stated in Table 12. The difference is lowest on the shortest trips but grows as the range increases, increasing the cruise phase of flight. This amplifies the difference between the aircraft. Even when omitting the climb and descent phase for the P-Volt, the flight time increase substantially compared to the Dash 8. The difference between the base case and only using cruise is significant for

Table 18: Parameter values for the ES-19 for each distance. For the comparison the shortest flight were used as reference

Component	**Kirkenes-Vadsø (38 km)**	**Bodø-Leknes (103 km)**		**Bodø-Stokmarknes (149 km)**		**Tromsø-Hammerfest (211 km)**	
Symbol	Value	Value	Change	Value	Change	Value	Change
P_{prop}	1208.9 kW	1299.9 kW	7.5 %	1497.3 kW	23.9 %	1872.1 kW	54.9 %
P_{TMS}	31.4 kW	33.8 kW	7.5 %	38.9 kW	23.9 %	48.7 kW	54.9 %
P_{bat}	1617.7 kW	1739.5 kW	7.5 %	2003.6 kW	23.9 %	2505.1 kW	54.9 %
E_{bat}	147.5 kg	375.7 kg	154.7 %	605.8 kg	310.8 %	1042.8 kg	607.1 %
m_{tot}	8671.4 kg	9323.7 kg	7.5 %	10739.5 kg	23.9 %	13427.8 kg	54.9 %
m_{bat}	1348.1 kg	1878.4 kg	39.3 %	3029.1 kg	124.7 %	5214.2 kg	286.8 %
m_{conv}	539.2 kg	579.8 kg	7.5 %	667.9 kg	23.9 %	835.0 kg	54.9 %
$m_{CB,bat}$	45.7 kg	49.1 kg	7.5 %	56.6 kg	23.9 %	70.7 kg	54.9 %
$m_{cable,1}$	338.7 kg	364.2 kg	7.5 %	419.5 kg	23.9 %	524.5 kg	54.9 %
$m_{CB,motor}$	21.7 kg	23.4 kg	7.5 %	26.9 kg	23.9 %	33.7 kg	54.9 %
m_{inv}	161.7 kg	173.8 kg	7.5 %	200.2 kg	23.9 %	250.4 kg	54.9 %
m_{mot}	236.8 kg	254.6 kg	7.5 %	293.2 kg	23.9 %	366.6 kg	54.9 %
$m_{cable,2}$	4.8 kg	5.2 kg	7.5 %	5.9 kg	23.9 %	7.4 kg	54.9 %
$m_{CB,TMS}$	0.5 kg	0.5 kg	7.5 %	0.6 kg	23.9 %	0.8 kg	54.9 %
$m_{inv,TMS}$	3.6 kg	3.9 kg	7.5 %	4.5 kg	23.9 %	5.6 kg	54.9 %
m_{TMS}	270.5 kg	290.8 kg	7.5 %	335.0 kg	23.9 %	418.9 kg	54.9 %

Table 19: Time comparison between the Dash 8-100, P-Volt and ES-19

Route	**Dash 8-100**	**Aircraft**	**Base case**		**Cruise only**	
	t_{ref}		t_{base}	Δt_{base}	t_{cruise}	Δt_{cruise}
Kirkenes-Vadsø (38 km)	10 min	P-Volt	19.1 min	91.3 %	12.8 min	28.4 %
		ES-19	13.0 min	30.4 %	8.6 min	-13.6 %
Bodø-Leknes (103 km)	21 min	P-Volt	41.3 min	96.7 %	34.8 min	65.7 %
		ES-19	28.0 min	33.1 %	23.4 min	11.5 %
Bodø-Stokmarknes (149 km)	27 min	P-Volt	56.5 min	109.3 %	50.3 min	86.4 %
		ES-19	38.2 min	41.4 %	33.9 min	25.4 %
Tromsø-Hammerfest (211 km)	35 min	P-Volt	76.3 min	118.1 %	71.3 min	103.7 %
		ES-19	51.5 min	47.2 %	48.0 min	37.0 %

the short distances. However, as the range increase, the difference decrease.

When considering cruise only, the shortest distance yields a shorter flight time for the ES-19 than for the Dash 8-100. As the Dash 8-100 use time during climb and descent the similar cruise speed of the two aircraft gives this effect. However, for the base case an increase in flight time of 30% is shown for the shortest distance and almost 50% for the longest. This increase makes the difference between the base case and cruise around 45% while it only diverges by 10% between Tromsø and Hammerfest. The difference is expected to converge for long distances. It shows that the cruise speed is sufficient for flight time calculations on long-distance travel. However, it is important to include the climb and descent for the short distances to get a precise result.

An additional case is added in Table 20. It uses the original flight duration from

Table 20: Comparison of total weight, battery capacity and battery power for the base case, cruise only and cruise with adjusted time.

Flight	**Aircraft**	**Base case** t = t_{base}			**Cruise** t = L/v_{cruise}			**Adjusted cruise** t = t_{base}		
		m_{total}	E_{bat}	P_{bat}	Δm_{total}	ΔE_{bat}	ΔP_{bat}	Δm_{total}	ΔE_{bat}	ΔP_{bat}
Kirkenes-Vadsø	P-Volt	4202.2 kg	68.6 kWh	527.4 kW	-12.6 %	-38.2 %	-166.2 %	-7.5 %	21.9 %	-60.2 %
	ES-19	8671.4 kg	147.5 kWh	1617.7 kW	-22.9 %	-47.7 %	-201.7 %	-18.9 %	3.9 %	-65.1 %
Bodø-Leknes	P-Volt	4774.5 kg	189.1 kWh	599.2 kW	-13.5 %	-31.7 %	-169.0 %	-4.4 %	12.0 %	-58.9 %
	ES-19	9323.7 kg	375.7 kWh	1739.5 kW	-19.9 %	-37.8 %	-190.3 %	-10.9 %	3.4 %	-61.7 %
Bodø-Stokmarknes	P-Volt	5409.7 kg	301.5 kWh	679.0 kW	-16.3 %	-32.0 %	-177.9 %	-4.3 %	9.1 %	-58.8 %
	ES-19	10739.5 kg	605.8 kWh	2003.6 kW	-23.4 %	-38.5 %	-203.7 %	-11.6 %	0.0 %	-62.0 %
Tromsø-Hammerfest	P-Volt	6560.6 kg	505.1 kWh	823.4 kW	-20.7 %	-33.9 %	-193.2 %	-4.1 %	6.9 %	-58.8 %
	ES-19	13427.8 kg	1042.8 kWh	2505.1 kW	-29.1 %	-41.5 %	-228.1 %	-13.2 %	-3.7 %	-62.7 %

the base case but assumes constant cruise. Hence, it accounts for the time increase observed due to climb and descent but omits the power frequencies found in Section 7. The table compares the total weight, battery energy, and battery power of the scenarios.

The discrepancy between the base case and the cruise is more significant than between the base case and the adjusted cruise. In both cases, the most significant change is for the power. It is a result of not including climb and takeoff. As these are the most power-consuming phases, the result is expected. Comparing the cruise and adjusted cruise for the P-Volt shows an increase in power for the cruise while the adjusted cruise stabilizes. For the ES-19, it increases at a slow rate.

While the energy consumption of the cruise increase with range, it can be noted that the energy of the adjusted cruise is higher for most flights than for the base case. The energy savings from the descent is not included, and the table shows that this offsets the high energy consumption in the climb and takeoff. This discrepancy is most prominent in the shortest flights and decreases with range. For the longest flight, the ES-19 shows a more energy-consuming base case.

An interesting observation is a variation between the base case and the cruise scenarios for the two shortest. Both aircraft show a lower difference for the parameters between Bodø and Leknes than between Kirkenes and Vadsø. This is an anomaly from trends where the difference tends to increase with longer flight distances. The drop occurs due to the battery's specific power being the limiting factor on the flight between Kirkenes and Vadsø, while the specific power is limiting for longer flights. This consideration is shown in Figs. 35 and 36 for the specific power is limiting for flights below 50 km and 75 km for the P-Volt and ES-19 respectively. It means that the base case battery is oversized with regards to the energy consumption only. As the cruise phase only is limited to energy, this effect is not present. Due to the high base weight of the ES-19 compared to the P-Volt, the change occurs at longer flight distances.

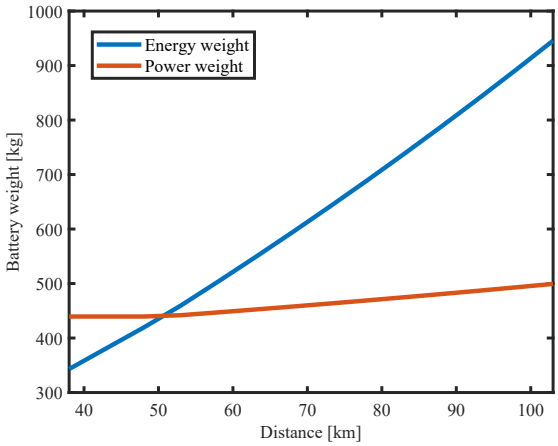

Figure 35: Aircraft weight with regards to the specific energy and specific power for the P-Volt. The highest weight is used for battery sizing.

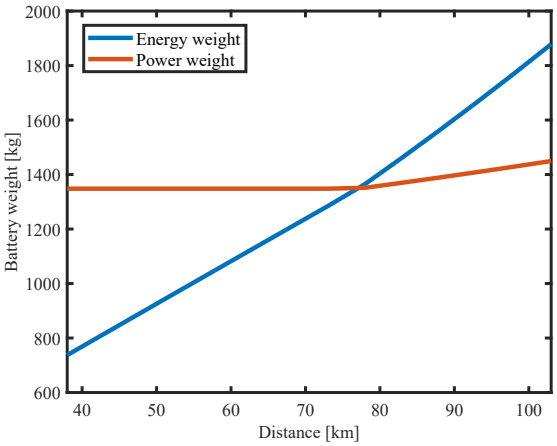

Figure 36: Aircraft weight with regards to the specific energy and specific power for the ES-19. The highest weight is used for battery sizing.

10.3 Scenario 2 - Voltage level sensitivity

Figure 37 and Fig. 38 shows the voltage level sensitivity of the P-Volt and ES-19 weight. It shows weight-savings for higher voltage levels, but these changes are modest. The most significant changes are observed for the ES-19, especially between Tromsø and Hammerfest.

Table 21 shows this more thoroughly. While the changes for the P-Volt are kept within 3%, the ES-19 displays change as high as 8.6%. However, despite the modest changes observed in the total weight of the P-Volt, the weight changes in the cables are substantial. As the cable weight is directly proportional to the current, and thus to the voltage, this is an expected result. Due to the proportionality, the cable weight is nearly doubled when the voltage level is reduced from 1000 V to 540 V. The opposite effect is seen when increasing the voltage. However, some incremental changes are observed beyond the changes caused directly by the voltage. It occurs as the aircraft weight reductions decrease the propulsion requirements. Hence, the requirements for the rest of the components are slightly lower, reducing their weight. This effect significantly impacts the ES-19 as it operates at higher power than the P-Volt. The cables are also a proportionally larger part of the weight, as shown in the previous sections.

10.4 Scenario 3 - Addition of gear

The benefits of adding gears to the EPS are dependent on whether the reduction in the motor weight outweighs the increased losses and weight addition of the gear. Figures 39 and 40 shows the effects of adding the gear at different gear ratios to the P-Volt and ES-19, respectively. As the specific power of the motor is expected to double for each gear ratio doubling, the motor weight is halved. Simultaneously, the gear increase in weight for higher gear ratios. However, the weight reductions

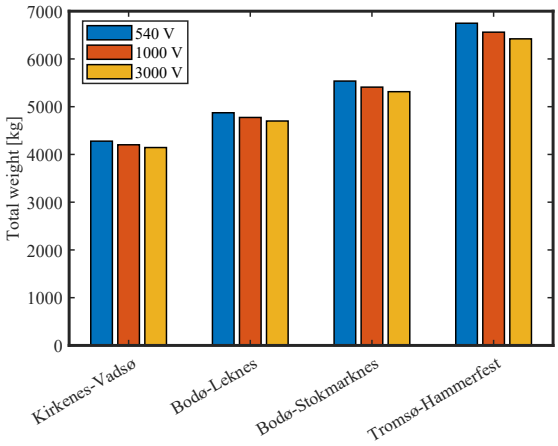

Figure 37: P-Volt weight at different voltage levels

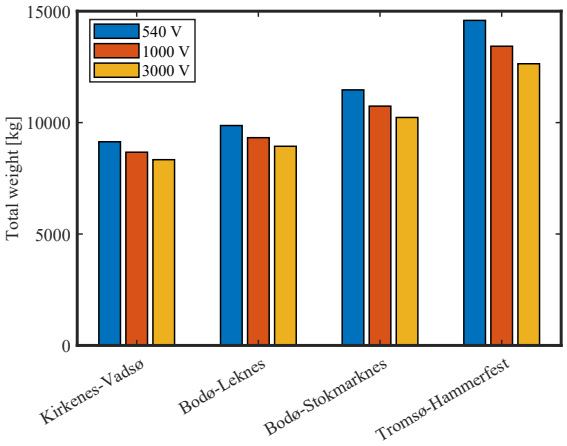

Figure 38: ES-19 weight at different voltage levels

Table 21: Sensitivity of total weight and total cable weight for each aircraft, distance and voltage level.

Case		**P-Volt**				**ES-19**			
		Cable weight		Total weight		Cable weight		Total weight	
Distance	Voltage level	Weight	Change	Weight	Change	Weight	Change	Weight	Change
Kirkenes-Vadsø (38 km)	540 V	129.1 kg	88.5 %	4278.3 kg	1.8 %	670.6 kg	95.2 %	9140.6 kg	5.4 %
	1000 V	68.5 kg	-	4202.2 kg	-	343.5 kg	-	8671.4 kg	-
	3000 V	22.5 kg	-67.1 %	4144.4 kg	-1.4 %	110.1 kg	-68.0 %	8336.4 kg	-3.9 %
Bodø-Leknes (103 km)	540 V	147.1 kg	89.0 %	4873.1 kg	2.1 %	724.0 kg	96.0 %	9868.5 kg	5.8 %
	1000 V	77.8 kg	-	4774.5 kg	-	369.4 kg	-	9323.7 kg	-
	3000 V	25.5 kg	-67.2 %	4700.1 kg	-1.6 %	118.0 kg	-68.0 %	8937.6 kg	-4.1 %
Bodø-Stokmarknes (149 km)	540 V	167.1 kg	89.5 %	5536.6 kg	2.3 %	841.4 kg	97.8 %	11468.7 kg	6.8 %
	1000 V	88.2 kg	-	5409.7 kg	-	425.5 kg	-	10739.5 kg	-
	3000 V	28.9 kg	-67.3 %	5314.4 kg	-1.8 %	135.1 kg	-68.2 %	10230.4 kg	-4.7 %
Tromsø-Hammerfest (211 km)	540 V	203.7 kg	90.5 %	6748.1 kg	2.9 %	1070.2 kg	101.2 %	14587.6 kg	8.6 %
	1000 V	106.9 kg	-	6560.6 kg	-	532.0 kg	-	13427.8 kg	-
	3000 V	34.9 kg	-67.4 %	6420.9 kg	-2.1 %	166.9 kg	-68.6 %	12641.3 kg	-5.9 %

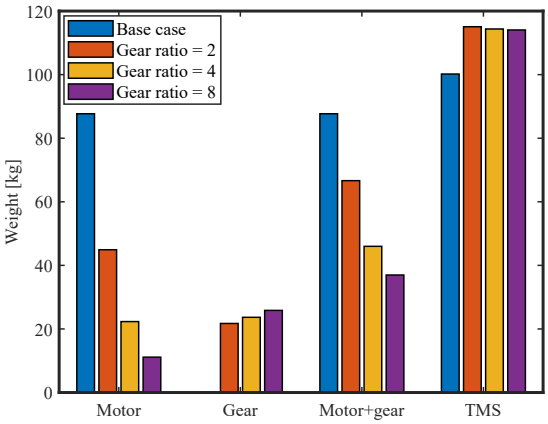

Figure 39: Weight of gear, motor and TMS at different gear ratios for the P-Volt between Bodø and Leknes.

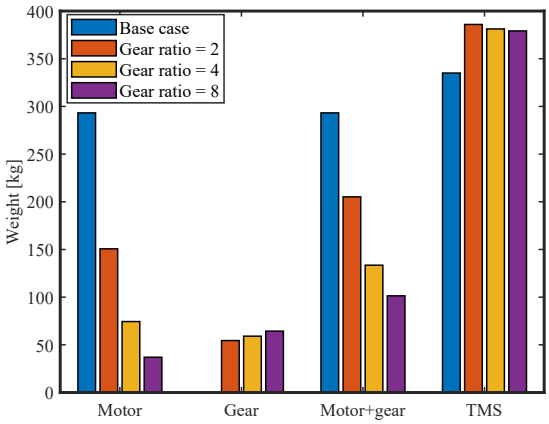

Figure 40: Weight of gear, motor and TMS at different gear ratios for the ES-19 between Bodø and Stokmarknes.

in the motor outweigh these increases, and the combined motor and gear weight is reduced. It improves as the gear ratio increase.

However, as the gear adds another inefficiency to the system, the heat dissipation in the EPS is increased. This heat is handled by the TMS, which increases in weight, as seen in the figures. It will also increase the size of the components in the TMS circuit as these are proportional to the TMS size. As the gear ratio increase, the TMS weight decreases slightly. Since the gear and motor weight decrease, this leads the propulsion power of the aircraft to reduce, reducing the power flow to the motors, thus reducing the heat losses.

Table 22 shows the effects the gear has on the power requirements of the battery and the aircraft weight. The general trend is that higher gear ratios are more advantageous than low gear ratios. Especially on short distances with high gear ratio it can result in significant weight-savings. The P-Volt only experience weight reductions on the two shortest distances, while the ES-19 shows weight improvements at all distances when applying a high gear ratio. The weight contribution of the motor is slightly higher for the ES-19, which leads to more significant improvements.

The battery power is, however, increased. It is due to the increased losses but is also a result of the increased size of the TMS. The increased power consumption adds weight to the battery, and as the flight distance increase, the effect on the battery capacity will increase. At long flights this capacity increase will outweigh the benefits of the EPS and result in weight additions for the aircraft. This trend is increased by the increased power requirement of the TMS circuit. However, as weight is considered the most critical parameter, gears can be advantageous, especially for shorter trips.

Table 22: Battery power and total weight comparison for the addition of gear for the P-Volt and ES-19.

Case		P-Volt				ES-19			
		Battery power		Total weight		Battery power		Total weight	
Distance	Gear ratio	Value	Change	Value	Change	Value	Change	Value	Change
	Base case	527.4 kW	-	4202.2 kg	-	1617.7 kW	-	8671.4 kg	-
Kirkenes-Vadsø	2	541.4 kW	2.6 %	4216.6 kg	0.3 %	1661.5 kW	2.7 %	8705.8 kg	0.4 %
(38 km)	4	538.4 kW	2.1 %	4193.8 kg	-0.2 %	1645.4 kW	1.7 %	8621.1 kg	-0.6 %
	8	537.2 kW	1.9 %	4183.8 kg	-0.4 %	1638.1 kW	1.3 %	8583.2 kg	-1.0 %
	Base case	599.2 kW	-	4774.5 kg	-	1739.5 kW	-	9323.7 kg	-
Bodø-Leknes	2	617.2 kW	3.0 %	4807.2 kg	0.7 %	1789.9 kW	2.9 %	9378.4 kg	0.6 %
(103 km)	4	613.4 kW	2.4 %	4777.5 kg	0.1 %	1771.1 kW	1.8 %	9280.1 kg	-0.5 %
	8	611.7 kW	2.1 %	4764.5 kg	-0.2 %	1762.7 kW	1.3 %	9236.1 kg	-0.9 %
	Base case	679.0 kW	-	5409.7 kg	-	2003.6 kW	-	10739.5 kg	-
Bodø-Stokmarknes	2	702.0 kW	3.4 %	5467.3 kg	1.1 %	2070.1 kW	3.3 %	10846.6 kg	1.0 %
(149)	4	697.0 kW	2.7 %	5428.8 kg	0.4 %	2045.0 kW	2.1 %	10715.0 kg	-0.2 %
	8	694.9 kW	2.3 %	5412.0 kg	0.0 %	2033.7 kW	1.5 %	10656.0 kg	-0.8 %
	Base case	823.4 kW	-	6560.6 kg	-	2505.1 kW	-	13427.8 kg	-
Tromsø-Hammerfest	2	857.1 kW	4.1 %	6675.8 kg	1.8 %	2608.3 kW	4.1 %	13666.5 kg	1.8 %
(211 km)	4	849.7 kW	3.2 %	6618.2 kg	0.9 %	2568.4 kW	2.5 %	13457.5 kg	0.2 %
	8	846.5 kW	2.8 %	6592.9 kg	0.5 %	2550.5 kW	1.8 %	13363.7 kg	-0.5 %

10.5 Scenario 4 - Battery losses

Including losses in the battery will increase the dissipated heat in the circuit and thus increase the strain on the TMS. The battery also needs to store more energy as more energy is lost in the system. Both of these effects will increase the weight of the system. These trends are observed in Figs. 41 and 42 where the change in weight with and without the battery loss are compared. The right-hand bar includes the losses, while the left-hand bar is the base case for each distance. The figure excludes the empty weight and the payload weight and only displays the weight of the electric system. A significant weight increase is observed for the battery in all cases. The increase is most evident for the longest flights. It is harder to observe changes in the other components. However, a weight gain in the TMS circuit can be observed.

The TMS increase is emphasized in Table 23 where the most significant parameter changes are shown. The aircraft's total weight follows the trends of the previous scenarios, where the changes are most evident for the longest flights and more significant for the ES-19 than for the P-Volt. Generally, including the battery losses affects the aircraft weight substantially, with more than 5% for the P-Volt and more than 7% for the ES-19. It is mainly a result of the battery and TMS weight increases, where the most significant increase is for the TMS. The same increase is expected for all TMS circuit components. Despite the battery losses only being 4.1% of the power, the effect on the battery weight is substantially higher. It occurs due to the weight increases seen for the other components and the system's interconnectedness.

The increased strain on the TMS is evident in Figs. 43 and 44 where the heat losses for the P-Volt and the ES-19 between Bodø and Stokmarknes are shown. The proportion of the losses is similar for each aircraft, but the amplitude is different. It is a result of using the same system architecture for both aircraft. The figures show that the losses in the TMS circuit are negligible. It is due to the low power

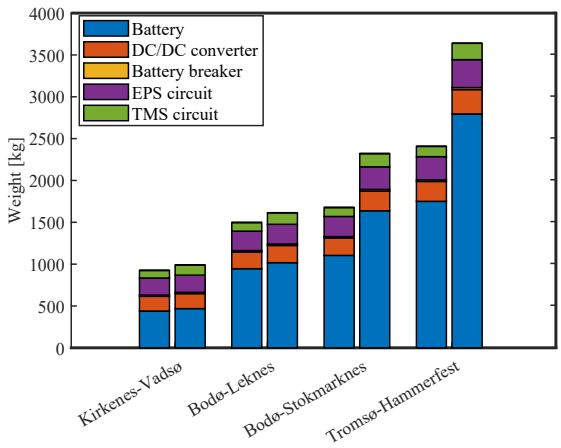

Figure 41: Weight of the electric power train for the ES-19 with battery losses.

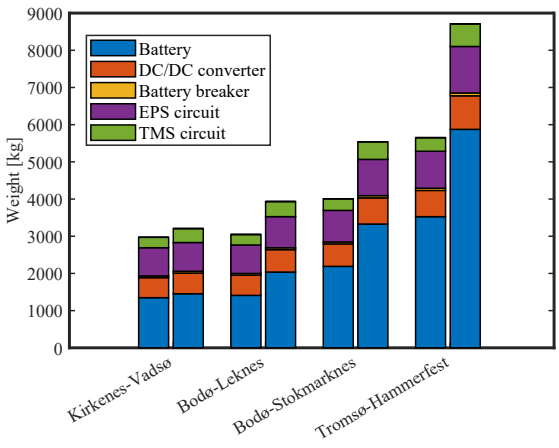

Figure 42: Weight of the electric power train for the ES-19 with battery losses.

Table 23: Parameter changes with battery losses compared to base case for the P-Volt.

Case		**P-Volt**			**ES-19**		
		Total weight	Battery weight	TMS weight	Total weight	Battery weight	TMS weight
Kirkenes-Vadsø (38 km)	Base case	4202.2 kg	439.5 kg	88.2 kg	8671.4 kg	1348.1 kg	270.5 kg
	Battery loss	4266.5 kg	468.4 kg	117.2 kg	8906.8 kg	1453.5 kg	363.7 kg
	Change	1.5 %	6.6 %	32.9 %	2.7 %	7.8 %	34.5 %
Bodø-Leknes (103 km)	Base case	4774.5 kg	945.7 kg	100.2 kg	9323.7 kg	1878.4 kg	290.8 kg
	Battery loss	4891.4 kg	1017.0 kg	134.4 kg	9633.6 kg	2037.3 kg	393.4 kg
	Change	2.4 %	7.5 %	34.1 %	3.3 %	8.5 %	35.3 %
Bodø-Stokmarknes (149 km)	Base case	5409.7 kg	1507.5 kg	113.5 kg	10739.5 kg	3029.1 kg	335.0 kg
	Battery loss	5598.4 kg	1637.6 kg	153.8 kg	11240.8 kg	3328.0 kg	459.0 kg
	Change	3.5 %	8.6 %	35.5 %	4.7 %	9.9 %	37.0 %
Tromsø-Hammerfest (211 km)	Base case	6560.6 kg	2525.3 kg	137.7 kg	13427.8 kg	5214.2 kg	418.9 kg
	Battery loss	6916.3 kg	2794.5 kg	190.0 kg	14410.7 kg	5874.0 kg	588.5 kg
	Change	5.4 %	10.7 %	38.0 %	7.3 %	12.7 %	40.5 %

demands of the TMS compared to the EPS. It is also a result of the high efficiencies of the cables and breakers, which is evident in the EPS circuit.

The single most significant contributor to heat losses is the battery. The battery feeds both circuits with power and needs to account for all the heat losses downstream towards the motors and TMS. Hence, it has the highest power rating, which results in the highest power losses as the efficiencies of the components are similar. The downstream losses are also evident for the other components, with the power losses decreasing due to lower power levels when approaching the motors.

10.6 Scenario 5 - Redundancy

While the other changes have been modest, only making minor changes to parameters in the original circuit, the redundancy requirement alters the circuit significantly. It includes multiple new CBs and a doubling of the distribution cables.

The weight results are shown in Figs. 45 and 46 for the P-Volt and ES-19, respect-

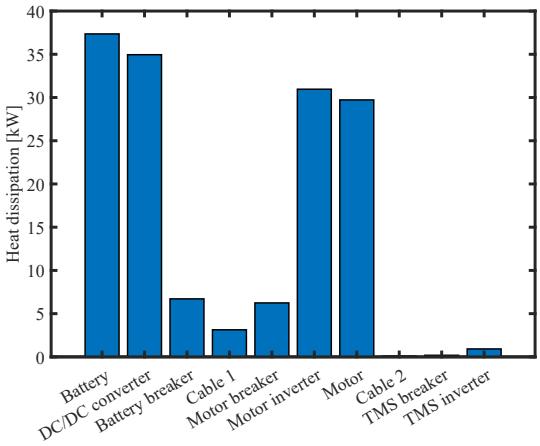

Figure 43: Heat losses of each component in the system for the P-Volt between Bodø and Stokmarknes (149 km).

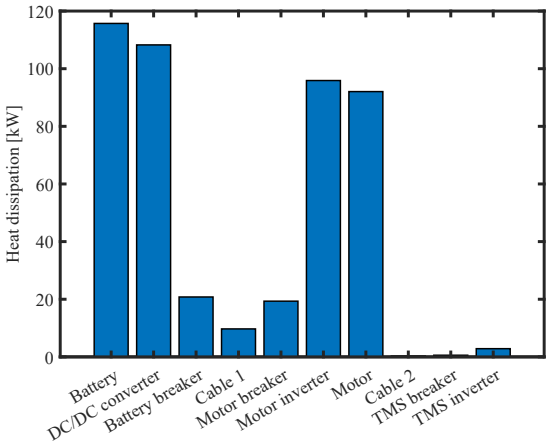

Figure 44: Heat losses of each component in the system for the ES-19 between Bodø and Stokmarknes (149 km).

ively. The figures show that while adding the components to the base case will give an additional weight gain, the weight gain is substantially lower than when including them prior to the sizing algorithm. Due to the system's interconnectivity, the weight spirals beyond the added weight of the new component. This effect is most apparent for the longer travel distances and the ES-19. However, it shows significant weight increases for the P-Volt with a weight gain of approximately 20% for the distance between Tromsø and Hammerfest. The ES-19, on the other hand, shows a weight gain of around 70% for the same distance, while the added components results in a minor increase.

In Table 24 the weight changes for the P-Volt are shown. The table only shows the results when redundancy is introduced before the sizing calculation. It shows a weight increase between 10% and 20% depending on the distance. This increase is almost the same as the battery changes. An exemption is between Kirkenes and Vadsø, where the battery weight is significantly increased compared to the total weight. An additional DC/DC converter is added, and three battery breakers are needed. However, the weight addition is higher than the weight of the components, with the DC/DC breaker adding another 24-40% weight even considering the doubling. The battery breaker experiences the same effect as it increases by more than 200%. The EPS and TMS circuits show more modest increases despite the additional components. It is due to the increases only applying to cables and breakers while the number of motors and inverters is kept constant. The redundancy requirements increase the TMS weight by 21.3% in the calculations. However, the weight added to the TMS is significantly larger due to additional losses.

The same trends are applicable for the ES-19 as shown in Table 25. However, the trends increase, and the battery weight is more than doubled for the distance between Tromsø and Hammerfest. The same applies to the rest of the components, where they all display at least a doubling, while the battery breaker weighs more than five times the base case value.

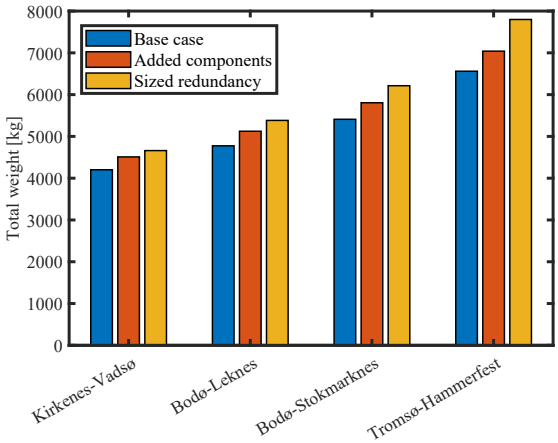

Figure 45: Weight of P-Volt for base case, with redundancy components added and with redundancy calculated through sizing algorithm. The empty weight and payload weight is omitted as they are constant.

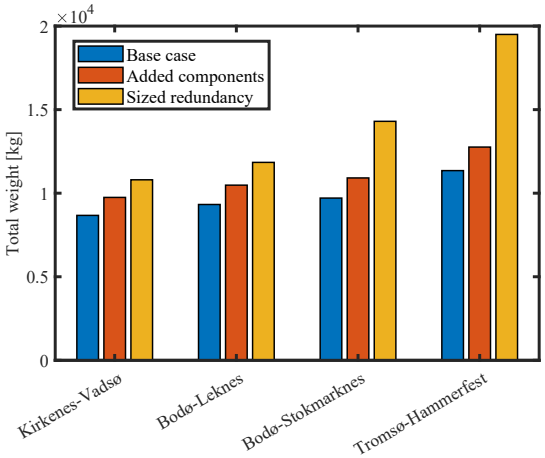

Figure 46: Weight of ES-19 for base case, with redundancy components added and with redundancy calculated through sizing algorithm. The empty weight and payload weight is omitted as they are constant.

Table 24: Comparison between the base case and the P-Volt with redundancy applied for the total weight and for each of the main components.

Case		m_{tot}	m_{bat}	m_{conv}	$m_{CB,bat}$	EPS circuit[1]	TMS circuit[1]
Kirkenes-Vadsø (38 km)	Base case	4202.2 kg	439.5 kg	175.8 kg	14.9 kg	204.2 kg	90.8 kg
	Redundancy	4660.6 kg	707.2 kg	393.6 kg	50.0 kg	317.7 kg	130.3 kg
	Change	10.9 %	60.9 %	123.9 %	235.8 %	55.6 %	43.5 %
Bodø-Leknes (103 km)	Base case	4774.5 kg	945.7 kg	199.7 kg	16.9 kg	232.0 kg	103.2 kg
	Battery loss	5382.9 kg	1076.1 kg	454.6 kg	57.8 kg	366.9 kg	150.5 kg
	Change	12.7 %	13.8 %	127.6 %	241.4 %	58.2 %	45.9 %
Bodø-Stokmarknes (149)	Base case	5409.7 kg	1507.5 kg	226.3 kg	19.2 kg	262.9 kg	116.9 kg
	Battery loss	6213.1 kg	1747.4 kg	524.7 kg	66.7 kg	423.5 kg	173.8 kg
	Change	14.8 %	15.9 %	131.8 %	247.8 %	61.1 %	48.6 %
Tromsø-Hammerfest (211 km)	Base case	6560.6 kg	2525.3 kg	274.5 kg	23.2 kg	318.8 kg	141.8 kg
	Battery loss	7798.9 kg	3029.9 kg	658.6 kg	83.7 kg	531.6 kg	218.1 kg
	Change	18.9 %	20.0 %	140.0 %	259.9 %	66.8 %	53.9 %

Table 25: Comparison between the base case and the ES-19 with redundancy applied for the total weight and for each of the main components.

Case		m_{tot}	m_{bat}	m_{conv}	$m_{CB,bat}$	EPS circuit[1]	TMS circuit[1]
Kirkenes-Vadsø (38 km)	Base case	8671.4 kg	1348.1 kg	539.2 kg	45.7 kg	758.9 kg	279.4 kg
	Redundancy	10801.4 kg	2300.9 kg	1355.9 kg	172.3 kg	1426.9 kg	451.4 kg
	Change	24.6 %	70.7 %	151.4 %	277.2 %	88.0 %	61.6 %
Bodø-Leknes (103 km)	Base case	9323.7 kg	1878.4 kg	579.8 kg	49.1 kg	816.0 kg	300.4 kg
	Battery loss	11843.2 kg	2408.1 kg	1486.7 kg	188.9 kg	1564.5 kg	495.0 kg
	Change	27.0 %	28.2 %	156.4 %	284.6 %	91.7 %	64.7 %
Bodø-Stokmarknes (149)	Base case	9707.7 kg	2190.5 kg	603.7 kg	51.1 kg	849.6 kg	312.8 kg
	Battery loss	14251.9 kg	4057.2 kg	1789.1 kg	227.3 kg	1882.7 kg	595.6 kg
	Change	46.8 %	85.2 %	196.4 %	344.5 %	121.6 %	90.4 %
Tromsø-Hammerfest (211 km)	Base case	11351.1 kg	3526.2 kg	705.9 kg	59.8 kg	993.4 kg	365.8 kg
	Battery loss	19474.0 kg	7632.4 kg	2444.6 kg	310.6 kg	2572.6 kg	813.9 kg
	Change	71.6 %	116.4 %	246.3 %	419.5 %	159.0 %	122.5 %

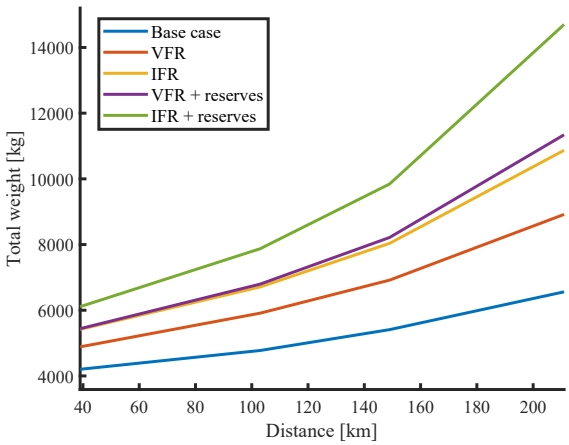

Figure 47: Weight of P-Volt as a function of flight distance with varying reserve requirements.

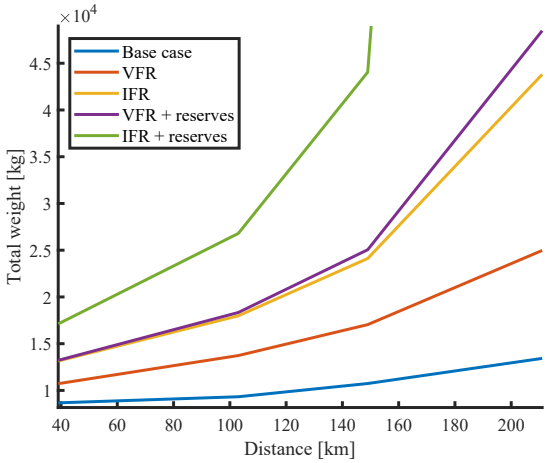

Figure 48: Weight of ES-19 as a function of flight distance with varying reserve requirements.

10.7 Scenario 6 - Energy reserves

The final regulation tested is the addition of reserves. Four reserve conditions are tested. These are the VFR, IFR, full VFR, and full IFR.

In Figs. 47 and 48 the weight of the the P-Volt and ES-19 are shown. They show that as the flight distance increase, the rate of weight increases for the aircraft quickens. For the ES-19, the high reserves scenario with IFR conditions and extra reserves, the aircraft reached its maximum distance at around 149 km. At longer distances, the aircraft's weight increases rapidly, making the system diverge.

It is observed that the difference between IFR conditions and the full VFR conditions is minor. Fifteen minutes of extra cruise is added for the transition from VFR to IFR conditions, while the full reserves add 15 minutes plus another 5% of the flight distance. The flight distance is generally short, so the additional 5% does not significantly impact the reserves. It is still evident that the impact increase as the flight distance does.

Table 26 shows the aircraft weight and the battery capacity for the different cases. The weight results underscore the aforementioned effects of the energy reserves. As the reserves directly impact the capacity needs of the battery, it also adds battery weight, and the battery weight increases. It will take up an increasingly significant proportion of the total weight. However, as the increase will affect the power requirements for the aircraft, the weight of the other components will also increase.

The capacity changes for the ES-19 battery are around twice the changes for the P-Volt. As the aircraft is twice the weight, this is an expected result. However, the increase is more significant on longer distances, leading to non-convergence for full IFR conditions between Tromsø and Hammerfest. Despite having convergence for the rest of the cases, the weight gains are substantial. Hence, adding reserve requirements for short-distance flights on the short-haul network can limit the implementation of electric aircraft.

Table 26: Parameter change for the P-Volt and ES-19 with the different reserve requirements added. Full VFR/IFR is the VFR or IFR conditions with extra reserves for rerouting and loiter.

Case		**P-volt**				**ES-19**			
		Total weight		Battery capacity		Total weight		Battery capacity	
Distance	Reserves	Value	Change	Value	Change	Value	Change	Value	Change
Kirkenes-Vadsø (38 km)	Base case	4202.2 kg	-	68.6 kWh	-	8671.4 kg	-	147.5 kWh	-
	VFR	4885.5 kg	16.3 %	208.8 kWh	204.3 %	10723.8 kg	23.7 %	603.3 kWh	309.1 %
	IFR	5418.8 kg	29.0 %	303.1 kWh	341.7 %	13151.6 kg	51.7 %	997.9 kWh	576.7 %
	Full VFR	5439.1 kg	29.4 %	306.7 kWh	347.0 %	13220.6 kg	52.5 %	1009.1 kWh	584.3 %
	Full IFR	6108.3 kg	45.4 %	425.1 kWh	519.5 %	17115.8 kg	97.4 %	1642.4 kWh	1013.6 %
Bodø-Leknes (103 km)	Base case	4774.5 kg	-	189.1 kWh	-	9323.7 kg	-	375.7 kWh	-
	VFR	5911.6 kg	23.8 %	390.3 kWh	106.3 %	13731.6 kg	47.3 %	1092.2 kWh	190.7 %
	IFR	6710.7 kg	40.6 %	531.6 kWh	181.1 %	17982.2 kg	92.9 %	1783.2 kWh	374.7 %
	Full VFR	6795.9 kg	42.3 %	546.7 kWh	189.0 %	18336.6 kg	96.7 %	1840.8 kWh	390.0 %
	Full IFR	7873.8 kg	64.9 %	737.3 kWh	289.8 %	26794.1 kg	187.4 %	3215.7 kWh	756.0 %
Bodø-Stokmarknes (149 km)	Base case	5409.7 kg	-	301.5 kWh	-	10739.5 kg	-	605.8 kWh	-
	VFR	6917.3 kg	27.9 %	568.2 kWh	88.4 %	17039.9 kg	58.7 %	1630.0 kWh	169.1 %
	IFR	8037.1 kg	48.6 %	766.2 kWh	154.1 %	24113.0 kg	124.5 %	2779.8 kWh	358.8 %
	Full VFR	8215.6 kg	51.9 %	797.8 kWh	164.6 %	25052.0 kg	133.3 %	2932.5 kWh	384.0 %
	Full IFR	9844.8 kg	82.0 %	1086.0 kWh	260.2 %	44047.4 kg	310.1 %	6020.4 kWh	893.7 %
Tromsø-Hammerfest (211 km)	Base case	6560.6 kg	-	505.1 kWh	-	13427.8 kg	-	1042.8 kWh	-
	VFR	8917.4 kg	35.9 %	922.0 kWh	82.5 %	24972.9 kg	86.0 %	2919.6 kWh	180.0 %
	IFR	10869.9 kg	65.7 %	1267.3 kWh	150.9 %	43803.4 kg	226.2 %	5980.7 kWh	473.5 %
	Full VFR	11342.0 kg	72.9 %	1350.8 kWh	167.5 %	48477.9 kg	261.0 %	6740.6 kWh	546.4 %
	Full IFR	14700.5 kg	124.1 %	1944.9 kWh	285.1 %				

Figures 49 and 50 shows the battery weight for the P-Volt and ES-19 as separated into the contribution from the EPS circuit, TMS circuit, reserves, and SOC requirement. The figures show that the reserves are the majority contributor to the battery weight, especially for the shortest routes. For both aircraft, the SOC is not a limitation for the shortest distance between Kirkenes and Vadsø. However, as the reserves are added, the energy is the limiting factor, and the SOC is included. For the ES-19 between Kirkenes and Vadsø, the full IFR reserves add nearly 7000 kg of battery weight compared to only 1000 kg needed for the propulsion, TMS, and SOC reserves. This ratio decreases with flight distance as the aircraft use more energy. It is still around half the battery weight when including full VFR between Bodø and Stokmarknes for the ES-19.

The EPS circuit requires more of the total battery capacity as the distance increase, while the contribution of the TMS is negligible for all cases.

11 Discussion

In the discussion, an attempt to gather the results presented in all the previous parts is conducted. The issues are addressed and possible solutions for all-electric flights are presented.

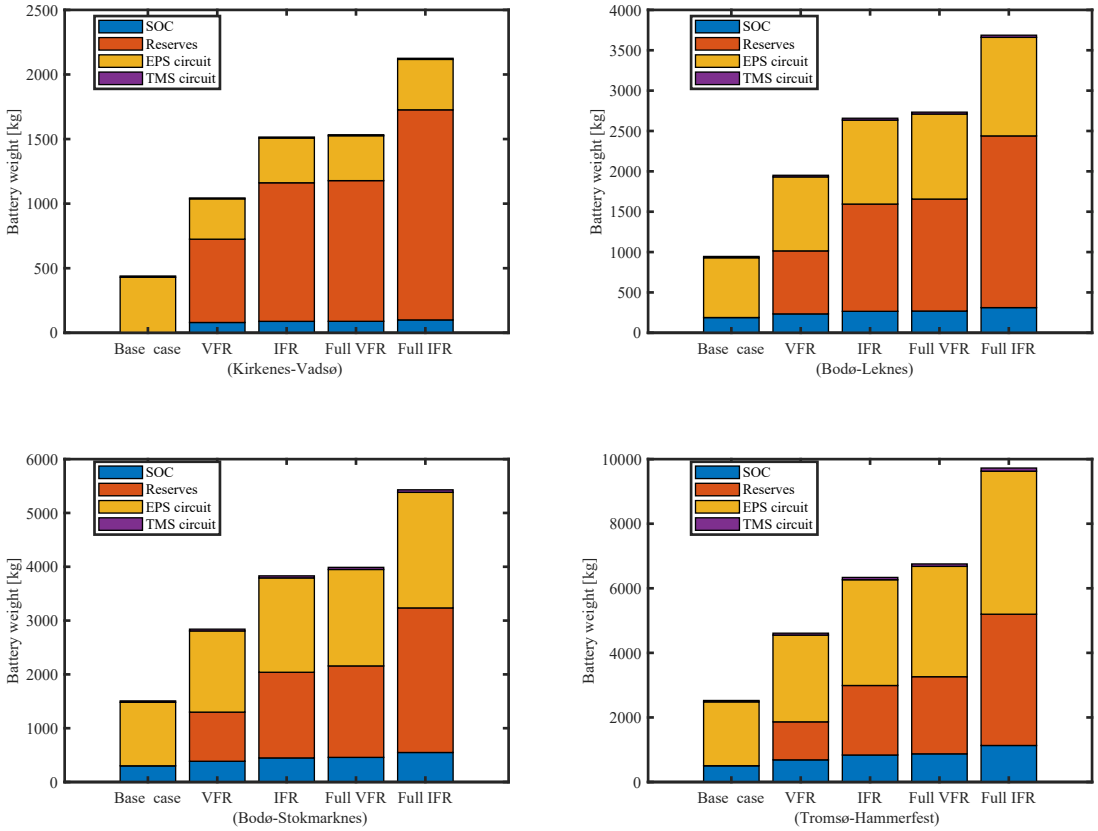

Figure 49: Battery weight shown by contribution from the EPS circuit the TMS circuit and the energy reserves for the P-Volt.

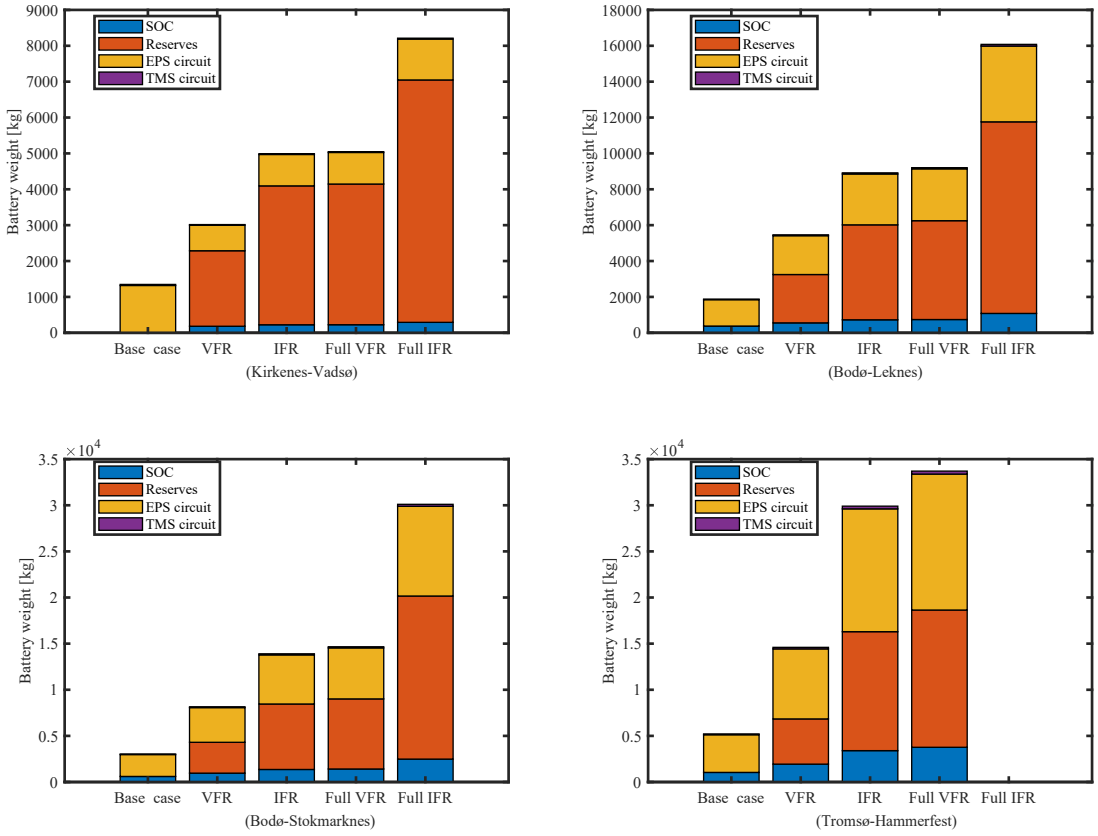

Figure 50: Battery weight shown by contribution from the EPS circuit the TMS circuit and the energy reserves for the ES-19.

11.1 Results

The results presented in this thesis give a bleak prospect for the electrification of the aviation industry. It shows that the conversion to electric propulsion is a challenge, even for the shortest routes. Even for the base case scenarios presented in Section 10.1, which only assumes the minimum requirements for flight, the total weight of the aircraft exceeds the limits of the MTOW. It is, however, only by a slim margin and could be manageable with minor improvements or reductions in payload weight. As the distance increase, this margin increases, and for the 211 km between Tromsø and Hammerfest, both aircraft exceed the MTOW by a considerable margin.

The battery is the most significant weight addition and adds almost 50% of the weight for the distance between Tromsø and Hammerfest for both aircraft. It has been pointed out as one of the main limiters for electric aviation, and the data from this thesis backs up the claim. New battery compositions exhibiting higher specific energy are needed even for the short flights on the short-haul network. The flight distances analyzed are in the lower half of the routes on the short-haul network, and if these distances are too long, the prospect for other routes is low.

Despite the most significant improvements being attributed to the battery's specific energy, the specific power is shown to affect the system. For the short distance flight between Kirkenes and Vadsø, the specific power limits the weight of the battery. Hence, the battery does not increase in weight before the specific energy becomes the limiting factor, which gives a constant power requirement until this event occurs. The flight distance this occurs on is shown in Figs. 35 and 36 and due to the required power being constant prior to the change, the weight of the aircraft would be constant. Hence, this establishes the minimum weight of the aircraft. The components are sized by the maximum power which occurs during takeoff regardless of flight distance. The battery need to deliver this power, making the specific power the dimensioning factor. Hence, the calculated weight of the base case scenarios are the minimum weight of each aircraft. Furthermore, it shows that while the distance is below 50 km for the P-Volt and below 75 km can operate them without any weight alterations.

The base case results do not show great promise for the electrification of the short-haul network. However, there are uncertainties for the parameter choices, and due to the interconnections of the electrical system, minor improvements for the components could yield significant improvements for the system as a whole. It is also possible to state that the choice of component performance is conservative despite the attempt to provide probable state-of-the-art values. Due to the uncertainties, the base results could be overly cautious, and more optimistic results could be attained. Adding constraints and weight to an already pessimistic result could be considered unnecessary. However, despite the uncertainties in the base results, the trends and limitations shown when adding regulations and additional weights will be applied independently of parameter choices. It will also enhance the insights into where improvements will yield the most significant impact.

The Breguet range equation for electric aircraft is commonly used to estimate the weight or range of an electric aircraft. However, the equation assumes that the

aircraft operates in cruise for the entire flight. As shown in Section 10.2 this gives a inaccurate result. The power requirement during cruise is substantially lower than for the takeoff and climb phase. Hence, sizing the components by the cruise power would result in underdimensioned components. The low power level will also decrease the losses in the circuit resulting in an underdimensioned TMS. The energy and weight of the aircraft are also substantially increased when accounting for takeoff and climb.

Additionally, by assuming constant cruise speed, the flight time is heavily reduced compared to using the flight data from the short-haul network. It is shown in Table 19 where it is evident that the most significant disparity is for the shortest flights. The time assumption could be sufficient for long-distance travel. However, as the travel distance increase, it is shown that the power discrepancy increase. So despite getting more precise results for the battery weight and flight time, this is traded for lower accuracy for the sizing of the components.

Significant effects were seen for the battery weight and the TMS by applying battery losses. These saw a rise in weight as the power stored in the battery increased and the heat produced in the battery needed to be handled. However, the battery's efficiency is likely to deteriorate over its lifetime. This reduction occurs as the internal resistance of the battery increases. Additionally, it will reduce the power and energy it can deliver and reduce the aircraft's range further. It will also increase the strain on the TMS, increasing the TMS weight. The results show that omitting the battery losses could lead to an undersized TMS, which could be a safety issue as its components would be overheated. The range of the aircraft would also be substantially decreased as the battery would be underdimensioned. However, a possibility would be to use the excess heat for secondary purposes as heating the cabin or de-icing the wings, reducing the power requirement in these processes.

The TMS is a minor contributor to the weight of the aircraft. However, it is an essential part of the electrical system and needs to be accounted for. It affects the capacity requirements of the battery, and despite the low weight attributed to it, the base case results show that the TMS is accountable for 2% and 3% of the total weight of the P-Volt and ES-19 respectively. This proportion is higher when including the battery losses. The rest of the TMS circuit is barely noticeable and could be omitted for more straightforward calculations.

The safety measures prove to be the most challenging requirements to implement. The inclusion of redundancy includes multiple new CBs and a new distribution line. These additions should enable the system to operate even if a fault is experienced at a critical location. However, as shown, the weight gain from the redundancy is significant. The inclusion of another loss component to the circuit increases the requirements for the TMS, resulting in a larger TMS. In addition to the direct weight gain caused by the increase in CBs and distribution lines, the power requirements caused by these additions propagate through the system. It leads to high weight increases for the ES-19, making it unfeasible for the longer distances as the weight is increased by 70% compared to the base case. It also explains why adding the components after the sizing procedure is unsatisfactory. As each weight gain affect the total system, the redundancy requirements need to be included at the beginning

of the design procedure to avoid an underdimensioned propulsion system. As the base case weights are already too high, the addition of redundancy would further increase the gap. The P-Volt does not experience as negative weight impact as the ES-19. However, adding redundancy results in a 20% increase in weight for long distances, which would affect its ability to operate on the routes.

The redundancy increases the aircraft's weight, which again increases the aircraft's required propulsion power. On the other hand, the reserve requirements add energy requirements directly to the battery. However, as this will increase the weight of the battery, it results in the same overall increase. The requirements are universal and apply to all operating aircraft which is a significant issue for the short distances on the short-haul network. As the flight duration is as low as 10-20 minutes for the shortest distance, it is evident that adding 30-60 minutes of energy reserves will impact the weight negatively. The results support this with the capacity for the shortest distances mainly retained for the energy reserves. The portion retained for the reserves reduce as the distance increase, but the effects on the weight increase. So despite the reserves changing the battery composition for the short flights to a greater extent than for the longer, the most significant impact occurs for the longer distances. For the distance from Tromsø to Hammerfest, the weight does not diverge for the full IFR conditions, which means that the flight is unachievable for the ES-19.

An opportunity could be present in the minimum SOC of the battery. In the sizing, it is not allowed to fall below 20% due to the deteriorating effects it has on the battery's lifetime. However, it could be viable for emergency use and as a reserve. As the aircraft is required to land with the reserves in the fuel tank (to avoid investigations), the use of these reserves is rare. Hence it could be viable to use the last 20% SOC to cover parts of the reserves. However, this would not suffice for the requirement on short routes as 20% would require a flight time of around 2 hours just for the VFR conditions. Based on the results, 2 hours of flight seem unrealistic. However, using them to cover parts of the reserve requirement would reduce the battery weight and should be included as new regulations for electrical aircraft are imposed.

The weight composition of the aircraft is of interest. It is regularly reported that new electric motors with increased power densities and efficiencies. However, as shown throughout the sizing procedure conducted in this thesis, this is only of limited interest for the electric aircraft. Of the components presented, the motor weight is amongst the lowest. It shows that improvements are needed for every part of the electrical system for an optimistic prospect of introducing electric aircraft. While many research articles solely focus on the EPS, it is shown in this thesis that the weight of the TMS weight is higher than the weight of the motor. The need for increased power density is of importance. However, the efficiency of the components will affect the system to a more significant extent. In a project report preceding the work in this thesis, it was shown that efficiency improvements improved the system more significantly than improvements in power density [78].

In general, the results show that the prospect of electrical aircraft on the shortest routes on the short-haul network is viable and that incremental improvements could increase the range. Increasing the voltage level and inclusion of gears could be

included as they result in weight reductions for the aircraft in many cases. However, the most pressing issue is the battery's specific energy, which to a large extent limits the range of the aircraft as the weight addition per increased kilometer is high. When adding in redundancy and energy requirements, the prospects deteriorate. In this thesis, these effects are tested individually, while a certification process would require them to be present simultaneously. It would compound the negative effects found from redundancy and energy reserves and would result in aircraft weights exceeding the MTOW to a great extent. The results also show that including battery losses are essential to include as it affects the thermal circuit of the aircraft. Excluding it could be hazardous as components could overheat, leading to fatal accidents. The battery is especially crucial as it could experience thermal runaway.

11.2 Short-haul analysis

The short-haul analysis is based on flights on the Norwegian short-haul network. The flights were manually chosen, and several requirements were set for them. These requirements made many of the distances unable to be a part of the database of short-haul flights analyzed. As shown in the Fig. 6, the collected flight matched the actual weekly flights to a certain extent. However, it does not give a fully representative impression of the short-haul network as multiple airports and flights were omitted due to the flight data not meeting the requirements. Different airports have different flight patterns in approach and takeoff, affecting the power, energy, and time profiles presented in the section.

Additionally, flights with unusual flight patterns are omitted due to the requirements imposed on the collected data. These include long loiters, diversions, and landing at the alternate airport. The power and energy consumption in these phases are important as they could be used to determine the energy reserves needed in the aircraft. Instead, the reserves used in this thesis are found in regulations for the aviation industry and estimated based on the vicinity of airports on the short-haul network. More detailed data on these events could yield more precise estimations for the required energy and power.

The power calculation applied to the data shows large fluctuations. These fluctuations are due to the sensitivity to speed and altitude changes between time steps. A moving average was applied to reduce them, but this manipulation of the data could yield inaccurate results. However, keeping the large fluctuations would give results where the power and propulsion force of the aircraft varies significantly from time step to time step. As the aircraft is expected that to operate at continuous propulsion, the result from the moving average is expected to be more accurate than the one without.

When comparing the standardized flight profile in Fig. 16 to the exemplary profile in Fig. 8 the main difference is during the climb phase. While the example profile stabilizes at an almost constant power output throughout the climb, the standardized flight profile shows a quick decline in power before stabilizing at the cruise level. The decline could be due to large differences in max power for the different flights. Due to the previously mentioned sensitivity, the maximum power output of

the aircraft could vary based on the sampling rate. As the maximum power is used to normalize the power consumption, variation in this value can significantly affect the power plot. It could be the reason for the different waveforms during the climb.

On average, the validity of the flight and power calculations seems realistic. Similar results are achieved in this thesis as the results presented by Jux et al. [47]. They examined an ATR 76-600 but over longer distances. However, this should not affect the results significantly. Their data shows approximately the same flight pattern, and their standardized flight is also similar to the one presented in this thesis, with the exemption of having a more even power requirement during the climb.

The short-haul network is mainly operated by Dash-8 100s, and all the data collection performed in this thesis is for this aircraft. Hence, the time and power profile of the aircraft is based on the Dash-8 100. However, the electric aircraft used for the sizing procedure does not have the same properties. So despite the collected data having validity for the Dash-8, it is not necessarily applicable to other aircraft.

The issue with using the Dash-8 100 data was discovered when using the time regressions for the P-Volt and the ES-19. It resulted in lower flight times for the P-Volt and the ES-19 than possible due to the comparably lower cruise speed of the electric aircraft. The time regressions were increased with the factor separating the cruise speed of the electric aircraft and the reference to account for this effect. this thesis does not explore whether this is an appropriate assumption, and it could give unrealistic flight scenarios. The amount of time spent on climb could, for example, be reduced to increase the lifetime of the batteries [104].

An additional concern for the viability of using data based on the Dash 8 for the electric aircraft is the operating altitude. The Dash 8-100 has a maximum operating altitude at 7600 meters which is more than 3000 meters higher than the maximum operation altitude for the P-Volt. The altitude regression shown in Fig. 9 shows that the regression line reach 7600 meters, and despite the altitude not being used directly in the sizing algorithm, the time spent on climb and descent will probably be higher for the Dash 8-100 than its electrical counterparts.

11.3 Modelling

Despite trying to include as many factors as possible during the sizing of the electric aircraft, several simplifications and assumptions were made. Many of these are presented in Section 9.2.1, but some significant simplifications are omitted.

11.3.1 Auxiliary power

As mentioned in Section 8.1.4 Zhang et al. [89] estimates that 10% of the propulsion force is needed for auxiliary power consumers as the environmental control. This power requirement is omitted from this thesis as the propulsion power of the aircraft varied significantly for the different scenarios. If 10% of the power were added for auxiliary sources, it would imply that the auxiliary demand also varied. It

is, however, expected to be a constant power consumption as the variation in the subsystems is limited. It could be modeled as a flat 10% of the initially installed power, but it was omitted in the sizing algorithm as this was unknown for the ES-19.

11.3.2 Weather conditions

Another factor that will significantly impact the power consumption and the flight pattern of the aircraft is the weather and especially the wind. It would directly impact the equations of motion for the aircraft by including an additional term accounting for the wind. The sign of the wind force would be dependent on the direction of the wind. However, as weather prediction only would yield additional uncertainties, the wind was omitted in the procedure. The data collection phase also omitted the weather conditions, which certainly affected the real-world data collected. The weather on the Norwegian short-haul network can be challenging, and it is important to include weather data in the calculations. A possibility for implementing the weather conditions would be to apply the worst-case scenario and calculate its effects on the aircraft.

11.3.3 Component Parameters

The parameter choices in this thesis are presented in Section 9.3 where a rationale for the choices is made. Nevertheless, it is important to emphasize the uncertainties in the parameters. For the motors, converters, inverters, and CBs, the data collection showed several different research projects and available products. It gives confidence that the parameters choices are realistic. However, as shown in the Section 8, it is a range in performance for the components. In this thesis, the average performances were chosen for the sizing procedure. As the goal of this thesis is to test the viability of a modern all-electric aircraft, it was desired to use the best performance components available. However, companies could be overstating their performance or omitting important factors from their results, and the time it takes for a successful academic demonstration to industrial implementation is long. Hence, the most optimistic performances were deemed too optimistic. These assumptions led to the middle-of-the-ground choices in component performances.

For the TMS, the available data was more limited. The TMS of an aircraft must be customized to handle the excess heat of the different components. However, the finalized design of a nine or 19-passenger all-electric aircraft is unavailable. It makes it hard to determine the performance of the TMS. In Rheaume et al. [176], who present the performance parameters used in this thesis, they suggest that the batteries can be pre-cooled due to the high thermal inertia of the battery. Whether this is possible is not considered here, but it emphasizes the uncertainties associated with the TMS.

11.3.4 Distribution system

The design of the distribution system was performed on a rough estimation. The distribution system for the EPS is assumed to cross the aircraft's wingspan, while the distribution for the TMS is sized by aircraft length. This modeling was chosen to include the aircraft size and could result in an over-dimensioned distribution. It could significantly impact the sizing as the cable weight contributed considerably to the weight of the ES-19.

Another consideration that could reduce the cable weight is the power requirements for the cable. The cable is dimensioned to handle the entire power flow downstream of the battery CB in the sizing procedure. However, the motors are separated on each wing. It could result in halving the propulsion power needed on either side. Nonetheless, there are issues attributed to this design. It is mainly due to the requirement for single motor failure operation. The aircraft would need to operate if one of the motors were faulted. This operation would increase the power flow in the distribution grid to one of the wings. Hence, it is safest to dimension the distribution grid for full-power operation. However, this would also affect the motors, which would need to handle operation in such a scenario. It would probably lead to an even higher power rating for the motors, yielding them over-dimensioned for regular operation. The use of four motors for the ES-19 would ease the requirements for the motors but would not affect the distribution system.

Finally, the voltage level of the distribution system is a debatable factor. 1000 V was chosen as the basis for the sizing procedure. However, this would be the highest voltage level installed on any aircraft. The current best practice is the 540 V DC grid installed at the most modern MEA. However, 540 V is expected to be too low for an all-electric aircraft, and 1000 V was chosen instead. This choice could have significant implications for the rest of the components as the insulation and performance would be impacted. However, this effect is not considered in this thesis. Every component has the same performance regardless of voltage level. Of course, this is not the case for the cable as it is scaled with the current.

The selectivity of the protection scheme has not been investigated thoroughly in this thesis. It could, for example, show the need for ACCBs on the AC side of the inverters. It is also a possibility that there is a need for fault current limiters (FCLs). These will operate during a fault, by increasing the resistance in the circuit and thus reducing the overcurrents experienced by the components. In Jones et al. [87] they incorporate FCLS on every distribution grid. However, they examine a superconducting distribution system with very low resistance in the cables. The low resistance would increase the need for FCLs as the overcurrents during faults would be high. Hence, it is not necessarily needed for the lower voltage DC system in this thesis.

11.3.5 Gear

When testing the weight and power effects of including a gear in the EPS, the weight sizing was based on a future scenario estimation made in [51]. However, this

article is from 2005, and the advancements in gear technology might have enhanced further than they projected. An example is the gear technology claimed by H3X as mentioned in Section 8.3 where a motor operating at 20 000 rpm could have a gear ratio of 4 and result in a gearbox only weighing 3 kg. They also claim that the efficiency is 99%. This efficiency is higher than the efficiency chosen in this thesis. In comparison, the gear weight is a little over 4.2 kg by using the gear equation used for the sizing. With the H3X values, the inclusion of gear could be more advantageous than shown in this thesis results.

However, there are reasons to doubt the positive effects of gearing the motor. The motor is expected to have a constant efficiency in the sizing regardless of the rotational velocity. As mentioned in Section 8.3, this is unrealistic as there is a trade-off between specific power and efficiency for the motor. As the motor speed increases, reliable and efficient PECs that enable a high electric frequency are needed. It could increase the weight of the motor inverter. Additionally, high-frequency motors experience more losses due to the frequency-dependent iron losses. In total, this could reduce the efficiency of the motor and gearbox, increase the heat losses, and potentially increase the battery's power requirements.

11.3.6 Maximum power

The sizing procedure in this thesis is based on the maximum power output of the aircraft. However, as shown in the standardized flight profile, the aircraft only operate in maximum power mode for a short time during takeoff and the initial climb. It results in the components being over-dimensioned for most of the flight. An advantageous alternative would be to have components enabling operation above their rated power for a short duration. It could reduce the component weight substantially throughout the electrical system and, hence, reduce the overall weight and power of the system. Alternatives increasing the thermal inertia of the components is a possibility as the 44% weight reduction found in Yi and Haran [133] where phase-shift materials were used in the motor.

The TMS is also sized by the maximum power requirement and could be substantially reduced if efforts decrease the heat generation in the initial phases of flight. The heat production will be highest during takeoff and climb as the maximum power is required and the ambient air is at its highest temperature. By delaying the heat generation, the aircraft could employ the colder ambient air at the top of climb to reduce the need for cooling air.

11.3.7 System architecture

The system architecture presented in this thesis is only a suggestion for the design procedure. It has a basis in articles for similar systems as presented in [44]. However, it is mainly designed to give an overview of the necessary components and their respective placement in the circuit. It shows the need for protection schematics and shows the effects of the downstream losses. An example is the interconnection of the TMS circuit and the EPS. It is expected that the TMS would run on a separate power

source distributed closer to the TMS than in the chosen architecture. However, to include all aspects of the aircraft, the TMS was placed in the aircraft's aft. For the sizing algorithm, the shared battery, DC/DC converter, and battery CB do not affect the result as these could be uncoupled without affecting the weight sizing.

As the components' scalability is linear and assumed independent of the number of devices, the weight and power ratings of the components are gathered into a single component before being presented. It is performed for most cases as it is the easiest and most transparent way of presenting them. However, as the P-Volt and ES-19 have multiple motors and thus multiple CBs and inverters, the size of each component would be smaller than the presented value.

11.3.8 Aircraft data

The empty weight and the payload weight are used as a basis in the sizing procedure of the electric aircraft. The empty weight of the ES-19 is based on the data presented by Heart Aerospace. This is only an estimate, and could be overly optimistic when considering the large weight savings compared to other aircraft in the same size range. For the P-Volt, the empty weight is based on the aircraft developed from the P2012 Caravan. Significant alterations may have been performed on the P2012 before introducing the new electric propulsion system for the P-Volt. However, in this thesis, the empty weight is assumed to be equal to the P2012 and thus being a retrofit only replacing the propulsion system.

The value of the empty weight is assumed constant regardless of the weight addition of the electric system. The demands for the landing gear would be substantially increased as the aircraft weight increased by multiple tonnes from the initial design. However, as the weight of the aircraft increase, the need for more structure in the aircraft body would also increase. It is not accounted for as this thesis's primary purpose is to show the weight gains caused by the onboard electric system.

The payload weight is estimated based on the number of passengers in the aircraft. Each passenger is assumed to weigh 80 kg with an additional 20 kg of luggage. The pilots are also included after the same model. This assumption could be an optimistic scenario as the payload weight might need to accommodate the transportation of goods. An example is post transportation which is a typical way for airliners to supplement their income and increase the delivery times in rural areas [182].

11.4 Practical considerations

There are several obstacles needed to overcome to use all-electric aircraft on the Norwegian short-haul network. The previous sections have tried to present the most pressing ones and discuss uncertainties in the procedure used in this thesis. This section will discuss some of the more practical evaluations and reasoning for the negative results.

If either of the electric aircraft presented in this thesis were implemented on the

short-haul network, the practical implications would be significant. From an infrastructure point of view, large power supplies would be needed in all the smaller airports on the short-haul network. As the airports were designed to be cost-efficient and simplistic, the necessary investments for high power distribution could be problematic.

It would affect the number of aircraft the fleet of the airliners. As discussed in Section 6.1.3, the number of aircraft is not required to increase to a large extent due to capacity needs if a 19-passenger aircraft could be used. However, acquiring some new aircraft would be necessary, and if the 19-passenger aircraft is unrealistic, the fleet would need a doubling with 9-passenger aircraft. this thesis shows that electric aircraft are highly sensitive to range increases. Hence there is a possibility of having electric aircraft operating the shortest routes, given slight improvements to the results presented here. However, as many of the routes have multiple stopovers, it would require passengers to change aircraft as the distance increase. It would probably be an inconvenience for both passengers and the aircraft and could be an issue for implementing the aircraft even on the shortest routes.

The increased flight time is also an issue as shown in Eq. (27) the flight time doubles for the P-Volt and is also substantially increased for the ES-19. It would affect the airliners by enabling less frequent flights. It would be counted as a cost for the airlines as the passengers pay per flight. It could also reduce the capacity of the short-haul network, which is the most vital requirement for the operator. For the passengers, it would give longer flight times and less mobility if the service were reduced.

However, despite all the considerations discussed and the negative results presented for the sizing algorithm, Widerøe has intentions to start electrifying its fleet. This intention is evident from the cooperation with Tecnam and Rolls Royce in creating the P-Volt. It could mean that they have better performing components than those chosen for this thesis. It could also be due to simpler architecture or other considerations not included in this thesis.

The difference between the base case scenario and the MTOW of the aircraft was not massive on the short distances, and minor improvements should yield a viable design. However, longer flights are unlikely based on the results in this thesis.

Anyhow, there are significant hurdles to overcome before electric aviation is viable for the short-haul network. These are found both in the performance of the electrical system components but are also due to regulations. Especially the demand for redundancy and energy reserves will be difficult to circumvent. Easing the rules in the implementation phase for the electric aircraft could be applied to the reserve requirements. It could enable the electric aircraft to start operation at an earlier stage, accelerating the technological development as seen in the automotive industry. However, the need for reserves will always be present for safety measures. The same holds for redundancy needed to avoid devastating disasters if faults occur in the electric circuit. Nevertheless, alternative designs and other measures could reduce the impact it has on the aircraft's weight. However, in the end, safety is the primary concern, and the implementation and regulation changes cannot compromise it.

12 Conclusion

The main purpose of this thesis is to explore the viability of electrifying the Norwegian short-haul network. It consists of three main parts; where the first section is a comprehensive analysis of the short-haul network. Based on 1500 real-world missions, a standardized profile of the propulsion power with respect to time is obtained. It also includes the time spent in each phase of flight for a standard commuter-class aircraft, dependent on the mission length. Except for the profiles, the main takeaways are an average power output during cruise at 37% of the rated power. It also shows that the proportion of the flight spent on climb and descent is higher for short missions than long ones.

The second part is a literature study. It is conducted to find state-of-the-art components for the electrical system needed in an all-electric aircraft. It also explores design opportunities and safety measures such as redundancy and fault handling. The section concludes with a proposed design for a 19-seat aircraft based on the ES-19, an electrical aircraft produced by Heart Aerospace, and the 9-seat Tecnam P-Volt. The design consists of a battery, DC/DC converter, DCCBs, inverters, and electric motors. The design also includes a secondary circuit powering the TMS.

The final part connects the above-mentioned results in a sizing algorithm. The algorithm employs the power and time data from the short-haul network and the component performance from the literature study in an iterative process determining the weight of the two selected aircraft. It shows that the minimum weight of the electrical powertrain increases the aircraft weight beyond the reported MTOW. The difference is small, and minor improvements could enable short-haul flights. However, due to the battery's low specific energy, the weight discrepancy increases for longer distances.

Through several scenarios, the effects of different technological and regulatory aspects are explored. They show that ignoring the power attributed to takeoff and climb results in an underdimensioned propulsion system. The need to account for a TMS is also established, despite only accounting for 2-3% of the total aircraft weight as its power consumption increase the battery size. As battery losses are included, this effect is further emphasized. Safety requirements such as redundancy and energy reserves have a significant impact, making the aircraft weight increase substantially. This weight gain is an important issue due to the high importance of safety in the certification process of an aircraft. Finally, it is established that high voltage levels for the DC distribution are advantageous as cable weight is reduced, and high gear ratios result in weight savings, especially on short distances.

The thesis shows that significant improvements for the components are needed and that even the minimum weight poses a challenge. It also shows the importance of including all factors of the electrical system throughout the design procedure as small changes can resonate through the system, increasing the significance of the change.

13 Further work

The thesis tries to give an overview of the challenges and opportunities for electrification of the Norwegian short-haul network. Hence, it has a relatively broad scope and does not provide detailed information on the different components of the electric system. It also includes several simplifications, many of them shortly discussed in Section 11.

However, the analysis performed in this thesis is built around the time and power profiles for the short-haul flights. These are based on the flight pattern of the Dash 8-100, and it should be verified whether these data apply to the 9- and 19-seat aircraft. It can be tested by performing data collection of similar aircraft and comparing it to the data presented in this thesis. Another improvement for the collected data would be to analyze the effects of long loiters, diversions, and different cruising altitudes. It could give more detailed power and energy estimations and could affect the regulations for reserve requirements.

A more thorough analysis of each component in the powertrain needs to be conducted. This thesis touches upon different topologies, but careful considerations are required. Another aspect of the components is their size. While the weight has been the main focus of this thesis, the size of the components has been omitted. Hence, an analysis of the size and placement of the components is needed. A custom design for the TMS and a more thorough analysis of the heat generation in the powertrain are necessary. The main emphasis should be on the takeoff and climb phase, as these pose the most significant challenge.

The effects caused by wind are of concern. The aircraft must operate in harsh weather conditions, and an estimate of worst-case wind conditions would reveal the increased constraints this effect poses. Other safety concerns omitted from this thesis are cosmic radiation and electromagnetic interference. Cosmic radiation can lead to discharges in the components and are of particular concern for switching devices, while electromagnetic interference will affect the design of the electrical system. The electromagnetic waves created by the electrical components could affect instruments or other components, which could be hazardous. The implications these factors have on the electrical system must be addressed.

As previously mentioned, the auxiliary power requirements are omitted from this thesis. However, the need for electrifying these and the increased battery power will affect the aircraft's weight. The different auxiliary processes need to be mapped, and a more in-depth analysis of their power requirements should be conducted. Including auxiliary functions will also increase the need for power-electronic converters as they are expected to operate at different power levels than the main distribution. The weight contributed to these also needs to be considered.

A complete electric system architecture with auxiliary processes needs to be produced. The architecture presented in this thesis is simplified but could still be valuable for testing the system's dynamic behavior. This could be tested in simulation tools where the system's selectivity and protection can also be assessed.

Finally, with the high power consumption of the aviation industry, the conversion to all-electric aircraft will have significant implications for the infrastructure of the short-haul network. A study estimating the power and energy requirements of electrification should be conducted. This study should also include a cost estimation for the infrastructure needed. Due to the high power operation of fast-charging, the transient effects it would impose on the electrical power system are also of interest.

Bibliography

[1] T. Mathisen and G. Solvoll, "Reconsidering the regional airport network in norway," *Eur. Transp. Res.*, vol. 4, pp. 39–46, 2012.

[2] A. Dominguez, "Derivation of the paschen curve law alpha laboratory immersion." [Online]. Available: www.compadre.org/advlabs/bfyii/files/Paschen_derivation.pdf

[3] Silicon Lightworks, "Li-ion voltage analysis." [Online]. Available: https://siliconlightworks.com/li-ion-voltage

[4] Airfleets, "Wideroe fleet details." [Online]. Available: https://www.airfleets.net/flottecie/Wideroe.htm

[5] "Flightradar.com." [Online]. Available: Flightradar.com

[6] A. Giannakis and D. Peftitsis, "Mvdc distribution grids and potential applications: Future trends and protection challenges," 09 2018.

[7] Eviation, "Alice." [Online]. Available: https://www.eviation.co/aircraft/#Alice

[8] A. Poleri, "Dubai 2021: Tecnam unveils the p-volt, an electric aircraft based on the p2012 traveller." [Online]. Available: https://www.aviacionline.com/2021/11/dubai-2021-tecnam-unveils-the-p-volt-an-electric-aircraft-based-on-the-p2012-traveller/

[9] Tecnam, "P2012 twin engine aircraft." [Online]. Available: https://www.tecnam.com/aircraft/p2012-traveller/

[10] Pilatus Aircraft, "Pc-12 ngx." [Online]. Available: https://www.pilatus-aircraft.com/data/document/Pilatus-Aircraft-Ltd-PC-12NGX-Brochure.pdf

[11] Globalair.com, "Beechcraft beechcraft 1900d." [Online]. Available: https://www.globalair.com/aircraft-for-sale/Specifications?specid=28

[12] ——, "British aerospace jetstream 31." [Online]. Available: https://www.globalair.com/aircraft-for-sale/Specifications?specid=529

[13] P. Callister and R. McLachlan, "Electric aircraft — coming soon to save us, or all hype & greenwash?" [Online]. Available: https://cleantechnica.com/2021/10/22/electric-aircraft-coming-soon-to-save-us-or-all-hype-greenwash/

[14] Heart Aerospace, "Electrifying regional air travel." [Online]. Available: https://heartaerospace.com

[15] Global Air, "Dornier dornier 228." [Online]. Available: https://www.globalair.com/aircraft-for-sale/Specifications?specid=797

[16] Skybrary, "Fairchild dornier 228." [Online]. Available: https://skybrary.aero/aircraft/d228

[17] One Air, "Commercial aviation." [Online]. Available: https://www.grupooneair.com/analysis-global-growth-commercial-aviation/

[18] G. Volker, A. Gangoli Rao, T. Grönstedt, C. Xisto, F. Linke, J. Melkert, J. Middel, B. Ohlenforst, S. Blakey, S. Christie, S. Matthes, and K. Dahlmann, "Evaluating the climate impact of aviation emission scenarios towards the paris agreement including covid-19 effects," *Nature Communications*, vol. 12, 06 2021.

[19] A. W. Schäfer, S. R. Barrett, K. Doyme, L. M. Dray, A. R. Gnadt, R. Self, A. O'Sullivan, A. P. Synodinos, and A. J. Torija, "Technological, economic and environmental prospects of all-electric aircraft," *Nat Energy*, vol. 4, pp. 160–166, 2019.

[20] ICAO, "Future of aviation." [Online]. Available: https://www.icao.int/Meetings/FutureOfAviation/Pages/default.aspx

[21] J. Z. Bird, "A review of electric aircraft drivetrain motor technology," *Transactions on Magnetics*, 2021.

[22] Air Transport Action Group, "Commitment to fly net zero by 2050," 2021. [Online]. Available: https://aviationbenefits.org/media/167501/atag-net-zero-2050-declaration.pdf

[23] P. Strathoff, H. A. Savic, and E. Stumpf, "Performance comparison of conventional, hybrid-electric, and all-electric powertrains for small aircraft," 06 2020.

[24] M. Hepperle, "Electric flight - potential and limitations," 10 2012.

[25] D. Lee, G. Pitari, V. Grewe, K. Gierens, J. Penner, A. Petzold, M. Prather, U. Schumann, A. Bais, T. Berntsen, D. Iachetti, L. Lim, and R. Sausen, "Transport impacts on atmosphere and climate: Aviation," *Atmospheric Environment*, vol. 44, no. 37, pp. 4678–4734, 2010, transport Impacts on Atmosphere and Climate: The ATTICA Assessment Report. [Online]. Available: https://www.sciencedirect.com/science/article/pii/S1352231009004956

[26] M. Lefèvre, A. Chaumond, P. Champelovier, L. Giorgis Allemand, J. Lambert, B. Laumon, and A.-S. Evrard, "Understanding the relationship between air traffic noise exposure and annoyance in populations living near airports in france," *Environment International*, vol. 144, p. 106058, 2020. [Online]. Available: https://www.sciencedirect.com/science/article/pii/S0160412020320134

[27] H. Schefer, L. Fauth, T. H. Kopp, R. Mallwitz, J. Friebe, and M. Kurrat, "Discussion on electric power supply systems for all electric aircraft," *IEEE Access*, vol. 8, pp. 84 188–84 216, 2020.

[28] P. J. Ansell and K. S. Haran, "Electrified airplanes: A path to zero-emission air travel," *IEEE Electrification Magazine*, vol. 8, no. 2, pp. 18–26, 2020.

[29] EASA, "Easa certifies electric aircraft, first type certification for fully electric plane world-wide." [Online]. Available: https://www.easa.europa.eu/newsroom-and-events/news/easa-certifies-electric-aircraft-first-type-certification-fully-electric

[30] Pipistrel, "Velis electro." [Online]. Available: https://www.pipistrel-aircraft.com/aircraft/electric-flight/velis-electro-easa-tc/#tab-id-3

[31] Wright Electric inc., "Wright," 2021, last accessed 08 November 2021. [Online]. Available: https://www.weflywright.com/

[32] E. Group, "Elfly group." [Online]. Available: https://el-fly.no/

[33] ZeroAvia, "We are zeroavia." [Online]. Available: ZeroAvia.com

[34] A. Lincoln, "Bye aerospace unveils 8-seat all-electric eflyer 800." [Online]. Available: https://byeaerospace.com/bye-aerospace-unveils-8-seat-all-electric-eflyer-800/

[35] Rolls Royce, "Rolls-royce and tecnam join forces with widerøe to deliver an all-electric passenger aircraft ready for service in 2026." [Online]. Available: https://www.rolls-royce.com/media/press-releases/2021/11-03-2021-rr-and-tecnam-join-forces.aspx

[36] NASA, "X-57," last accessed 10 November 2021. [Online]. Available: https://www.nasa.gov/specials/X57

[37] T. P. Dever, K. P. Duffy, A. J. Provencza, P. L. Loyselle, B. B. Choi, C. R. Morrison, and A. M. Love, "Assessment of technologies for noncryogenic hybrid electric propulsion," 2015.

[38] S. Sahoo, X. Zhao, and K. Kyprianidis, "A review of concepts, benefits, and challenges for future electrical propulsion-based aircraft," *Aerospace*, vol. 7, no. 4, 2020. [Online]. Available: https://www.mdpi.com/2226-4310/7/4/44

[39] C. Riboldi and F. Gualdoni, "An integrated approach to the preliminary weight sizing of small electric aircraft," *Aerospace Science and Technology*, vol. 58, pp. 134–149, 2016.

[40] C. E. Riboldi, F. Gualdoni, and L. Trainelli, "Preliminary weight sizing of light pure-electric and hybrid-electric aircraft," *Transportation Research Procedia*, vol. 29, pp. 376–389, 2018.

[41] A. R. Gnadt, R. L. Speth, J. S. Sabnis, and S. R. Barrett, "Technical and environmental assessment of all-electric 180-passenger commercial aircraft," *Progress in Aerospace Sciences*, vol. 105, pp. 1–30, 2019.

[42] R. H. Jansen, C. Bownman, and A. Jonkovsky, "Sizing power components of an electrically driven tail cone thruster and a range extender," 2016.

[43] M. Armstrong, C. Ross, M. Blackwelder, and K. Rajashekara, "Propulsion system component considerations for nasa n3-x turboelectric distributed propulsion system," *SAE Internatinoal Journal of Aerospace*, vol. 121, no. 1, pp. 344–353, 2012.

[44] T. C. Cano, I. Castro, A. Rodríguez, D. G. Lamar, Y. F. Khalil, L. Albiol-Tendillo, and P. Kshirsagar, "Future of electrical aircraft energy power systems: An architecture review," *IEEE Transactions on Transportation Electrification*, vol. 7, no. 3, pp. 1915–1929, 2021.

[45] I. Staack, A. Sobron, and P. Krus, "The potential of full-electric aircraft for civil transportation: from the breguet range equation to operational aspects," *CEAS Aeronautical Journal*, vol. 12, pp. 803–819, 2021.

[46] Avinor, "Utslippsfri luftfart i 2040?" [Online]. Available: https://avinor.no/elfly-konferansen

[47] B. Jux, S. Foitzik, and M. Doppelbauer, "A standard mission profile for hybrid-electric regional aircraft based on web flight data," in *2018 IEEE International Conference on Power Electronics, Drives and Energy Systems (PEDES)*, 2018, pp. 1–6.

[48] AeroToolbox, "Fundamental forces in flight," 2017. [Online]. Available: https://aerotoolbox.com/forces-in-flight/

[49] D. G. Hull, *Fundamentals of Airplane Flight Mechanics*, 2007.

[50] D. Raymer, *Aircraft Design: A Conceptual Approach, Sixth Edition*, 09 2018.

[51] G. V. Brown, A. F. Kascak, B. Ebihara, D. Johnson, B. Choi, M. Siebert, and C. Buccieri, "Nasa glenn research center program in high power density motors for aeropropulsion," 2005. [Online]. Available: https://ntrs.nasa.gov/api/citations/20060003628/downloads/20060003628.pdf

[52] Lars Engerengen, "Kortbaneflyplass." [Online]. Available: https://snl.no/kortbaneflyplass

[53] G. Thorsnæs and L. Engerengen, "Værøy." [Online]. Available: https://snl.no/V%C3%A6r%C3%B8y

[54] J. BAILEY, "Shaping norway's regional air connectivity - the story of widerøe." [Online]. Available: https://simpleflying.com/wideroe-history/

[55] DAT, "Dat." [Online]. Available: DAT.dk

[56] K. J. Sunnevåg, "Utforming av anbudskonkurranser i samferdselssektoren," no. 18, 2000.

[57] Samferdselsdepartementet. Innbydning til konkurranse; drift av regionale ruteflygingar i nord-noreg. [Online]. Available: https://www.regjeringen.no/no/dokumenter/drift-av-regionale-ruteflygingar-i-nord-noreg/id2873231/

[58] Samferdseldepartementet. Innbydning til konkurranse; drift av regionale ruteflygingar i sør-noreg. [Online]. Available: https://www.regjeringen.no/no/dokumenter/innbyding-til-konkurranse--drift-av-regionale-ruteflygingar-i-sor-noreg-1.-april-2020--31.-mars-2024/id2628355/

[59] Y. Jarslett, "Twin otter." [Online]. Available: https://snl.no/Twin_Otter

[60] P. E. Dalløkken, "Slik har widerøe gjort 16 gamle fly "nye"." [Online]. Available: https://e24.no/privatoekonomi/i/3JVMlL/slik-har-wideroee-gjort-16-gamle-fly-nye

[61] AOPA, "Understanding part 23 rewrite." [Online]. Available: https://www.aopa.org/advocacy/advocacy-briefs/understanding-part-23-rewrite

[62] Norsk Offentlig Utredning, "Fra statussymbol til allemannseie – norsk luftfart i forandring," 2019, samferdselsdepartementet. [Online]. Available: https://www.regjeringen.no/contentassets/19a211ff48814d09b9939631924cf48d/no/pdfs/nou201920190022000dddpdfs.pdf

[63] Samferdselsdepartementet, "Nasjonal Transportplan 2018-2029," 2016.

[64] Avinor og Luftfartstilsynet, "Forslag til program for introduksjon av elektrifiserte fly i kommersiell luftfart," 2020, last accessed 08 November 2021. [Online]. Available: https://luftfartstilsynet.no/globalassets/dokumenter/andre-dokumenter/forslag-til-program-for-introduksjon-av-elektrifiserte-fly-i-kommersiell-luftfart.pdf

[65] A. Budalen, O. M. Rørstad, S. S. Fallmyr, and S. Skjelvik, "Dette elflyet fra rolls-royce kan være i lufta i norge om fem år." [Online]. Available: https://www.nrk.no/nordland/wideroe-satser-pa-elfly-fra-rolls-royce-_-kan-vaere-i-lufta-pa-norske-flyplasser-i-2026-1.15413067

[66] H. Løvik, "Norge produserer 98 prosent fornybar kraft, men bruker 46 prosent fossil varmekraft fra europa." [Online]. Available: https://www.tu.no/artikler/i-norge-produserer-vi-98-prosent-fornybar-kraft-men-vi-bruker-hele-57-prosent-fossil-varmekraft-fra-europa/441422

[67] B. Sarlioglu and C. T. Morris, "More electric aircraft: Review, challenges, and opportunities for commercial transport aircraft," *IEEE Transactions on Transportation Electrification*, vol. 1, no. 1, pp. 54–64, 2015.

[68] Cornell Law School, "14 cfr § 91.151 - fuel requirements for flight in vfr conditions." [Online]. Available: https://www.law.cornell.edu/cfr/text/14/91.151

[69] ——, "14 cfr § 91.167 fuel requirements for flight in ifr conditions." [Online]. Available: https://www.law.cornell.edu/cfr/text/14/91.167

[70] EASA, "Vedlegg til forslag til kommisjonsforordning om drift av luftfartøyer – ops." [Online]. Available: https://www.easa.europa.eu/sites/default/files/dfu/EASA_2011_00060002_NO_TRA.pdf

[71] C. Y. Justin, A. P. Payan, S. I. Briceno, B. J. German, and D. N. Mavris, "Power optimized battery swap and recharge strategies for electric aircraft operations," *Transportation Research Part C: Emerging Technologies*, vol. 115, p. 102605, 2020. [Online]. Available: https://www.sciencedirect.com/science/article/pii/S0968090X19310241

[72] Eurocontrol, "Aircraft performance database." [Online]. Available: https://contentzone.eurocontrol.int/aircraftperformance/details.aspx?ICAO=DH8A

[73] A. Barzkar and M. Ghassemi, "Electric power systems in more and all electric aircraft: A review," *IEEE Access*, vol. 8, pp. 169 314–169 332, 2020.

[74] V. Gkoutzamanis, S. Tsentis, O. Valsamis Mylonas, A. Kalfas, K. Kyprianidis, P. Tsirikoglou, and M. Sielemann, "Thermal management system considerations for a hybrid-electric commuter aircraft," *Journal of Thermophysics and Heat Transfer*, pp. 1–17, 03 2022.

[75] R. S. F. Patròn, R. M. Botez, and D. Labour, "New altitude optimisation algorithm for the flight management system cma-9000 improvement on the a310 and l-1011," *Aeronautical Journal*, vol. 117, pp. 787–805, 2013.

[76] B. J. Brelje and J. R. Martins, "Electric, hybrid, and turboelectric fixed-wing aircraft: A review of concepts, models, and design approaches," *Progress in Aerospace Sciences*, vol. 104, pp. 1–19, 2019.

[77] K. Yokota, H. Fujimoto, and Y. Hori, "Descent angle control by regenerative air brake using observer-based thrust control for electric aircraft," in *2020 AIAA/IEEE Electric Aircraft Technologies Symposium (EATS)*, 2020, pp. 1–13.

[78] M. Anker, "Sizing of electric propulsion system for an all-electric aircraft," 2021.

[79] K. V. Papathakis and A. M. Sessions, "A nasa approach to safety considerations for electric propulsion aircraft testbeds," 2017.

[80] D. C. Loder, A. Bollman, and M. J. Armstrong, "Turbo-electric distributed aircraft propulsion: Microgrid architecture and evaluation for eco-150," in *2018 IEEE Transportation Electrification Conference and Expo (ITEC)*, 2018, pp. 550–557.

[81] Wright Electric. (2021) Wright spirit energy storage discussion paper. [Online]. Available: https://docsend.com/view/faijiijzkvqdccjg

[82] S. Teichel, M. Dörbaum, O. Misir, A. Mertens, J. R. Seume, and B. Ponick, "Design considerations for the components of electrically powered active high-lift systems in civil aircraft." *CEAS Aeronaut J*, vol. 6, pp. 49–67, 2015.

[83] L. Dorn-Gomba, J. Ramoul, J. Reimers, and A. Emadi, "Power electronic converters in electric aircraft: Current status, challenges, and emerging technologies," *IEEE Transactions on Transportation Electrification*, vol. 6, no. 4, pp. 1648–1664, 2020.

[84] T. Spierling and C. Lents, "Parallel hybrid propulsion system for a regional turboprop: Conceptual design and benefits analysis," in *AIAA Propulsion and Energy 2019 Forum*, 2019.

[85] J. L. Kratz and G. L. Thomas, "Dynamic analysis of the starc-abl propulsion system," in *AIAA Propulsion and Energy 2019 Forum*, 2019.

[86] A. Dubois, M. van der Geest, J. Bevirt, S. Clarke, R. J. Christie, and N. K. Borer, "Design of an electric propulsion system for sceptor," 06 2016. [Online]. Available: https://ntrs.nasa.gov/api/citations/20160007774/downloads/20160007774.pdf

[87] C. E. Jones, P. J. Norman, S. J. Galloway, M. J. Armstrong, and A. M. Bollman, "Comparison of candidate architectures for future distributed propulsion aircraft," *IEEE Transactions on Applied Superconductivity*, vol. 26, no. 6, pp. 1–9, 2016.

[88] M. Yildiz, "Electric energy use in aviation, perspective, and applications," *Journal of Polytechnic*, vol. 24, 2021.

[89] X. Zhang, C. Bowman, T. O'Connell, and K. Haran, "Large electric machines for aircraft electric propulsion," *IET Electric Power Applications*, vol. 12, pp. 767–779, 2018.

[90] Bombardier, "C-series." [Online]. Available: https://web.archive.org/web/20150908154642/http://commercialaircraft.bombardier.com/content/dam/Websites/bca/literature/cseries/Bombardier-Commercial-Aircraft-CSeries-Brochure-en.pdf.pdf

[91] Boeing. 787 airplane characteristics for airport planning. [Online]. Available: https://www.boeing.com/assets/pdf/commercial/airports/acaps/787.pdf

[92] Airbus. Aircraft characteristics airport and maintenance planning. [Online]. Available: https://web.archive.org/web/20161128050613/http://www.airbus.com/fileadmin/media_gallery/files/tech_data/AC/Airbus-AC_A350-900-1000-Nov16.pdf

[93] Boeing. 777-200lr / -300er / -freighter airplane characteristics for airport planning. [Online]. Available: https://www.boeing.com/assets/pdf/commercial/airports/acaps/777_2lr3er.pdf

[94] ——. 737 airplane characteristics for airport planning. [Online]. Available: https://www.boeing.com/assets/pdf/commercial/airports/acaps/737.pdf

[95] Modernairliners, "Bombardier dash-8 regional airliner." [Online]. Available: https://modernairliners.com/bombardier-dash-8-regional-airliner/

[96] R. Buckingham, T. Asset, and P. Atanassov, "Aluminum-air batteries: A review of alloys, electrolytes and design," *Journal of Power Sources*, vol. 498, p. 229762, 2021. [Online]. Available: https://www.sciencedirect.com/science/article/pii/S0378775321003037

[97] A. Misra, *Electrified Aircraft Propulsion: Powering the Future of Air Transportation.* Cambridge University Press, 2022, ch. Electrochemical Energy Storage and Conversion for Elecrified Aircraft.

[98] J. K. Nøland, "Hydrogen electric airplanes: A disruptive technological path to clean up the aviation sector," *IEEE Electrification Magazine*, vol. 9, no. 1, pp. 92–102, 2021.

[99] C. Liu, Z. G. Neale, and G. Cao, "Understanding electrochemical potentials of cathode materials in rechargeable batteries," *Materials Today*, vol. 19, no. 2, pp. 109–123, 2016.

[100] Battery University, "Battery basics," 2021, last accessed 09 November 2021. [Online]. Available: https://batteryuniversity.com

[101] A. Turksoy, A. Teke, and A. Alkaya, "A comprehensive overview of the dc-dc converter-based battery charge balancing methods in electric vehicles," *Renewable and Sustainable Energy Reviews*, vol. 133, p. 110274, 2020. [Online]. Available: https://www.sciencedirect.com/science/article/pii/S1364032120305633

[102] S. Jafari, T. Nikolaidis, and R. Sureddi, "Physics-based thermal management system components design for all-electric propulsion systems," 06 2021.

[103] S. Sripad, A. Bills, and W. Viswanathan, "A review of safety considerations for batteries in aircraft with electric propulsion," *MRS Bulletin*, vol. 46, pp. 435–442, 2021.

[104] M. Clarke and J. J. Alonso, "Lithium–ion battery modeling for aerospace applications," *Journal of Aircraft*, vol. 58, no. 6, pp. 1323–1335, 2021. [Online]. Available: https://doi.org/10.2514/1.C036209

[105] T. Huang, J. Ge, and X. Wang, "Review on air transport safety of lithium ion battery: Thermal explosion hazards," 06 2021.

[106] M. Armand, P. Axmann, D. Bresser, M. Copley, K. Edström, C. Ekberg, D. Guyomard, B. Lestriez, P. Novák, M. Ptranikova, W. Porcher, S. Trabesinger, M. Wohlfahrt-Mehrens, and H. Zhang, "Lithium-ion batteries - current state of the art and anticipated developments," *Journal of Power Sources*, vol. 479, 2020.

[107] B. Scrosati, J. Hassoun, and Y.-K. Sun, "Lithium-ion batteries. a look into the future," *Energy & Environmental Science*, vol. 4, no. 9, pp. 3287–3295, 2011.

[108] P. Wheeler, T. S. Sirimanna, S. Bozhko, and K. S. Haran, "Electric/hybrid-electric aircraft propulsion systems," *Proceedings of the IEEE*, vol. 109, no. 6, pp. 1115–1127, 2021.

[109] N. Thapa, S. Ram, S. Kumar, and J. Mehta, "All electric aircraft: A reality on its way," *materialstoday: PROCEEDINGS*, vol. 43, pp. 175–182, 2021.

[110] A. Bills, S. Sripad, W. L. Fredericks, M. Sing, and V. Viswanathan, "Performance metrics required of next-generation batteries to electrify commercial aircraft," *ACS Energy Lett*, vol. 5, no. 2, pp. 663–668, 2020.

[111] P. G. Bruce, S. A. Freunberger, L. J. Hardwick, and J.-M. Tarascon, "Li-o_2 and li-s batteries with high energy storage," *Nature Materials*, vol. 11, pp. 19–29, 2012.

[112] A. Manthiram, S.-H. Chung, and C. Zu, "Lithium–sulfur batteries: Progress and prospects," *Advanced Materials*, vol. 27, no. 12, pp. 1980–2006, 2015.

[113] S. Huang, E. Huixiang, Y. Yang, Y. Zhang, M. Ye, and C. C. Li, "Transition metal phosphides: new generation cathode host/separator modifier for li–s batteries," *Journal of Materials Chemistry A*, vol. 9, pp. 7458–7480, 2021.

[114] K. Ueno, *Fundamental Properties and Solubility Toward Cathode Active Materials*. Springer Singapore, 2021, pp. 277–286.

[115] J. Liang, Z.-H. Sun, F. Li, and H.-M. Cheng, "Carbon materials for li–s batteries: Functional evolution and performance improvement," *Energy Storage Materials*, vol. 2, pp. 76–106, 2016. [Online]. Available: https://www.sciencedirect.com/science/article/pii/S2405829715300465

[116] H. Hizarci, K. Kalayci, and U. Arifoglu, *New Frontiers in Sustainable Aviation*. Springer, 2022, ch. An Overview of Aircraft Electric Power System for Sustainable Aviation.

[117] Oxis Energy, "Lithium sulfur: An energy revolution." [Online]. Available: https://oxisenergy.com/technology/

[118] M. Kane, "Oxis faces bankruptcy a month after announcing 450 wh/kg cells." [Online]. Available: https://insideevs.com/news/509878/oxis-faces-bankruptcy/

[119] C. Randall, "Lyten to launch li-s battery for 2025/26." [Online]. Available: https://www.electrive.com/2021/09/28/lyten-to-launch-li-s-battery-for-2025-26/

[120] Lyten, "Lyten." [Online]. Available: https://lyten.com/

[121] G. Girishkumar, B. McCloskey, A. C. Luntz, S. Swanson, and W. Wilcke, "Lithium - air battery: Promise and challenges," *The Journal of Physical Chemistry Letters*, vol. 1, no. 14, pp. 2193–2203, 2010.

[122] T. Liu, J. P. Vivek, E. W. Zhao, J. Lei, N. Garcia-Araez, and C. P. Grey, "Current challenges and routes forward for nonaqueous lithium–air batteries," *Chemical Reviews*, vol. 120, no. 14, pp. 6558–6625, 2020. [Online]. Available: https://doi.org/10.1021/acs.chemrev.9b00545

[123] K. G. Gallagher, S. Goebel, T. Greszler, W. Oelerich, D. Eroglu, and V. Srinvasan, "Quantifying the promise of lithium–air batteries for electric vehicles," *Energy & Environmental Science*, vol. 5, 2014.

[124] B. Andresen, "Over halvparten av nye personbiler er elbiler." [Online]. Available: https://www.ssb.no/transport-og-reiseliv/artikler-og-publikasjoner/over-halvparten-av-nye-personbiler-er-elbiler

[125] H. Lin, H. Guo, and H. Qian, "Design of high-performance permanent magnet synchronous motor for electric aircraft propulsion," 10 2018, pp. 174–179.

[126] M. Spangenberg, "D2.1 economic feasibility study for a 19 pax hybrid-electric commuter aircraft," 03 2020. [Online]. Available: https://www.rolls-royce.com/~/media/Files/R/Rolls-Royce/documents/innovation/elica-d2-1-economic-feasibility-study-for-a-19-pax-hybrid-electric-commuter-aircraft.pdf

[127] S. Sirimanna, B. Thanatheepan, D. Lee, S. Agraval, Y. Yu, Y. Wang, A. Anderson, A. Banerjee, and K. Haran, "Comparison of electrified aircraft propulsion drive system with different electric motor topologies," *Journal of Propulsion and Power*, vol. 37, no. 6, pp. 733–747, 2021.

[128] A. D. Anderson, N. J. Renner, Y. Wang, S. Agrawal, S. Sirimanna, D. Lee, A. Banerjee, K. Haran, M. J. Starr, and J. L. Felder, "System weight comparison of electric machine topologies for electric aircraft propulsion," in *2018 AIAA/IEEE Electric Aircraft Technologies Symposium (EATS)*, 2018, pp. 1–16.

[129] J. Benzaquen, J. He, and B. Mirafzal, "Toward more electric powertrains in aircraft: Technical challenges and advancements," *CES Transactions on Electrical Machines and Systems*, vol. 5, no. 3, pp. 177–193, 2021.

[130] G. Brando, A. Dannier, A. Pizzo, and L. Di Noia, "A direct drive solution for contra-rotating propellers in electric unmanned aerial vehicle," 03 2015.

[131] A. Yoon, X. Yi, J. Martin, Y. Chen, and K. Haran, "A high-speed, high-frequency, air-core pm machine for aircraft application," in *2016 IEEE Power and Energy Conference at Illinois (PECI)*, 2016, pp. 1–4.

[132] D. Gerada, A. Mebarki, N. L. Brown, C. Gerada, A. Cavagnino, and A. Boglietti, "High-speed electrical machines: Technologies, trends, and developments," *IEEE Transactions on Industrial Electronics*, vol. 61, no. 6, pp. 2946–2959, 2014.

[133] X. Yi and K. S. Haran, "Transient performance study of high-specific-power motor integrated with phase change material for transportation electrification," in *2020 IEEE Transportation Electrification Conference Expo (ITEC)*, 2020, pp. 119–124.

[134] Federal Aviation Administration and U.S. Department of Transportation, *Pilot's Handbook of Aeronautical Knowledge*, 2018.

[135] J. P. Fielding, *Introduction to aircraft design*. Cambridge University Press, 1999.

[136] J. J. Scheidler, V. M. Asnani, and T. F. Tallerico, "Nasa's magnetic gearing research for electrified aircraft propulsion," in *2018 AIAA/IEEE Electric Aircraft Technologies Symposium (EATS)*, 2018, pp. 1–12.

[137] T. V. Frandsen, L. Mathe, N. I. Berg, R. K. Holm, T. N. Matzen, P. O. Rasmussen, and K. K. Jensen, "Motor integrated permanent magnet gear in a battery electrical vehicle," *IEEE Transactions on Industry Applications*, vol. 51, no. 2, pp. 1516–1525, 2015.

[138] T. F. Tallerico, J. J. Scheidler, and Z. A. Cameron, "Electromagnetic mass and efficiency of magnetic gears for electrified aircraft," in *2019 AIAA/IEEE Electric Aircraft Technologies Symposium (EATS)*, 2019, pp. 1–25.

[139] H. Y. Wong, H. Baninajar, B. Dechant, and J. Bird, "Designing a magnetic gear for an electric aircraft drivetrain," in *2020 IEEE Energy Conversion Congress and Exposition (ECCE)*, 2020, pp. 1–6.

[140] A. El-Refaie and M. Osama, "High specific power electrical machines: A system perspective," in *2017 20th International Conference on Electrical Machines and Systems (ICEMS)*, 2017, pp. 1–6.

[141] EMRAX, "Emrax e-motors," last accessed 08 November 2021. [Online]. Available: https://emrax.com/

[142] F. Anton, "eaircraft: Hybrid-elektrische antriebe für luftfahrzeuge." [Online]. Available: https://www.bbaa.de/fileadmin/user_upload/02-preis/02-02-preistraeger/newsletter-2019/02-2019-09/02_Siemens_Anton.pdf

[143] A. N. Varyukhin, P. S. Suntsov, M. V. Gordin, V. S. Zakharchenko, and D. Y. Rakhmankulov, "Efficiency analysis of hybrid electric propulsion system for commuter airliners," in *2019 International Conference on Electrotechnical Complexes and Systems (ICOECS)*, 2019, pp. 1–3.

[144] H3X, "Tech," last accessed 09 December 2021. [Online]. Available: https://www.h3x.tech/

[145] MagniX, "Magnix," last accessed 08 November 2021. [Online]. Available: https://www.magnix.aero/

[146] J. O. Reimers, "Introduction of electric aviation in norway." [Online]. Available: https://avinor.no/contentassets/c29b7a7ec1164e5d8f7500f8fef810cc/introduction-of-electric-aircraft-in-norway.pdf

[147] MGM COMPRO, "About us," 2021, last accessed 08 December 2021. [Online]. Available: https://www.mgm-compro.com/

[148] YASA, "Yasa products," last accessed 09 December 2021. [Online]. Available: https://www.yasa.com/products/yasa-p400/

[149] Magnax, "Products," last accessed 09 December 2021. [Online]. Available: https://www.traxial.com/products/

[150] L. Blain, "H3x claims it's tripled the power density of electric aircraft motors," 2020, last accessed 09 December 2021. [Online]. Available: https://newatlas.com/aircraft/h3x-electric-aircraft-motor-power-density/

[151] Safran, "Engineus," last accessed 02 May 2022. [Online]. Available: https://www.safran-group.com/products-services/engineustm

[152] R. H. Jansen, C. Bownman, A. Jonkovsky, R. Dyson, and J. L. Felder, "Overview of nasa electrified aircraft propulsion research for large subsonic transports," 2017.

[153] G. Buticchi, S. Bozhko, M. Liserre, P. Wheeler, and K. Al-Haddad, "On-board microgrids for the more electric aircraft—technology review," *IEEE Transactions on Industrial Electronics*, vol. 66, no. 7, pp. 5588–5599, 2019.

[154] L. Tarisciotti, A. Costabeber, L. Chen, A. Walker, and M. Galea, "Current-fed isolated dc/dc converter for future aerospace microgrids," *IEEE Transactions on Industry Applications*, vol. 55, no. 3, pp. 2823–2832, 2019.

[155] N. Keshmiri, M. I. Hassan, R. Rodriguez, and A. Emadi, "Comparison of isolated bidirectional dc/dc converters using wbg devices for more electric aircraft," *IEEE Open Journal of the Industrial Electronics Society*, vol. 2, pp. 184–198, 2021.

[156] P. Channegowda, Z. S. Du, S. Dwari, and P. Kshirsagar, "Megawatt class ultra high density dc-dc converters for future electric aircraft systems," in *2019 AIAA/IEEE Electric Aircraft Technologies Symposium (EATS)*, 2019, pp. 1–11.

[157] R. Nilsen, "Electric drives," Blackboard, 2018, compendium in TET4120 electric drives.

[158] M. Innocenti, L. Pollini, R. Mati, and L. Sani, "Design of an all-electric propulsion system and control management for a general aviation aircraft," 08 2015.

[159] D. Zhang, J. He, D. Pan, M. Dame, and M. Schutten, "Development of megawatt-scale medium-voltage high efficiency high power density power converters for aircraft hybrid-electric propulsion systems," in *2018 AIAA/IEEE Electric Aircraft Technologies Symposium (EATS)*, 2018, pp. 1–5.

[160] A. Deshpande, Y. Chen, B. Narayanasamy, Z. Yuan, C. Chen, and F. Luo, "Design of a high-efficiency, high specific-power three-level t-type power electronics building block for aircraft electric-propulsion drives," *IEEE Journal of Emerging and Selected Topics in Power Electronics*, vol. 8, no. 1, pp. 407–416, 2020.

[161] Q. Huo, J. Xiong, N. Zhang, X. Guo, L. Wu, and T. Wei, "Review of dc circuit breaker application," *Electric Power Systems Research*, vol. 209, p. 107946, 2022. [Online]. Available: https://www.sciencedirect.com/science/article/pii/S0378779622001766

[162] F. Mohammadi, K. Rouzbehi, M. Hajian, K. Niayesh, G. B. Gharehpetian, H. Saad, M. Hasan Ali, and V. K. Sood, "Hvdc circuit breakers: A comprehensive review," *IEEE Transactions on Power Electronics*, vol. 36, no. 12, pp. 13 726–13 739, 2021.

[163] S. Beheshtaein and R. Cuzner, "A new y- igct-based dc circuit breaker for nasa n3-x spacecraft," in *2021 IEEE Applied Power Electronics Conference and Exposition (APEC)*, 2021, pp. 1215–1218.

[164] B. Perea-Mena, J. A. Valencia-Velasquez, J. M. López-Lezama, J. B. Cano-Quintero, and N. Muñoz-Galeano, "Circuit breakers in low- and medium-voltage dc microgrids for protection against short-circuit electrical faults: Evolution and future challenges," *Applied Sciences*, vol. 12, no. 1, 2022. [Online]. Available: https://www.mdpi.com/2076-3417/12/1/15

[165] M. Barnes, D. S. Vilchis-Rodriguez, X. Pei, R. Shuttleworth, O. Cwikowski, and A. C. Smith, "Hvdc circuit breakers–a review," *IEEE Access*, vol. 8, pp. 211 829–211 848, 2020.

[166] G. Valente, S. Sumsurooah, C. I. Hill, M. Rashed, G. Vakil, S. Bozhko, and C. Gerada, "Design methodology and parametric design study of the on-board electrical power system for hybrid electric aircraft propulsion," in *The 10th International Conference on Power Electronics, Machines and Drives (PEMD 2020)*, vol. 2020, 2020, pp. 448–454.

[167] C. Hartmann, J. K. Nøland, R. Nilssen, and R. Mellerud, "Conceptual design, sizing and performance analysis of a cryo-electric propulsion system for a next-generation hydrogen-powered aircraft," 12 2021.

[168] J. Freeman, P. Osterkamp, M. Green, A. Gibson, and B. Schiltgen, "Challenges and opportunities for electric aircraft thermal management," *Aircraft Engineering and Aerospace Technology: An International Journal*, vol. 86, no. 6, pp. 519–524, 2014.

[169] F. Berg, J. Palmer, P. Miller, M. Husband, and G. Dodds, "Hts electrical system for a distributed propulsion aircraft," *IEEE Transactions on Applied Superconductivity*, vol. 25, no. 3, pp. 1–5, 2015.

[170] J. Palmer, E. Shehab, I.-S. Fan, and M. Husband, "Quality function deployment and sensitivity analysis of requirements for future aircraft propulsion cryogenic cooling systems," *International Conference on Manufacturing Research*, vol. 11, pp. 77–82, 2013.

[171] D. Dezhin, N. Ivanov, K. Kovalev, I. Kobzeva, and V. Semenihin, "System approach of usability of hts electrical machines in future electric aircraft," *IEEE Transactions on Applied Superconductivity*, vol. 28, no. 4, pp. 1–5, 2018.

[172] F. Berg, J. Palmer, L. Bertola, P. Miller, and G. Dodds, "Cryogenic system options for a superconducting aircraft propulsion system," *IOP Conference Series Materials Science and Engineering*, vol. 101, 2015.

[173] M. Popescu, D. Staton, A. Boglietti, A. Cavagnino, D. Hawkins, and J. Goss, "Modern heat extraction systems for electrical machines - a review," in *2015 IEEE Workshop on Electrical Machines Design, Control and Diagnosis (WEMDCD)*, 2015, pp. 289–296.

[174] J. W. Chapman, S. L. Schnulo, and M. P. Nietzsche, "Development of a thermal management system for electrified aircraft," 01 2020.

[175] H. Kellermann, M. Lüdemann, M. Pohl, and M. Hornung, "Design and optimization of ram air–based thermal management systems for hybrid-electric aircraft," *Aerospace*, vol. 8, no. 3, 2020.

[176] J. M. Rheaume, M. Macdonald, and C. E. Lents, "Commercial hybrid electric aircraft thermal management system design, simulation, and operation improvements," in *2019 AIAA/IEEE Electric Aircraft Technologies Symposium (EATS)*, 2019, pp. 1–23.

[177] J. Hemmerdinger, "Tecnam reveals expected performance of in-development p-volt electric aircraft." [Online]. Available: https://www.flightglobal.com/airframers/tecnam-reveals-expected-performance-of-in-development-p-volt-electric-aircraft/146500.article

[178] Zoran Cale, "Därför storsatsar bill gates i svenska succén – klimatsatsning drar in miljarder." [Online]. Available: https://www.tn.se/hallbarhet/darfor-storsatsar-bill-gates-i-svenska-succen-klimatsatsning-drar-in-miljarder

[179] Richard Schuurman, "United and mesa orders boost for heart." [Online]. Available: https://airinsight.com/united-and-mesa-orders-boost-for-heart/

[180] B. Fehrm, "The true cost of electric aircraft. part 2." [Online]. Available: https://leehamnews.com/2021/07/08/the-true-cost-of-electric-aircraft-part-2/

[181] P. M. Sforza, "Chapter 10 - propellers," in *Theory of Aerospace Propulsion (Second Edition)*, second edition ed., ser. Aerospace Engineering, P. M. Sforza, Ed. Butterworth-Heinemann, 2017, pp. 487–524. [Online]. Available: https://www.sciencedirect.com/science/article/pii/B9780128093269000105

[182] T.-E. S. Hanssen, J. Løvland, S. Nerdal, and G. Solvoll, "Transportinfrastruktur i nord-norge; status, utviklingsplaner og betydning for verdiskapning," 2013. [Online]. Available: https://www.regjeringen.no/contentassets/9a4393660e6643cca1c5039a8dac6406/transportinfrastruktur_i_nord_norge_del1.pdf.pdf